ภาคผนวก

ก. บทความตีพิมพ์ในวารสารวิชาการระดับนานาชาติ

1. C. Soemphol, A. Sonsilphong and **N. Wongkasem**, "Metamaterials with near-zero refractive index produced using fishnet structures," *Journal of Optics* **16** 015104, December 2013. **(IF 1.990)**

2. A. Sonsilphong and **N. Wongkasem**, "Low Loss Circular Birefringence in Artificial Triple Helices," *Progress In Electromagnetics Research M*, Vol. **29**, 267-278, March 2013. **(IF 0.428)**

3. A. Sonsilphong and **N. Wongkasem**, "Three-dimensional artificial double helices with high negative refractive index," *Journal of Optics* **14** 105103, September 2012. **(IF 1.990)**

4. W. Panpradit, A. Sonsilphong, C. Soemphol and **N. Wongkasem**, "High Negative Refractive Index Chiral Metamaterials," *Journal of Optics* **14** 075101, July 2012. **(IF 1.990)**

ข. สิทธิบัตรประเทศไทย

1. นันทกานต์ วงศ์เกษม และ อมรเทพ สอนศิลพงศ์, "วัสดุป้องกันคลื่นสัญญาณแม่เหล็กไฟฟ้าใน ย่านรังสีเอกซ์" ยื่นจดสิทธิบัตรประเทศไทย เมื่อวันที่ 2 เมษายน 2557 เลขที่คำขอ 1401001981

2. นันทกานต์ วงศ์เกษม และ มนตรี มาลาทอง, "วัสดุปิดกั้นคลื่นสัญญาณแม่เหล็กไฟฟ้า" ยื่นจดสิทธิบัตรประเทศไทย เมื่อวันที่ 31 มกราคม 2556 เลขที่คำขอ 1301000619

ค. บทความตีพิมพ์ใน Proceedings การประชุมวิชาการระดับนานาชาติ

1. **N. Wongkasem** and A. Sonsilphong, "Narrow-Band Wave Block by Chiral Metamaterials," PIER 2013, Stockholm, Sweden, August 2013.

2. A. Sonsilphong and **N. Wongkasem**, "Light-weight radiation protection by non-lead materials in x-ray regimes," ICEAA – IEEE APWC 2014, Aruba, August 2014.

บทความตีพิมพ์ในวารสารวิชาการระดับนานาชาติ

ก1.   C. Soemphol, A. Sonsilphong and **N. Wongkasem**, "Metamaterials with near-zero refractive index produced using fishnet structures," *Journal of Optics* **16** 015104, December 2013. **(IF 1.990)**

Metamaterials with near-zero refractive index produced using fishnet structures

C Soemphol, A Sonsilphong and N Wongkasem

Metasolver Laboratory, Department of Electrical Engineering, Faculty of Engineering,
Khon Kaen University, Khon Kaen, 40002, Thailand

E-mail: nantakan@kku.ac.th

Abstract

Metamaterials with near-zero refractive index designed using fishnet structures are proposed. The near-zero-index band is generated with the overlap of electric and magnetic resonances, where the transition from a negative-n region to a positive-n region is found. Both the permittivity and the permeability are controlled via geometrical parameters and the structure orientation, and are near-zero within the operating band, resulting in low loss transmission. As the number of layers increases, the transmission band becomes broader and moves to lower frequency. The experimental results confirm that such designs can generate a near-zero refractive index with low loss within an operating frequency band.

Keywords: near-zero, refractive index, metamaterials, fishnet

(Some figures may appear in colour only in the online journal)

1. Introduction

Metamaterials have been designed to achieve electromagnetic properties which are rarely found or do not exist at all in nature. The permittivity (ε), permeability (μ) and refractive index (n) can be manipulated to generate unusual values, for instance, refractive indices with extreme positive and negative [1] or near-zero [2–11] values, by designing the shape, the orientation and the content of the metamaterial structures.

The electrodynamic properties of a matched metamaterial having a zero or near-zero refractive index have been discussed intensively [2]. It has been shown that the electromagnetic fields in these media are static in space, but remain dynamic in time. Typically, near-zero bands are considered when n is positive, less than 1 and near-zero [8]. According to Snell's law, transmitted waves propagating from near-zero-refractive-index materials (NZRIM) are nearly normal to the outgoing surface; NZRIM can be applied in controlling wave directivity [2–6] and the radiation pattern [7]. Several NZRIM structures [3, 4, 8–12] have been designed for integrating with different kinds of antennas, phase shifters, couplers, and resonators. Furthermore, in a subset of NZRIM for which $\varepsilon \sim 0$ (ENZ),

there are various exciting EM phenomena, e.g., tunneling through extremely narrow ENZ channels [13], extremely nonlinear electrodynamics [14], harmonic generation with low absorption [15], low threshold multistability, all-optical switching, and inherently nonlocal effects [16], to name but a few.

In this paper, fishnet structures are modified to achieve near-zero refractive index, where both the permittivity and the permeability are near-zero at the operating frequency in microwave regimes. The structures designed shown in figure 1 are composed of pairs of short slabs connected with continuous wires printed on both sides of a substrate. The electrical and magnetic resonances can be adjusted respectively via the continuous wires and the slabs. The near-zero-index band is generated within the matching resonances, where the transition from a double-negative (DNG) region to a double-positive (DPG) one is expected [2]. Another advantage of the slab pair design is that it is simple, yet can generate negative n where the excitation is normal to the structure plane [17–22]. Here, a single layer and multiple (two and three) layers of fishnet structures are investigated. The simulation and experimental results show that these designs can generate near-zero refractive index with low loss within an operating frequency band.
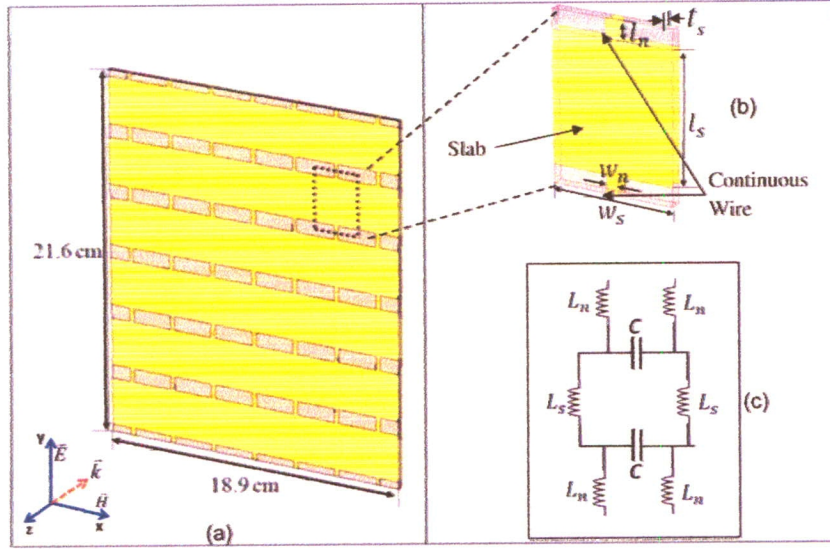
Figure 1. (a) A 6 × 7 unit cell, (b) a unit cell and (c) the *LC* equivalent circuit for the fishnet structures.

2. Near-zero refractive index in fishnet structures

Pairs of short slabs and continuous wires are combined to construct fishnet structures, as illustrated in figures 1(a) and (b). The pair of short slabs (front and back) provides a magnetic resonance, while the arrays of continuous wires generate an electric resonance. The *LC* equivalent circuit of the fishnet structure is presented in figure 1(c), where the magnetic resonance frequency can be determined from $f_m \sim \sqrt{\frac{1}{l_s^2} + \frac{1}{l_s l_n} \frac{w_n}{w_s}}$ [20]. l_s represents the length of the slab, l_n is the length of the neck line, and w_s and w_n are the width of the slab and the neck line, respectively. The refractive index ($n = \sqrt{\varepsilon \mu}$) of the structure is near-zero or close to zero when either ε or μ for the structure is close to zero, or both ε and μ are close to zero. ε and μ are directly related to the geometry of the structure, i.e. the permeability can be controlled through the inductance of the slab width (w_s) and the capacitance between layers by changing the substrate thickness (t_s) and ε_r for the substrate; furthermore, the width of the neck line (w_n) and the spacing between the wires ($w_s - w_n$) are the main factors used to manage the permittivity.

A 2.4 mm thick FR4 dielectric substrate ($\varepsilon_r = 4.3$ and $\tan(\delta) = 0.025$) with the copper thickness of 30 μm is used to fabricate 6 × 7 fishnet structures. The simulation results are obtained from CST Microwave Studio where a finite integration technique is performed. The excitation is launched on the fishnet plane, along the $-z$ axis, perpendicular to the x–y plane, as shown in figure 1. The boundary condition is set as open spaces for all the axes. The scattering parameters of these fishnets are obtained from the xy plane. The structure dimensions are as follows: $w_s = 26$ mm, $w_n = 2.5$ mm, $l_s = 27$ mm, $l_n = 4$ mm. The short slab is as wide as the unit cell (along the x axis). The unit cell size is 26 mm × 35 mm. These parameters will be employed in the rest of the paper.

Figures 2(a) and (b) illustrate the amplitude and phase of the transmission (S_{21}) and reflection (S_{11}) coefficients of the single-layer fishnet. A broad passband ($S_{21} > -6$ dB
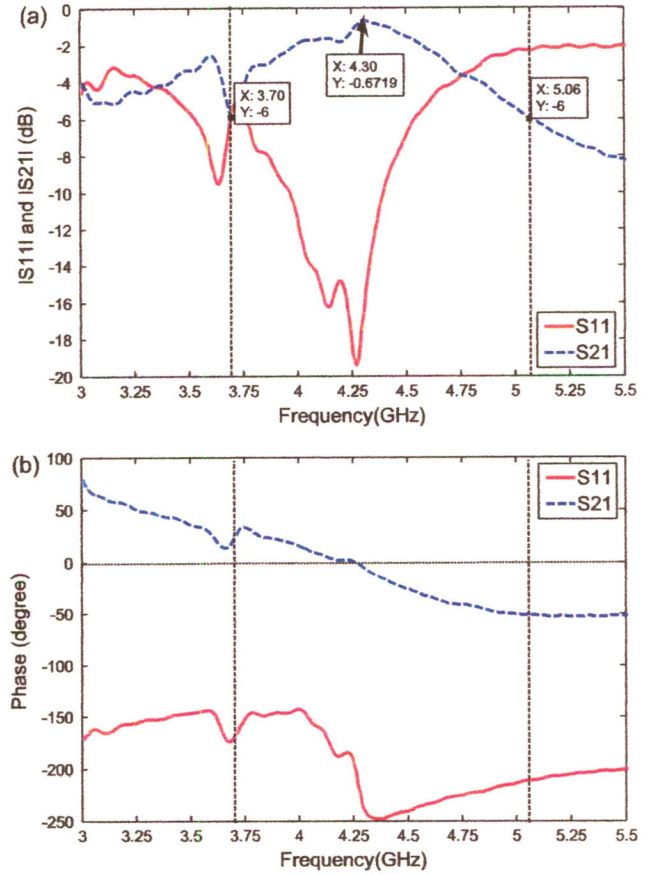

Figure 2. (a) Amplitude and (b) phase of the *S*-parameters of single-layer fishnet structures.

or minimum 50% transmission) is found from 3.70 to 5.06 GHz or 31.68% bandwidth with a transmission peak at 4.30 GHz. The transmission (S_{21}) and reflection (S_{11}) coefficients obtained from the simulations are then used to retrieve other EM parameters [23, 24]. The EM properties are presented in figure 3.
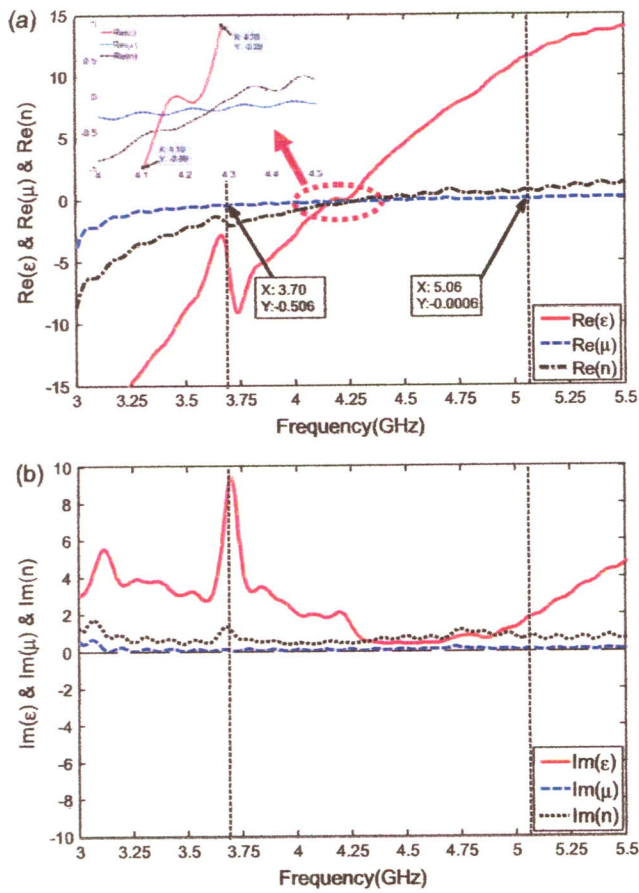
Figure 3. (a) Real and (b) imaginary parts of ε, μ and n for single-layer fishnet structures.
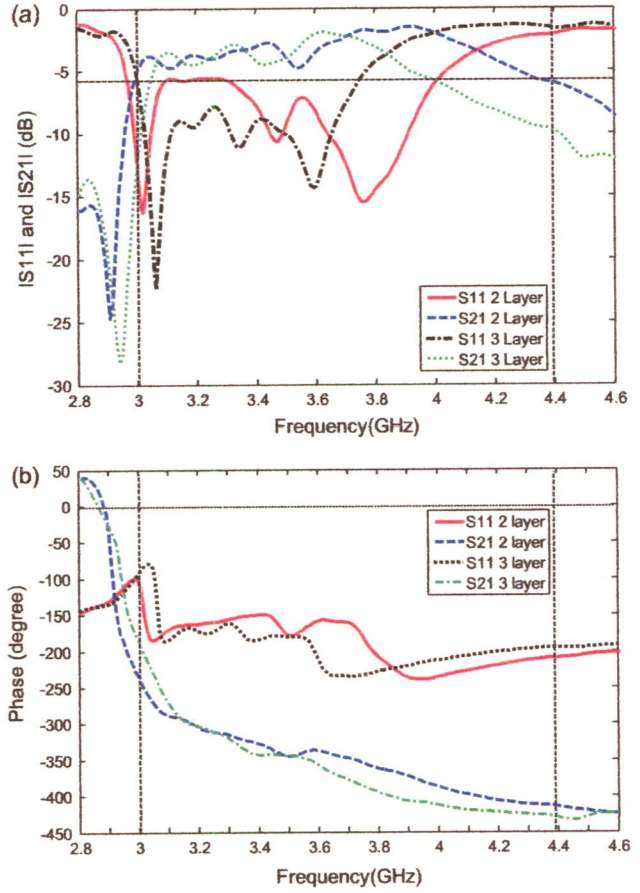

Figure 4. (a) Two-layer and (b) three-layer fishnet structures.

Figure 5. (a) Amplitude and (b) phase of the *S*-parameters of two-layer and three-layer fishnet structures.
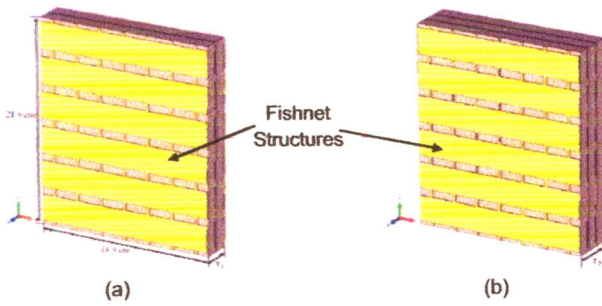

Figure 6. Real parts of ε, μ and n for two-layer and three-layer fishnet structures.

We focus on the near-zero-index band (4.0–4.5 GHz) generated within the passband (3.70–5.06 GHz) where good transmission is observed. The real part of μ is close to zero ($-0.506 < \mathrm{Re}(\mu) < -0.0006$) within the transmission band range; on the other hand, however, the real part of ε is near-zero from 4.10 to 4.28 GHz, as marked in the zoomed plot of figure 3. n is found to be near-zero from 4.00 to 4.50 GHz. It is important to state that an $n < 0$ region is found below the transmission peak (4.30 GHz), while an $n > 0$ region begins after the peak. These results support the idea of where the near-zero-index band should be generated, i.e. the transition from a double-negative region to a double-positive one.
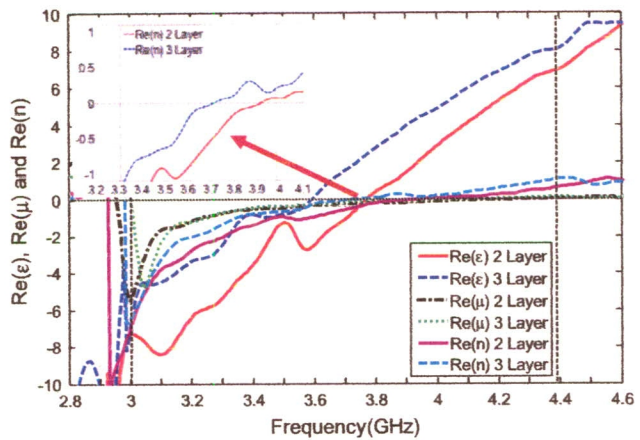
3. Multilayer fishnet structures

Here, two ($t_1 = 4.92$ mm) and three ($t_2 = 7.38$ mm) layers of the fishnet structures, as shown in figure 4, are investigated. Figure 5 presents S_{11} and S_{21} for the multiple-layer fishnet structures.

As the number of layers increases, the total capacitance of the structure also increases, resulting in lowering the location of the resonance frequency. The transmission band where
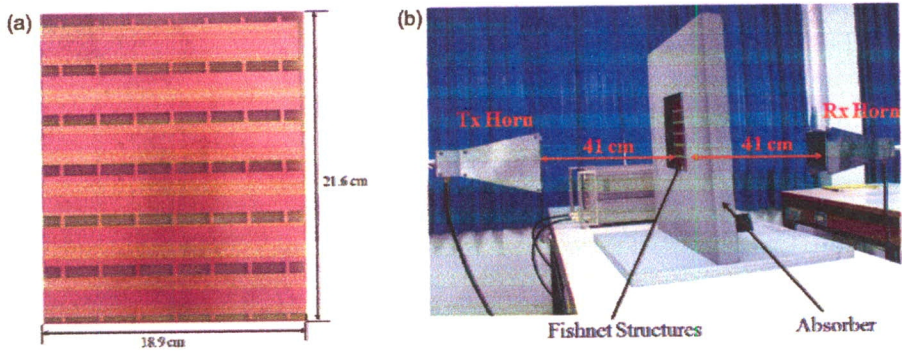
Figure 7. (a) Fabricated fishnets and (b) the experiment setup.

$S_{21} > -6$ dB for the multiple layers is therefore lower than that for the single layer. It can be seen in figure 6 that Re(n) is near-zero from 3.32 to 4.00 GHz. The near-zero bands of the multiple-layer designs are significantly broad—almost in the same range as the operating band.

4. Fabrication and measurement

The fishnet structures shown in figure 7(a) are fabricated using a standard printed circuit board process with 30 μm thick copper patterns on 2.4 mm thick FR4 dielectric substrates ($\varepsilon_r = 4.3\varepsilon_r$ and loss tangent $\tan(\delta) = 0.025$). The transmission and reflection coefficients of the fabricated fishnet structures are measured by using a vector network analyzer (HP8753D). Microwave standard-gain horn antennas are used as the transmitting and receiving ports, as shown in the experimental setup, illustrated in figure 7(b). The transmitter and receiver horns have 13 cm × 13 cm diagonal mounts, with 50° 3 dB beam width at 3.5 GHz. The far-field range of the horn antennas starts from 22.53 cm. The transmission distance from the horn to the front of the fishnets and the distance from that same point to the receiver horn are set equal, at 41.0 cm, which fulfills the far-field condition. From this setup, one can also conclude that the input wave is approximately a planar wave. The vertical linear polarization waves are launched from the transmitter horn antenna through the fishnets and then are collected by the receiver horn with a frequency step of 0.0125 GHz, from 3 to 5.5 GHz. The ECCOSORB® AN absorbers are used to eliminate the unwanted scattering and reflected waves; therefore one only obtains the measurement data from the interaction between the propagated waves and the fishnets. Figure 8(a) shows the S-parameters of single-layer fishnet structures.

The transmission bands ($S_{21} > -6$ dB) from the simulation and measurement results are similar in the range from 3.18 to 5.22 GHz, where the transmission peak is at 4.33 GHz. Some variations between the theoretical and measured results are caused by the limited dimensions of the fabricated prototype, and fabrication imperfections, as well as the accuracy limits of the measuring instruments. ε, μ and n in figure 8(b) are near-zero in the transmission band and at the frequency band from 4.30 to 5.20 GHz. The loss factor (LF $= (\frac{\mathrm{Im}(n)}{\mathrm{Re}(n)})$) shown in figure 9 indicates low loss transmission (LF < 1.0) from 4.30 to 4.57 GHz. An efficient way to reduce
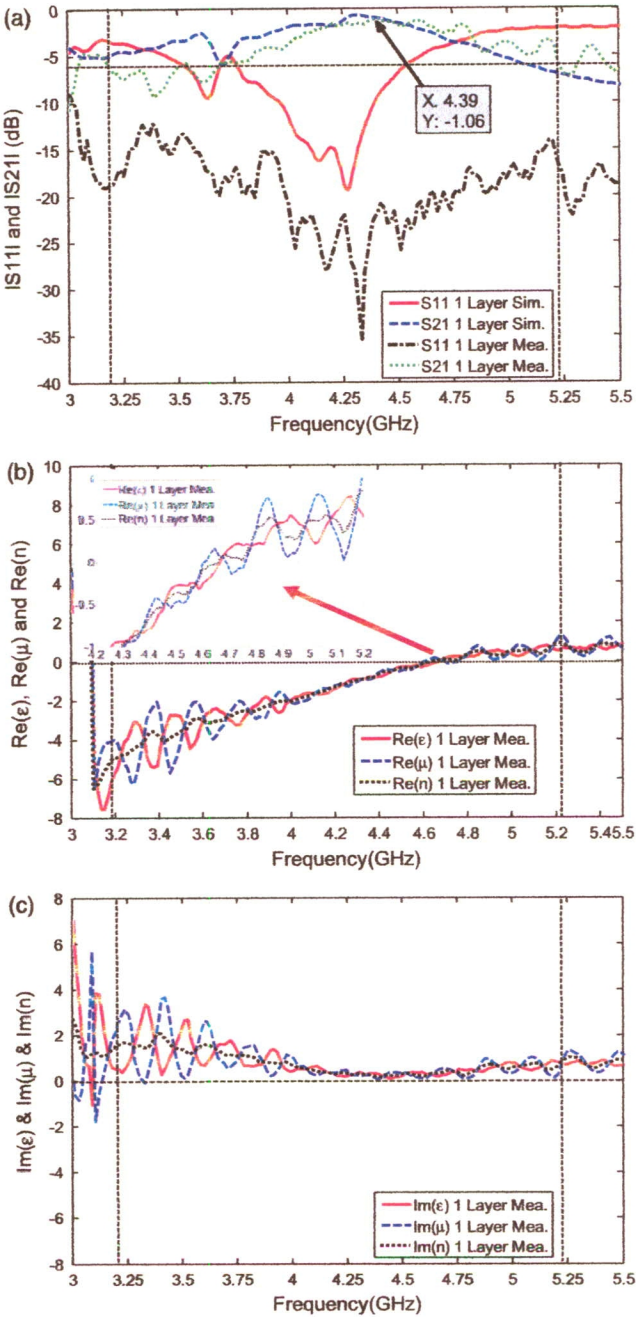

Figure 8. Measurement results for single-layer fishnets: (a) S-parameters, (b) real parts and (c) imaginary parts of ε, μ and n.
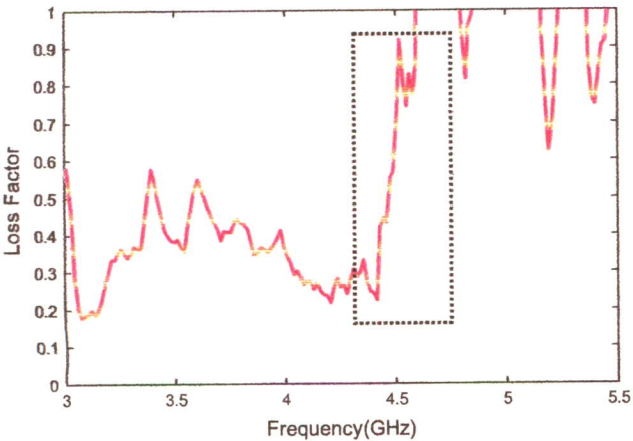
Figure 9. Loss factors of single-layer fishnet structures.
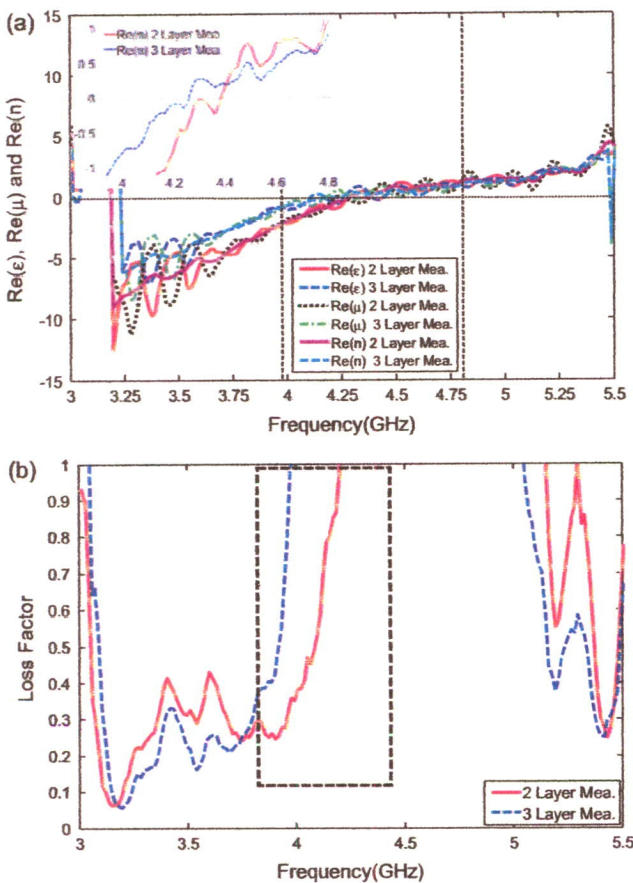

Figure 10. Measurement results for two-layer and three-layer fishnets: (a) real parts of ε, μ and n and (b) the loss factor.

losses of fishnet structures can be by increasing the effective inductance to capacitance ratio [25] which directly affects the Q factor of the structure.

As discussed earlier, the near-zero bands (3.96–4.80 GHz) of the two-layer and three-layer fishnets are lower and broader than that of the single layer, showing the same trend as those from the simulation results. ε, μ and n are shown in figure 10(a). The refractive index is near-zero within the transmission band. The loss factors of both multiple-layer fishnets shown in figure 10(b) also confirm the low loss for

near-zero transmission at 4.16–4.20 GHz and 3.96–4.00 GHz for two and three layers, respectively.

Conclusions

A near-zero-index band is generated around the transition from a negative-n region to a positive-n region where the electric and magnetic resonances are matched. Both the permittivity and the permeability are designed to be close to zero within the near-zero transmission band in order to achieve low loss transmission. The near-zero band is broader and located at lower frequency when more layers are added due to the impact of the total capacitance and the couplings among the additional structures. These proposed structures are additional promising candidates for metamaterials of near-zero refractive index which will facilitate different applications.

Acknowledgments

References

[1] Panpradit W, Sonsilphong A, Soemphol C and Wongkasem N 2012 High negative refractive index in chiral metamaterials *J. Opt.* **14** 075101

[2] Ziolkowski R W 2004 Propagation in and scattering from a matched metamaterial having a zero index of refraction *Phys. Rev.* E **70** 046608

[3] Silveirinha M and Engheta N 2006 Tunneling of electromagnetic energy through subwavelength channels and bends using ε-near-zero materials *Phys. Rev. Lett.* **97** 157403

[4] Lui R, Cheng Q, Hand T, Mock J J, Cui T J, Cummer S A and Smith D R 2008 Experimental demonstration of electromagnetic tunneling through an epsilon-near-zero metamaterial at microwave frequencies *Phys. Rev. Lett.* **100** 023903

[5] Zhou H, Pei Z, Qu S, Zhang S, Wang J, Duan Z, Ma H and Xu Z 2009 A novel high-directivity microstrip patch antenna based on zero index metamaterial *IEEE Antennas Propag. Lett.* **8** 538–41

[6] Zhou B and Cui T J 2011 Directivity enhancement to Vivaldi antennas using compactly anisotropic zero-index metamaterials *IEEE Antennas Wirel. Propag. Lett.* **10** 326–9

[7] Wang B and Huang K M 2010 Shaping the radiation pattern with mu and epsilon-near-zero metamaterials *Prog. Electromagn. Res.* **106** 107–19

[8] Enoch S, Tayeb G, Sabouroux P, Guerin N and Vincent P 2002 A metamaterial for directive emission *Phys. Rev. Lett.* **89** 213902

[9] Franson S J and Ziolkowski R W 2009 Confirmation of zero-N behavior in a high gain grid structure at millimeter-wave frequencies *IEEE Antennas Wirel. Propag. Lett.* **8** 387–90

[10] Kim D and Choi J 2009 Study of antenna gain enhancement using a near-zero refractive index and Fabry–Perot cavity

resonance *3rd Int. Congr. on Advanced Electromagnetic Materials in Microwave and Optic*

[11] Huang H C, Lin K H, Su H L, Wu C Y and Lin H H 2009 Design of dual-polarized high-gain antenna radome by using Jerusalem cross metamaterial structure *APSURSI: Antennas and Propagation Society Int. Symp.*

[12] Wang X, Feng Y, Chen S, Zhao Z and Zhou C 2010 Beam *combination* using near-zero index metamaterials *INEC: 3rd Int. Nanoelectronics Conf.*

[13] Rui R, Cheng Q, Hand T, Mock J, Cui T J, Cummer S A and Smith D R 2008 Experimental demonstration of electromagnetic tunneling through an epsilon-near-zero metamaterial at microwave frequencies *Phys. Rev. Lett.* **100** 023903

[14] Ciattoni A, Rizza C and Palange E 2010 Extreme nonlinear electrodynamics in metamaterials with very small linear dielectric permittivity *Phys. Rev. A* **81** 043839

[15] Vincenti M A, de Ceglia D, Ciattoni A and Scalora M 2011 Singularity-driven second- and third-harmonic generation at ε-near-zero crossing points *Phys. Rev. A* **84** 063826

[16] de Ceglia D, Campione S, Vincenti M A, Capolino F and Scalora M 2013 Low-damping epsilon-near-zero slabs: nonlinear and nonlocal optical properties *Phys. Rev. B* **87** 155140

[17] Zhang S, Fan W, Malloy K J, Brueck S R, Panoiu N C and Osgood R M 2005 Near-infrared double negative metamaterials *Opt. Express* **13** 4922–30

[18] Zhou J, Economou E N, Koschny T and Soukoulis C M 2006 A unifying approach to left handed materials design *Opt. Lett.* **31** 3620–2

[19] Dolling G, Wegener M, Soukoulis C M and Linden S 2007 Negative-index metamaterial at 780 nm wavelength *Opt. Lett.* **32** 53–5

[20] Kafesaki M, Tsiapa I, Katsarakis N, Koschny Th, Soukoulis C M and Economou E N 2007 Left-handed metamaterials: the fishnet structure and its variations *Phys. Rev. B* **75** 235114

[21] Alici K B and Ozbay E 2008 A planar metamaterials: polarization independent fishnet structure photonics and nanostructures—fundamentals and applications *ScienceDirect* **6** 102–7

[22] Tung N T, Lee Y P and Lam V D 2009 Transmission properties of electromagnetic metamaterials: from split-ring resonator to fishnet structure *Opt. Rev.* **16** 578–82

[23] Smith D R, Shultz S, Markos P and Soukoulis C M 2002 Determination of effective permittivity and permeability of metamaterials from reflection and transmission coefficients *Phys. Rev. B* **65** 195104

[24] Chen X, Grzegorczyk T, Wu B I, Pacheco J and Kong J A 2004 Robust method to retrieve the constitutive effective parameters of metamaterial *Phys. Rev. E* **70** 016608

[25] Zhou J F, Koschny Th and Soukoulis C M 2008 An efficient way to reduce losses of left-handed metamaterials *Opt. Express* **16** 11147

บทความตีพิมพ์ในวารสารวิชาการระดับนานาชาติ

ก2.   Sonsilphong and **N. Wongkasem**, "Low Loss Circular Birefringence in Artificial Triple Helices," *Progress In Electromagnetics Research M*, Vol. **29**, 267-278, March 2013. **(IF 0.428)**

LOW LOSS CIRCULAR BIREFRINGENCE IN ARTIFICIAL TRIPLE HELICES

Amornthep Sonsilphong and Nantakan Wongkasem[*]

Metasolver Laboratory, Department of Electrical Engineering, Faculty of Engineering, Khon Kaen University, Khon Kaen 40002, Thailand

Abstract—Low loss circular birefringence is found in three-dimensional artificial triple helices. High values of chirality index are generated. Within the transmission bandwidth, there is a significant difference in the refractive index value of the right- and left-circularly polarized waves. The outgoing waves from a wedge structure designed from these triple helices are proved to split with a wide angle. The wave polarizations agree with earlier simulation results.

1. INTRODUCTION

Helices are one of the well-known chiral structures found in several natural molecules, e.g., DNA, sucrose, proteins, etc., as well as solid elements such as quartz and crystal. Optical activity presented in helix structures in terms of chirality parameter, κ, has been reported [1, 2]. The chirality parameter based on the constitutive relations [3] describes the cross-coupling between electric and magnetic field. Due to optical activity or optical rotary dispersion (ORD), any arbitrary polarization wave splits into a right-circularly polarized (RCP) wave and a left-circularly polarized (LCP) wave with different phase velocity and different refractive index, i.e., n_+ of the RCP wave and n_- of the LCP wave, while propagating independently inside the chiral media. This double refraction of the circular polarized waves is also called circular birefringence from where the optical rotation is derived, as it rotates the plane of polarization of the polarized waves. The two circularly polarized waves are then coupled at the boundaries and exit the media in one polarization configuration, typically as an elliptically polarized

wave, based on the absorption loss or circular dichroism (CD) of the media. The effective refractive index ($n_{eff} = (n_+ + n_-)/2$) of the chiral media is used to determine the direction of the leaving wave. However, the RCP and LCP waves can both continue to propagate outside the chiral media if the outgoing surface plane of the media is not perpendicular to the direction of the incoming waves. This can be done by constructing the media in different shapes, for instance in a wedge [4, 5] or triangle shape [6]. The two outgoing waves will propagate separately according to their refractive index generated earlier based on ORD. This wave/light splitting control is useful in beam splitters, polarizers, etc..

Artificial single and double helices have been proposed for broadband circular polarizers [7–9] and have improved the signal to noise ratio [10]. Multi-band circular polarizers using multilayered planar spiral metamaterials, where different transformation responses for the LCP and RCP waves were demonstrated, have been investigated [11, 12]. Chiral split-ring resonators (SRRs) formed in 3D double helix shape have been proposed as a resonant microwave absorber [13]. Several bi-layer and multi-layer chiral structures [14–17], as well as non-planar chiral SRRs [18] with strong optical activity and negative refractive index were studied in both microwave and optical regimes. Electromagnetic (EM) properties and negative refractive index of multiple helices, i.e., single, double, triple, quadruple, and quintuple helix were extensively studied [19]. High negative refractive index was found in three-dimensional double helices [20]. As the number of helical backbones increases it results in higher values of chirality index and lower loss [19]. The number of helical backbones is associated with an overlapping area of opposite handedness of the helix [21]. By changing the balance between left- and right-handed helices, the chirality index of the structures increases [22]. The chirality is also linked to transmission properties through the transmission phases [23].

This paper presents three-dimensional artificial triple helices where both RCP and LCP waves propagate inside the triple helix stack with low loss, unlike single and double helices, where one of the two circularly polarized waves is normally filtered out. The transmission coefficients and electromagnetic properties, i.e., refractive indices (n_+, n_- and n_{eff}), chirality and loss factor are investigated. The 3D planar triple helices are fabricated and measured to validate the EM properties. The wedge design of these 3D triple helices is implemented to observe the circular birefringence. It has been found that these triple helices can generate wide splitting angle waves with low loss.

2. ARTIFICIAL HELICAL STRUCTURES

Three conventional helical structures, e.g., single, double, and triple helix, illustrated in Figures 1(a), 1(b), and 1(c), respectively, are initially investigated. Figure 1(d) shows the proposed 3D triple planar helix whose fabrication and testing is discussed in the next section. The geometric parameters of these helices are set as follows: pitch height, $H = 20$ mm and radius of wire, $R = 0.5$ mm. The transmission and reflection coefficients of these conventional helices are obtained by CST Microwave studio [24].
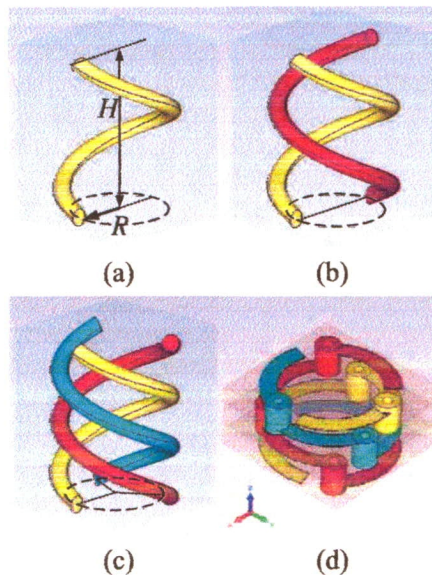

Figure 1. (Color online) conventional (a) single, (b) double, and (c) triple helix, (d) 3D triple planar helix.

The RCP and LCP waves are excited along the $-z$ direction. A periodic boundary is set on the x-y plane and therefore the helices are seen as a periodic array on the x-y plane with one row along the z axis. The effective refractive index, n_{eff}, chirality, $\kappa = (n_+ - n_-)/2$, and loss factor of RCP (LF_+) and LCP (LF_-), $LF_\pm = |\mathrm{Im}(n_\pm)/\mathrm{Re}(n_\pm)|$ are extracted from transmission and reflection coefficients [25] illustrated in Figure 2.

The transmission properties of single and double conventional helices indicate filter ability where an unwanted polarized wave can be eliminated. Based on its right-handed orientation, the RCP wave can propagate through both single and double helices, while the LCP wave
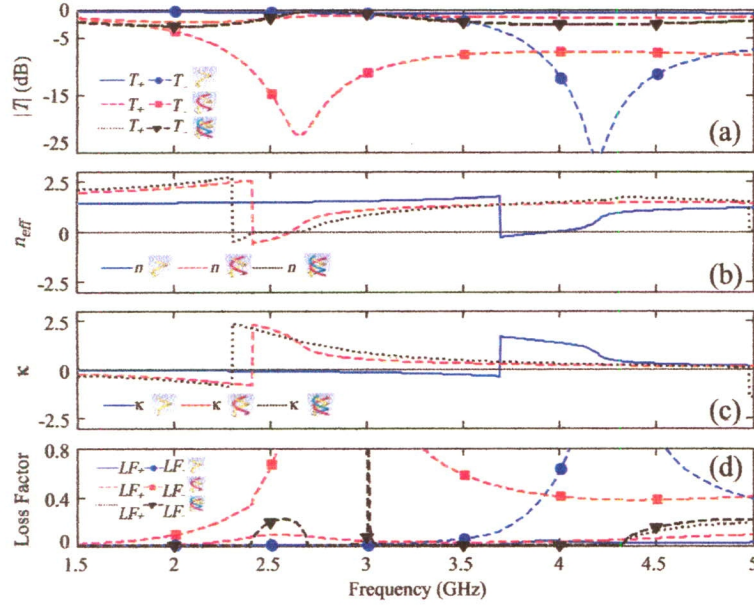
Figure 2. (Color online) (a) transmission coefficient: T_+ for RCP wave and T_- for LCP wave, (b) effective refractive index, (c) chirality and (d) loss factor: LF_+ for RCP wave and LF_- for LCP wave of single, double, and triple helix.

is almost blocked [7–10, 19] at the resonance frequency, at 4.20 GHz for single helix and 2.60 GHz for double helix. As the balance between left- and right-handed helices is improved, the triple helix allows both RCP and LCP waves to travel through. The transmission coefficient of both RCP and LCP waves is then enhanced. The amplitude of the RCP and LCP waves is almost identical, as shown in Figure 2(c). The low loss illustrated in the loss factor plot also supports this design. It is important to stress that all three helical structures can generate negative refractive index, which was also demonstrated in an earlier study [19].

3. THREE-DIMENSIONAL TRIPLE HELICES

The schematics of 3D planar triple helix chiral metamaterials are shown in Figure 3. The structures are fabricated on FR-4 boards. The dielectric constant of the FR-4 board is $\varepsilon = 4.3 + 0.23i$. The thickness of copper is 0.03 mm. CST Microwave Studio based on finite integration technique (FIT) is used to determine the reflection and transmission
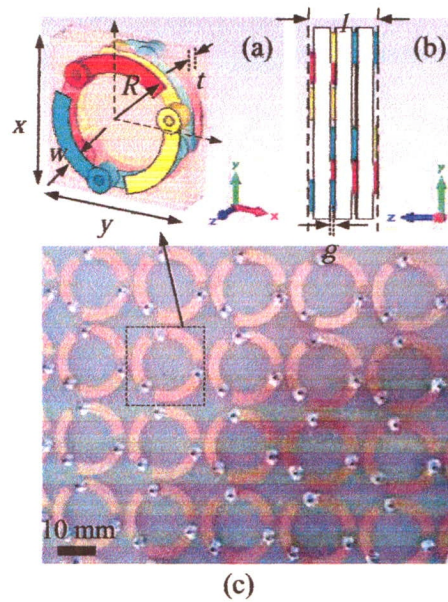
Figure 3. (Color online) a unit cell of 3D planar triple helix in (a) perspective, and (b) side view, and (c) a photograph of fabricated sample. The geometric parameters are: $x = y = 18.75$ mm, $w = 2.25$ mm, $l = 6.94$ mm, $g = 0.535$ mm, $R = 8.75$ mm, and $t = 1.6$ mm.

coefficients. Tetrahedral meshing is set in a frequency domain solver operating from 1.4 GHz to 3.0 GHz. The unit cell boundary condition of CST dictates the periodic orientation of the helices on the surface plane. The helix unit lattice is 18.75 mm × 18.75 mm × 6.94 mm. The right- and left-circularly polarized waves are excited along the $-z$ direction. The transmission and reflection coefficients obtained from the simulations are then used to retrieve other EM parameters [25].

Exactly the same material parameters and orientations used in fabricated helices are implemented throughout these EM full wave simulations. The ring with R radius is split into three equal arcs. An array of the three arcs is printed on each layer. At the adjacent layer, the array is rotated by 120° as illustrated in Figure 1(d). The arc from the previous layer is connected with the rotated arc (same color) of the neighboring layer through a created hole. To complete a helix pitch, these triple helices require four layers printed on three substrates. The diameters of the outer and inner hole are 3.25 mm and 1.25 mm respectively. Three FR4 substrates are used to complete a stack of arrays of one pitch triple helices. Figures 3(a) and 3(b)

illustrate the unit cell of 3D planar triple helix in a perspective view
and side view. The 3D planar triple helices are manufactured with
10×10 unit cells. Some fabricated parts of the first layer are shown in
Figure 3(c), where the dashed square indicates a unit cell of each helix.
Note that to obtain multiple "n" backbone helices [11], there will be
unconnected identical "n" arcs printed on each layer. Furthermore,
the number of helix pitches can be increased by adding extra sets of
multilayer stacks.

The reflection and transmission coefficients of the fabricated
helix stack are measured by a vector network analyzer HP8753D.
Horn antennas are used as transmitting and receiving ports. The
vertical linear polarization waves are launched from the transmitter
horn antenna through the helix stack and then are collected by the
receiver horn in vertical and horizontal directions with a frequency
step of 0.0125 GHz, from 1.4 GHz to 3.0 GHz. More details about the
experiment procedure and setup can be found in an earlier report [20].

The transmission coefficients of RCP (T_+) and LCP (T_-) from the
simulation and experiment are illustrated in Figure 4. The frequency
is investigated in the 1.4 GHz–3.0 GHz range. The amplitude of the
RCP and LCP waves has a similar pattern, illustrated in Figures 4(a)
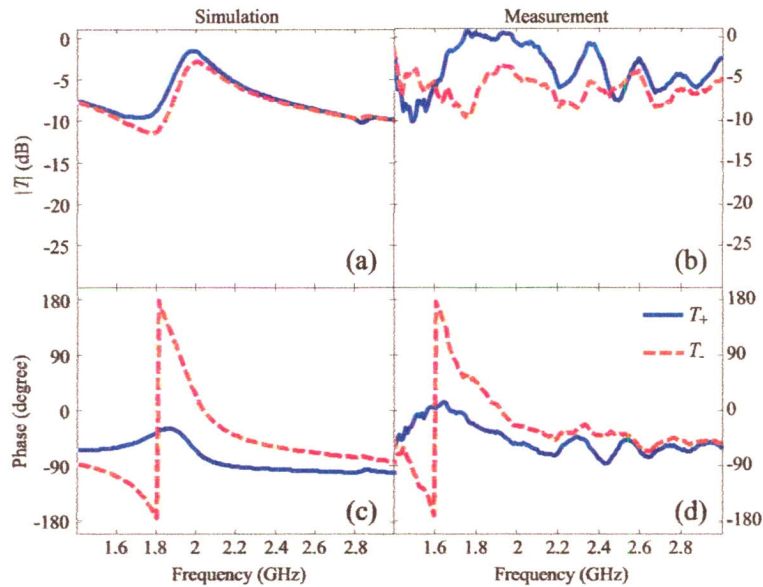(simulation) and 4(b) (experiment), showing a pass band at the

Figure 4. (Color online) simulation and experiment results
of 3D planar triple helix: (a) and (b) transmission amplitude,
(c) and (d) transmission phase from RCP and LCP excitation waves.

operating frequency from 1.8 GHz to 2.2 GHz. On the other hand, the phase of the RCP and LCP waves is different for both simulation (Figure 4(c)) and experiment (Figure 4(d)), confirming the chirality of the structures [23]. The effective refractive index and index of the RCP and LCP excitations, and chirality retrieved from the transmission and reflection coefficients [23, 25] are shown in Figures 5(a) (simulation) and 5(b) (measurement). The loss factor of RCP, LF_+, and LCP, LF_-, and effective loss factor, LF_{eff}, are observed and presented in Figures 5(c) (simulation) and 5(d) (measurement).

The refractive index of the LCP wave, n_-, is negative from 1.80 GHz to 2.01 GHz (dash line, simulation) and from 1.60 GHz to 1.85 GHz (dash line, measurement), while the refractive index of the RCP wave, n_+, (solid line, simulation) and the chirality, κ, (dashed-dotted line, simulation) are positive, as shown in Figure 5(a). As illustrated in Figure 5(b), κ from measured data is also positive from 1.60 GHz to 1.85 GHz, while n_+ changes from negative to positive. In Figure 5(c), from 1.80 GHz to 2.01 GHz, the loss factor of both RCP and LCP excitations (simulation) is low (< 0.5), while the loss factors of the measured data shown in Figure 5(d), from 1.60 GHz to 1.85 GHz, are higher, varying from 0.3 to 1.0. Some variations between the theoretical and measured results are caused by the limited
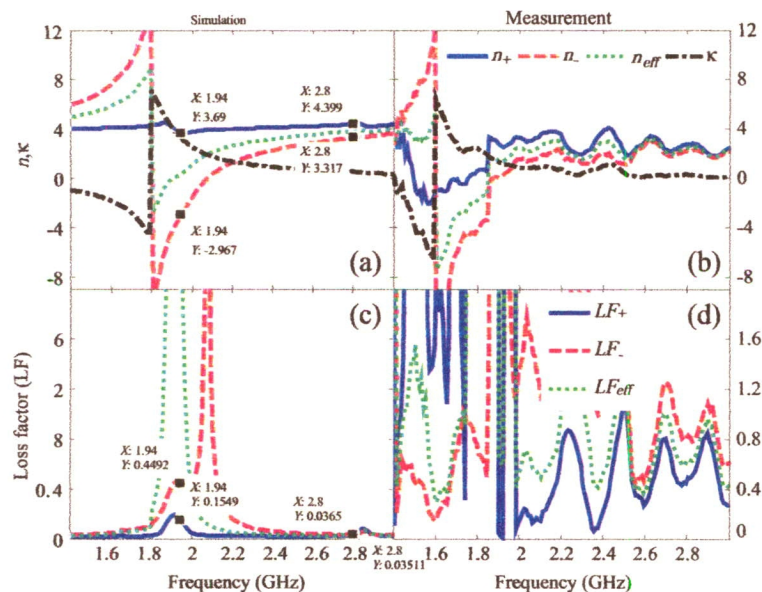

Figure 5. (Color online) simulation and experiment results of 3D planar triple helix: (a) and (b) refractive and chirality index, and (c) and (d) loss factor of RCP and LCP waves.

dimensions of the fabricated prototype [26], fabrication imperfections, as well as accuracy limit of the measuring instruments. However, we may conclude that there is low loss transmission for both excitations within the operating frequency. The RCP and LCP waves propagate through these triple helix stacks with a different refractive index stating circular birefringence. For instance, at 2.01 GHz, n_+ is 3.79 with the transmission amplitude of -1.96 dB, and n_- is -1.09 with the RCP *amplitude of -3.03 dB.*

Figure 6 illustrates the transmission of the RCP and LCP waves through a wedge constructed from the designed triple helix stack. Two frequencies where both LCP and RCP waves propagate with low loss, 1.94 GHz (located within the transmission bandwidth) and 2.8 GHz, marked in Figure 5(a) and Figure 5(c), are selected to investigate the circular birefringence. A TEM linear polarization wave is lunched from the base to the top of the wedge along $\bar{k}$, as shown in Figure 6. The wedge dimension is set as 8 unit cells (height, h) $\times$3 unit cells (width, w) or 150 mm $\times$56.25 mm. In order to build an 8.5° wedge, 9 unit cells have to be placed along the propagation direction (wedge length) of the short side (A), and 12 unit cells along the propagation direction of the long side (B). The adjacent cells are separated by 0.5 mm; therefore the short side is 65.39 mm and the long side is 87.71 mm. Hence, the 8.5° wedge, $\tan^{-1}((A - B)/w)$, is constructed.

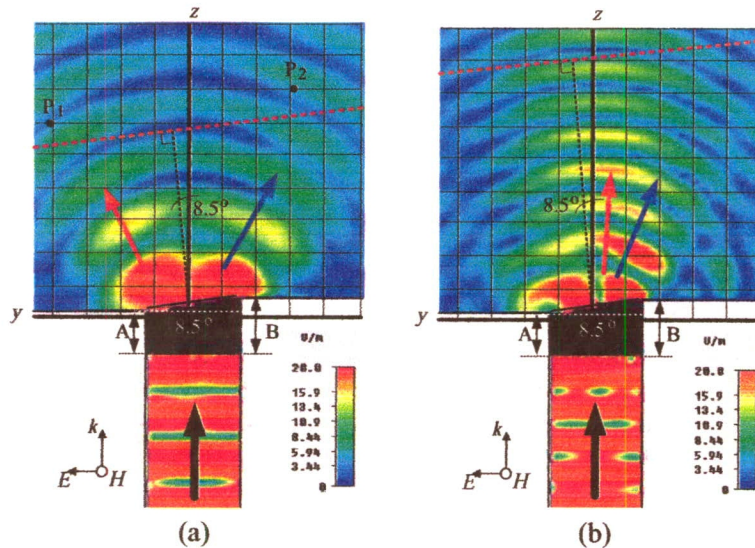At 1.94 GHz (Figure 5(a)), n_+ and n_- are 3.69 and respectively

Figure 6. Transmission of RCP and LCP waves through triple helix wedge at (a) 1.94 GHz and (b) 2.80 GHz.

-2.97. Based on Snell's law and the wedge angle of $8.5°$, the RCP wave will propagate to free space with the outgoing angle of $+32.88°$ (blue arrow), with respect to the normal line of the outgoing surface, while the LCP wave will travel out with a $-25.91°$ outgoing angle (red arrow). The direction of the two transmitted waves in Figure 6(a) supports the previous results shown in Figure 5(a). This confirms that the RCP and LCP waves are split with a $58.79°$ wide angle. Another example is at $2.80\,GHz$, where n_+ and n_- are 4.40 and 3.32, respectively (Figure 5(a)). Based on Snell's Law, the transmitted RCP and LCP waves will propagate through the chiral wedge with an outgoing angle of $40.34°$ and respectively $29.24°$, therefore having the splitting angle of $11.10°$. The direction of the two waves presented in Figure 6(b) supports the refractive index values retrieved earlier.

To further investigate the polarization of the outgoing wave within the operating frequency of $1.94\,GHz$, electric field components, E_x and E_y at points P_1 and P_2 marked in Figure 6(a) are collected. Point P_1 $(0, 206\,mm, -300\,mm)$ and P_2 $(0, -158\,mm, -350\,mm)$ lay outside the far-field region on the $-25.91°$ and $+32.88°$ line, respectively. The amplitude (A_1, A_2) and phase (θ_1, θ_2) of E_x and E_y at point P_1 and P_2 are presented in Table 1. The phase difference between E_x and E_y, θ, is determined by $\theta_1 - \theta_2$. Since $A_1 \neq A_2$ and $\theta \neq 0$, or $\theta \neq \pi$, the outgoing wave is proved to be elliptically polarized [18, 19]. If the angle θ is arbitrary and it is not equal to $\pm\pi/2$, the major axis (E_x) and minor axis (E_y) of the ellipse will be rotated with the rotation angle of $(1/2)\tan^{-1}(2A_1 A_2 \cos\theta/(A_1^2 - A_2 2))$ [27, 28]. If $\sin(\theta) > 0$, the rotation is counterclockwise or left-elliptically polarized, and clockwise or right-elliptically polarized when $\sin(\theta) < 0$ [29]. At the observed points, P_1 and P_2, $\sin(\theta)$ is negative and positive, respectively, stating that the outgoing waves at point P_1 and P_2 are left-handed and right-handed. Figure 7 illustrates the left-and right elliptical polarization at points P_1 and P_2 at $1.94\,GHz$.

Table 1. E_x and E_y, rotation of electric field, and polarization configuration of the outgoing wave at point P_1 and P_2 at $1.94\,GHz$.

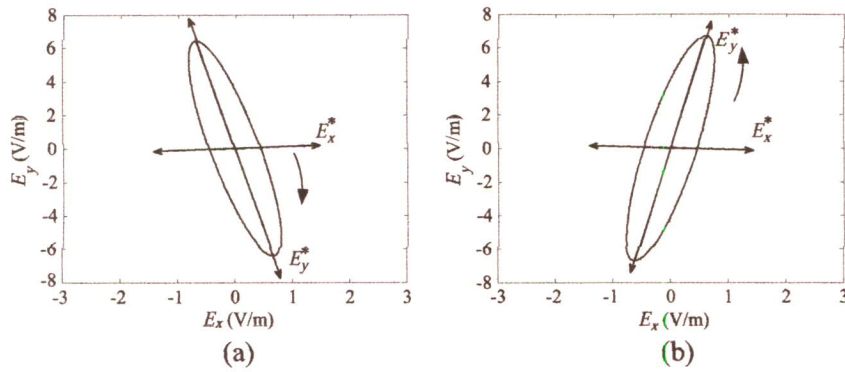| Positions	E_x		E_y		θ (°)	$\sin(\theta)$	Rotation angle	Polarization Configuration
	A_1 (V/m)	θ_1 (°)	A_2 (V/m)	θ_2 (°)				
P_1	0.80	129.50	6.41	−84.67	214.17	−0.56	5.92°	Left/Elliptical
P_2	0.77	−118.58	6.70	−156.08	37.23	0.61	−5.25°	Right/Elliptical

Figure 7. Left- and right-elliptical polarization at point (a) P_1 and (b) P_2 at 1.94 GHz.

4. CONCLUSIONS

Simple three-dimensional artificial triple helices are designed to generate circular birefringence with low loss in microwave regimes. High chirality is found within the transmission bandwidth where low loss transmission of RCP and LCP excitation waves propagate through triple helix stacks with a different refractive index. At 1.94 GHz, a wide splitting angle of 58.79° from the RCP wave with $n_+ = 3.69$ and from the LCP wave with $n_- = -2.97$ is obtained. The measurement results confirm the simulation results. The results of the wedge structure also support this design.

ACKNOWLEDGMENT

REFERENCES

1. Lakhtakia, A., V. K. Varadan, and V. V. Varadan, *Lecture Note in Physics: Time-harmonic Electromagnetic Fields in Chiral Media*, Springer, Heidelberg, Berlin, 1989.

2. Xia, Y., Y. Zhoua, and Z. Tang, "Chiral inorganic nanoparticles:

Origin, optical properties and bioapplications," *Nanoscale*, Vol. 3, 1374–1382, 2011.

3. Lindell, I. V., A. H. Sihvola, S. A. Tretyakov, and A. J. Viitanen, *Electromagnetic Waves in Chiral and Bi-isotropic Media*, Artech House Publishers, Boston, MA, 1994.

4. Wongkasem, N. and A. Akyurtlu, "Light splitting effects in chiral metamaterials," *J. Opt.*, Vol. 12, 035101, 2010.

5. Sonsilphong, A. and N. Wongkasem, "Novel technique for high refractive index manifestation," *International Conference on Electromagnetics in Advanced Applications*, 536–539, 2011.

6. Wongkasem, N., A. Akyurtlu, J. Li, A. Tibolt, Z. Kang, and W. D. Goodhue, "Novel broadband terahertz negative refractive index metamaterials: Analysis and experiment," *Progress In Electromagnetics Research*, Vol. 64, 205–218, 2006.

7. Gansel, J. K., M. Thiel, M. S. Rill, M. Decker, K. Bade, V. Saile, G. V. Freymann, S. Linden, and M. Wegener, "Gold helix photonic metamaterial as broadband circular polarizer," *Science* Vol. 325, 1513, 2009.

8. Gansel, J. K., M. Wegener, S. Burger, and S. Linden, "Gold helix photonic metamaterials: A numerical parameter study," *Optics Express*, Vol. 18, 1059, 2010.

9. Yang, Z. Y., M. Zhao, P. X. Lu, and Y. F. Lu, "Ultrabroadband optical circular polarizers consisting of double-helical nanowire structures," *Optics Letters*, Vol. 35, 2588–2590, 2010.

10. Yang, Z. Y., M. Zhao, and P. X. Lu, "How to improve the signal-to-noise ratio for circular polarizers consisting of helical metamaterials?" *Optics Express*, Vol. 19, 4255–4260, 2011.

11. Ma, X., C. Huang, M. Pu, C. Hu, Q. Feng, and X. Luo, "Multi-band circular polarizer using planar spiral metamaterial structure," *Optics Express*, Vol. 20, 16050–16058, 2012.

12. Ma, X., C. Huang, M. Pu, Y. Wang, Z. Zhao, C. Wang, and X. Luo, "Dual-band asymmetry chiral metamaterial based on planar spiral structure," *Appl. Phys. Lett.*, Vol. 101, 161901, 2012.

13. Wang, B., T. Koschny, and C. M. Soukoulis, "Wide-angle and polarization independent chiral metamaterials absorbers," *Phys. Rev. B.*, Vol. 80, 033108, 2009.

14. Plum, E., J. Zhou, J. Dong, V. A. Fedotov, T. Koschny, C. M. Soukoulis, and N. I. Zheludev, "Metamaterial with negative index due to chirality," *Phys. Rev. B*, Vol. 79, 035407, 2009.

15. Zhou, J., J. Dong, B. Wang, T. Koschny, M. Kafesaki, and C. M. Soukoulis, "Negative refractive index due to chirality," *Phys.*

Rev. B, Vol. 79, 121104(R), 2009.

16. Li, Z., R. Zhao, T. Koschny, M. Kafesaki, K. B. Alici, E. Colak, H. Caglayan, E. Ozbay, and C. M. Soukoulis, "Chiral metamaterials with negative refractive index based on four 'U' split ring resonators," *Appl. Phys. Lett.*, Vol. 97, 081901, 2010.

17. Zhao, R., L. Zhang, J. Zhou, T. Koschny, and C. M. Soukoulis, "Conjugated gammadion chiral metamaterial with uniaxial optical activity and negative refractive index," *Phys. Rev. B*, Vol. 83, 035105, 2011.

18. Wang, B., J. Zhou, T. Koschny, and C. M. Soukoulis, "Nonplanar chiral metamaterials with negative index," *Appl. Phys. Lett.*, Vol. 94, 151112, 2009.

19. Wongkasem, N., C. Kamtongdee, A. Akyurtlu, and K. Marx, "Artificial multiple helices: EM and polarization properties," *J. Opt.*, Vol. 12, 075102, 2010.

20. Sonsilphong, A. and N. Wongkasem, "Three-dimensional artificial double helices with high negative refractive index," *J. Opt.*, Vol. 14, 105103, 2012.

21. Raos, G., "Degrees of chirality in helical structures," *Macromol. Theory Simul.*, Vol. 11, 739–750, 2002.

22. Green, M. M., N. C. Peterson, T. Sato, A. Teramoto, R. Cook, and S. Lifson, "A helical polymer with a cooperative response to chiral information," *Science*, Vol. 268, 1860–1866, 1995.

23. Sonsilphong, A. and N. Wongkasem, "Transmission properties in chiral metamaterials," *International Journal of Physical Sciences*, Vol. 7, No. 21, 2829–2837, 2012.

24. CST Microwave Studio: http://www.cst.com/.

25. Wang, B., J. Zhou, T. Koschny, M. Kafesaki, and C. M. Soukoulis, "Chiral metamaterials: Simulations and experiments," *J. Opt. A: Pure Appl. Opt.*, Vol. 11, 114003, 2009.

26. Ranga, Y., L. Matekovits, K. P. Esselle, and A. R. Weily, "Multi-octave frequency selective surface reflector for ultrawideband antennas," *IEEE Antennas and Wireless Propagat. Letters*, Vol. 10, 219–222, 2011.

27. Balanis, C. A., *Advanced Engineering Electromagnetic*, John Wiley & Sons, 1989.

28. Orfanidis, S. J., "Electromagnetic waves and antennas," Online *URL: http://www.ece.rutgers.edu/~orfanidi/ewa/*.

29. "IEEE standard definitions of terms for antennas," IEEE Std 145-1983, Revised IEEE Std 145-1993, 1993.

บทความตีพิมพ์ในวารสารวิชาการระดับนานาชาติ

ก3.   Sonsilphong and **N. Wongkasem**, "Three-dimensional artificial double helices with high negative refractive index," *Journal of Optics* **14** 105103, September 2012. **(IF 1.990)**

Three-dimensional artificial double helices with high negative refractive index

A Sonsilphong and N Wongkasem

Metasolver Laboratory, Department of Electrical Engineering, Faculty of Engineering, Khon Kaen University, Khon Kaen, 40002, Thailand

E-mail: nantakan@kku.ac.th

Abstract

Chirality can be manipulated in multilayer three-dimensional helices. Multiple backbone helices can be effectively designed and fabricated, preserving their unique electromagnetic properties of chiral metamaterials. Chirality is boosted in double helices. The chirality index is four times higher than in single helices. Based on the extreme chirality, the effective refractive index of the 3D double helices is proved to be negative, with low loss.

Keywords: metamaterials, chirality, helices, negative refractive index

(Some figures may appear in colour only in the online journal)

1. Introduction

Chiral metamaterials (CMMs) are some of the most promising electromagnetic artificial materials, with an important function in wave control, e.g. negative refraction [1], light splitting [2], focusing lenses [3], and Casimir forces [4, 5], to name a few. Two particular electromagnetic (EM) properties of chiral media are optical rotary dispersion (ORD) or optical activity, and circular dichroism (CD). ORD controls the EM polarization of the two splitting waves, with different phase velocity, propagating inside CMMs. The two waves have opposite polarization: left-circular polarization (LCP) and right-circular polarization (RCP). CD features the effect of the absorption of electromagnetic waves traveling through CMMs. Any arbitrary polarization is therefore transformed to elliptical polarization. These properties are essential for applications using polarization control. With the condition $|\kappa^R| > (\sqrt{\varepsilon_r \mu_r})^R$, as the chirality, κ, is higher, the separated LCP and RCP waves will certainly have opposite signs of refractive index, n, and therefore negative refractive index [2]. It is important to stress that the effective index of refraction of chiral media is determined by the indices of the two eigenmodes inside the media, which are the refractive indices of LCP and RCP, n_+, n_-, meaning that the wave with a larger index is dominant. Several chiral structures, such as bilayer and multilayer chiral metamaterials [6–9], Swiss rolls [10,

11], non-planar chiral SRRs [12], and chiral resonators [13], with strong optical activity and negative refractive index have been studied in microwave and optical regimes.

Helices, known as one of the most promising three-dimensional (3D) chiral structures, have been fabricated with the intention of being used as a compact broadband circular polarizer [14, 15]. Low-loss ultrabroadband circular polarizers consisting of double-helical structures were also proposed in the visible regime [16]. Multiple helical metamaterials have been intensively studied to construct circular polarizers with high signal-to-noise ratio [17], as well as negative refractive index [18]. The chirality is larger as the number of backbones or helical wires of multiple helices increases [19]. Hence, helical structures can exhibit a very large chirality index, which has a significant impact on the EM properties of the structures, especially refractive index. In this paper, we propose 3D artificial single and double helix structures formed in a stack of planar patterns. These chiral structures are designed based on conventional 3D helices. The one pitch conventional and the proposed 3D planar single and double helices are illustrated in figure 1.

The chirality index of 3D planar single and double helices is observed to depend on orientation and geometrical parameters: helix pitch, radius of ring, line width, and coupling length. The unit cell size of the studied structures is less than $\lambda/8$, confirming the homogeneous properties. n, n_+,
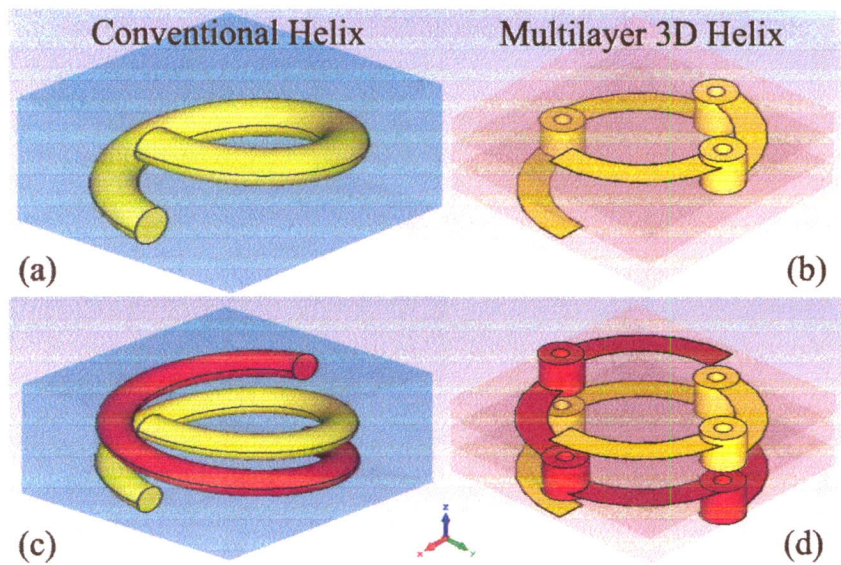
Figure 1. (a) Conventional and (b) 3D planar single helices. (c) Conventional and (d) 3D planar double helices.
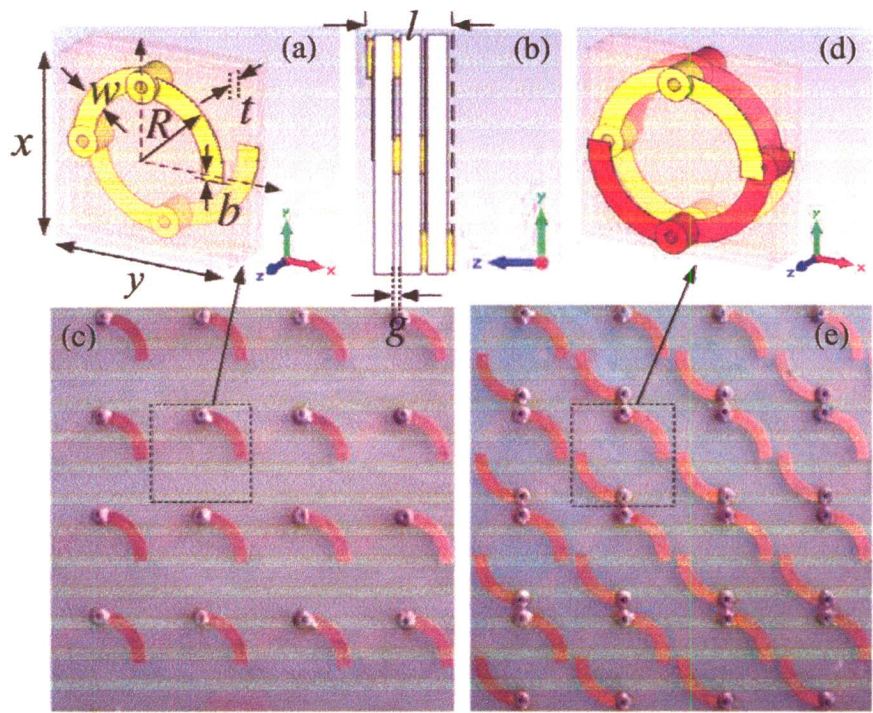

Figure 2. Unit cell of the 3D planar single helix in (a) perspective and (b) side view, and (c) a photograph of the fabricated sample. (d) Unit cell of the 3D planar double helix and (e) a photograph of the fabricated 3D planar double helices. The geometrical parameters of the two structures are: $x = y = 18.75$ mm, $w = 2.25$ mm, $l = 6.94$ mm, $g = 0.535$ mm, $b = 0.5$ mm, $R = 8.75$ mm, and $t = 1.6$ mm.

n_-, and the loss factor (LF) will be investigated as well. At their operating frequency, both 3D planar single and double helices can filter out one of the circularly polarized waves, indicating the handedness of chiral media, i.e. the polarized wave with the same handedness type as that of the helices can propagate through the structure stack. The 3D planar double helices also generate a strong negative refraction and modifiable chirality with an impressively low loss. Both types of structure are fabricated and then measured to validate the EM properties.

2. Three-dimensional artificial helices

The schematics of 3D planar single and double helix chiral metamaterials are shown in figure 2. Both structures are fabricated on FR-4 boards. The dielectric constant of the FR-4 board is $\varepsilon = 4.3 + 0.23i$. The thickness of copper is 0.03 mm. CST Microwave Studio [20], which is based on the finite integration technique (FIT), is used to determine the reflection and transmission coefficients. Tetrahedral meshing is set in a frequency domain solver operating from 1.5 to 4.0 GHz.
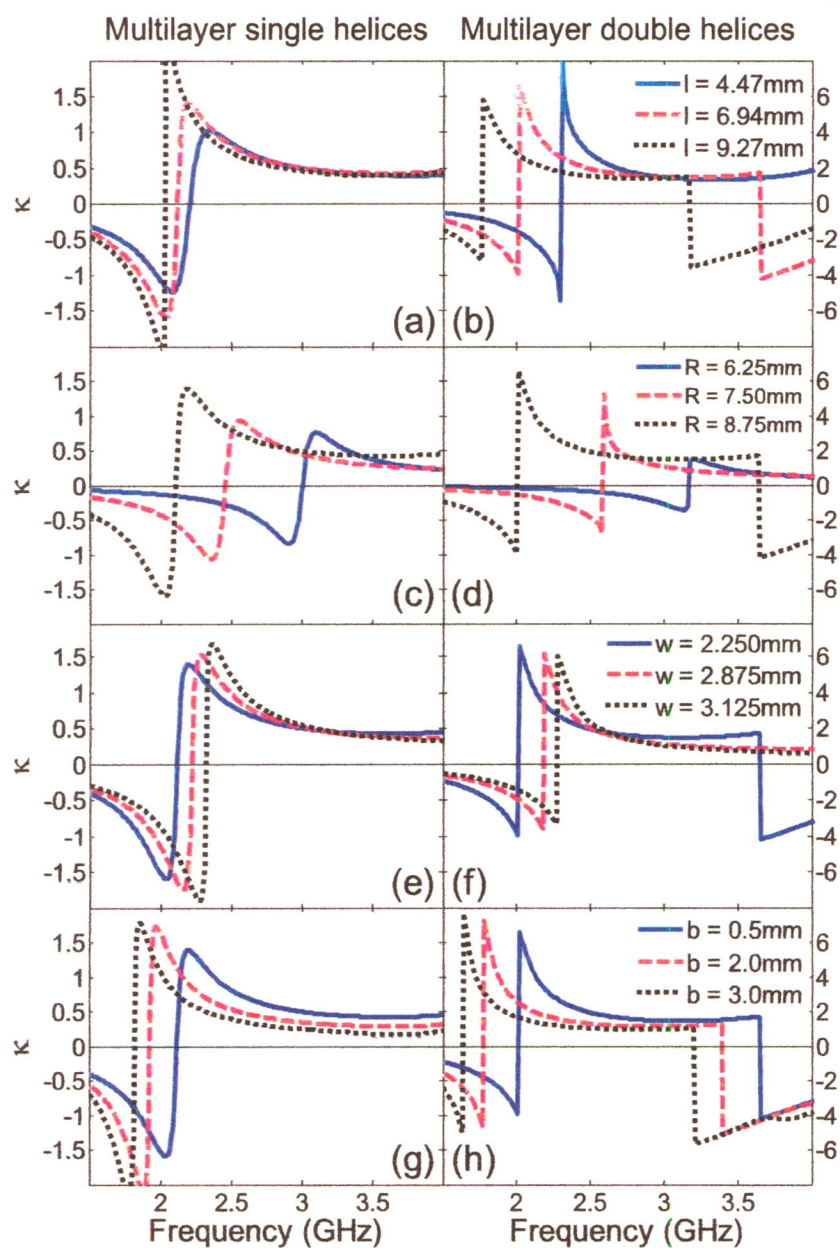
Figure 3. Chirality study when (a) and (b) helix pitch, (c) and (d) helix radius, (e) and (f) line width, and (g) and (h) coupling length of 3D planar single and double helices are varied.

The unit cell boundary condition of CST dictates the periodic orientation of the helices on the surface plane. The helix unit lattice is 18.75 mm × 18.75 mm × 6.94 mm. The right- and left-circularly polarized waves are excited along the $-z$ direction. Transmission and reflection coefficients obtained from the simulations are then used to retrieve other EM parameters [21].

Exactly the same material parameters and orientations used in fabricated helices are implemented throughout these EM full-wave simulations. The ring with R radius is split into four equal parts. An array of each part is then printed on each layer. The quarter rings of each layer are connected with the quarter rings of the adjacent layer through the created holes, as shown in figures 1(b) and (d). The diameters of the outer and inner hole are 3.25 and 1.25 mm respectively. Three FR4 substrates are used to complete a stack of arrays

of one pitch single helices. Figures 2(a) and (b) illustrate the unit cell of a 3D planar single helix in a perspective view and side view. Similarly, the 3D planar double helices are designed by adding another array of quarter rings on the same layer. The two quarter ring sets are placed opposite each other, or 180° apart (darker color), as illustrated in figure 2(d). To complete a helix pitch, these double helices also require four layers printed on three substrates. The 3D planar single and double helices are manufactured with 10 × 10 unit cells. Some fabricated parts of the first layer are shown in figures 2(c) and (e), where the dashed square indicates a unit cell of each helix. Note that to obtain multiple 'n' backbone helices [18], there will be unconnected identical 'n' parts printed on each layer. Furthermore, the number of helix pitches can be increased by adding extra sets of multilayer stacks.
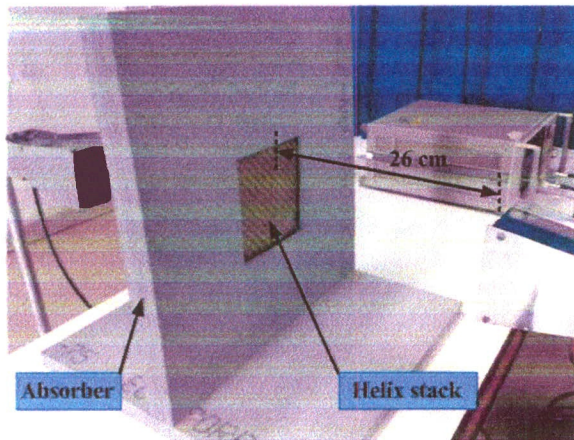
Figure 4. Helix stack with transmitter and receiver horns for the experimental measurement system.

The real part of the chirality of 3D planar single and double helices is investigated with respect to several physical parameters, i.e. substrate thickness or helix pitch, l, ring radius or helix radius, R, line width, w, and coupling length, b. Because of the extra backbone, the phase difference between the RCP and LCP wave of the double helices is more prominent than that of single helices; therefore, the chirality index, κ, of the double helices is larger than κ of the single helices. As illustrated in figure 3, κ of the double helices in all cases is approximately four times greater than in single helices. Figures 3(a) and (b) present a study of the chirality index based on the helix pitch. Other parameters are fixed as discussed previously in figure 2. As the helix pitch is wider, the resonance position shifts to a lower frequency, and κ increases. This is true for single and double helices and also matches the results from conventional 3D helices [15, 18]. Based on the two backbones of the double helices, there are two resonances generated within the frequency regimes of interest.

The effects of R on the chirality index are presented in figures 3(c) and (d). As the helix radius increases, the chirality index increases and shifts to a lower frequency. In figures 3(e) and (f), w is varied. In contrast with other cases, the chirality shifts to a higher frequency as the linewidth is wider. Lastly, the coupling length is studied. The results are shown in figures 3(g) and (h) for multilayer single and double helices, respectively. When the coupling length increases, the index resonance also increases and shifts to a lower frequency. The simulation results, focusing particularly on the chirality index, have proved that these 3D planar helices can provide the same EM properties as those from conventional 3D helices [15, 18]. Sets of 3D planar helices are fabricated and measured to further investigate the EM properties.

The reflection and transmission coefficients of the fabricated helix stack are measured by a vector network analyzer (HP8753D). Horn antennas are used as transmitting and receiving ports, as shown in the experimental setup illustrated in figure 4. The transmitter and receiver horns have 13 cm × 13 cm diagonal mounts, with 50° 3 dB beam width at 2.0 GHz. The far-field range of horn antennas

starts from 22.53 cm. The transmission distance from the horn to the front of the helix stack, as well as the receive distance from that same point to the receiver horn, are set equally at 26.0 cm, which satisfies the far-field condition. From this setup, one can also conclude that the input wave is approximately a planar wave. The vertical linear polarization waves are launched from the transmitter horn antenna through the helix stack and are then collected by the receiver horn in vertical and horizontal directions with a frequency step of 0.0125 GHz, from 1.5 to 4.0 GHz. The reflection and transmission coefficients of the RCP and LCP wave can be achieved by converting linear cross- and co-polarization data [21]. The absorbers ECCOSORB®AN are used to eliminate the unwanted scattering and reflected waves; therefore the measurement data is only achieved by the interaction between the propagated waves and the helix stack. Figures 5(a) and (b) show the transmission coefficients of the RCP and LCP wave, T_+ and T_-, of the 3D planar single helices.

Within the operating frequency, the transmission amplitudes of the RCP and LCP waves are different, similar to those of conventional single 3D helices [15, 18], as well as other well-known chiral metamaterial structures [6, 7, 9]. A resonance dip is found in the LCP wave (T_-) located respectively at 2.11 GHz (simulation) and 2.38 GHz (measurement), as presented in figures 5(a) and (b). On the other hand, the transmission coefficient of the RCP wave (T_+) in the same frequency location generates a fair passband. This means that while the LCP wave is almost entirely blocked, the RCP wave can propagate through the helix stack. Due to the phase difference between the RCP and LCP wave, the refractive indices of the RCP and LCP wave are generated, confirming the chirality occurrence [22]. The simulated and measured phase of the RCP and LCP wave, and their refractive index and chirality are illustrated in figures 5(c) and (d) and figures 5(e) and (f), respectively. The results from the simulations and measurements are in good agreement in terms of both location and value. The effective loss factor, $LF = |Im(n)/Re(n)|$, and the loss factor of RCP and LCP, $LF_\pm = |Im(n_\pm)/Re(n_\pm)|$, are observed. κ (black dashed dotted line) in figures 5(e) and (f) is in the range from -2 to 2. Negative refraction is found in the LCP wave, n_- (red dashed line), around the chirality peak, while n_+ (blue solid line) is positive. At 2.1 GHz, LF_+ is significantly lower (<0.3), as presented in figure 5(g), while LF_- is high (>1.0). Therefore, this media can block the LCP wave.

Figures 6(a) and (b) present the transmission coefficients of the 3D double helices. The LCP resonance dip location obtained from the simulation (2.04 GHz) and measurement (2.05 GHz) is slightly different. Similar to the single helices, the RCP wave can propagate through these right-handed double helices, while the LCP wave is truncated. Hence, if the LCP wave is desired instead of the RCP wave, it can be accomplished by reversing the helix orientation into a left-handed format. The difference between the transmission phase of the RCP and LCP wave is significant; therefore κ is greater [22] than in single helices. The transmission phases of the LCP and RCP are shown in figures 6(c) and
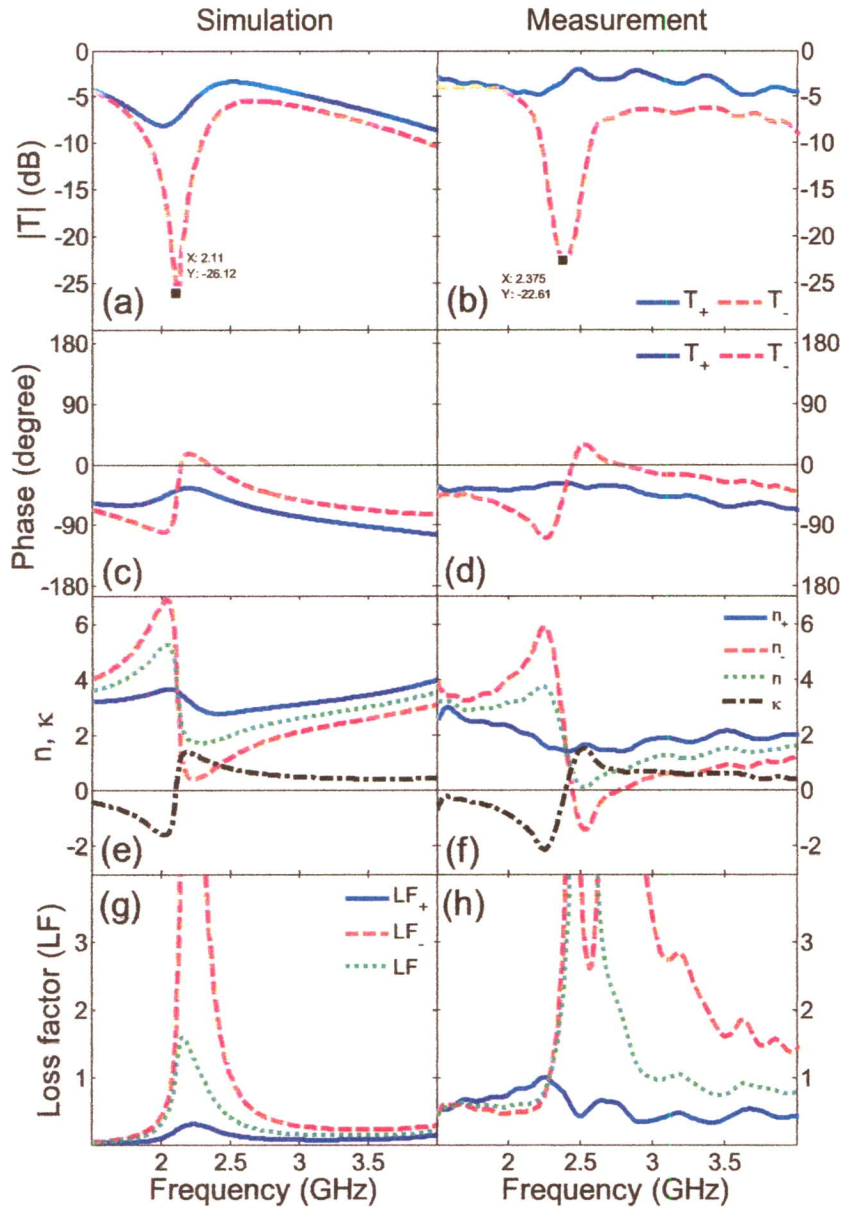
Figure 5. Simulation and experiment results of 3D planar single helices: (a) and (b) transmission amplitude, (c) and (d) transmission phase from the RCP and LCP excitation wave, (e) and (f) refractive and chirality index, and (g) and (h) loss factor of the RCP, LCP wave and of the average value.

(d). n, n_+, n_- and κ are illustrated in figures 6(e) and (f). The results from the simulation and measurement show the same overall tendency. In the frequency region from 2.0 to 2.4 GHz (measurement), n_- (red dashed line) is negative, while n_+ (blue solid line) and κ (black dashed dotted line) are positive. It is important to state that at the LCP resonance dip the negative index peak from the LCP wave is significantly high ($n_- = -9.91$, measurement) compared to the positive index peak of the RCP wave ($n_+ = +1.01$, measurement). Hence, the effective or average refractive index is negative with a high value ($n = -4.45$, measurement). Note that it is rare for the effective refractive index of chiral metamaterials to be negative [23]. The LF is shown in figure 6(g), with LF_+ being less than 0.3, and LF_- higher (>1.0).

3. Conclusions

Simple 3D planar single and double helices are proposed. The chirality index of the two types of helices can be controlled by adjusting the structure orientation. Their electromagnetic properties are similar to those of the conventional helices. Due to their strong optical activity, the effective refractive index of 3D planar double helices is found to be negative. The simulation results are in good agreement with the measurement results.
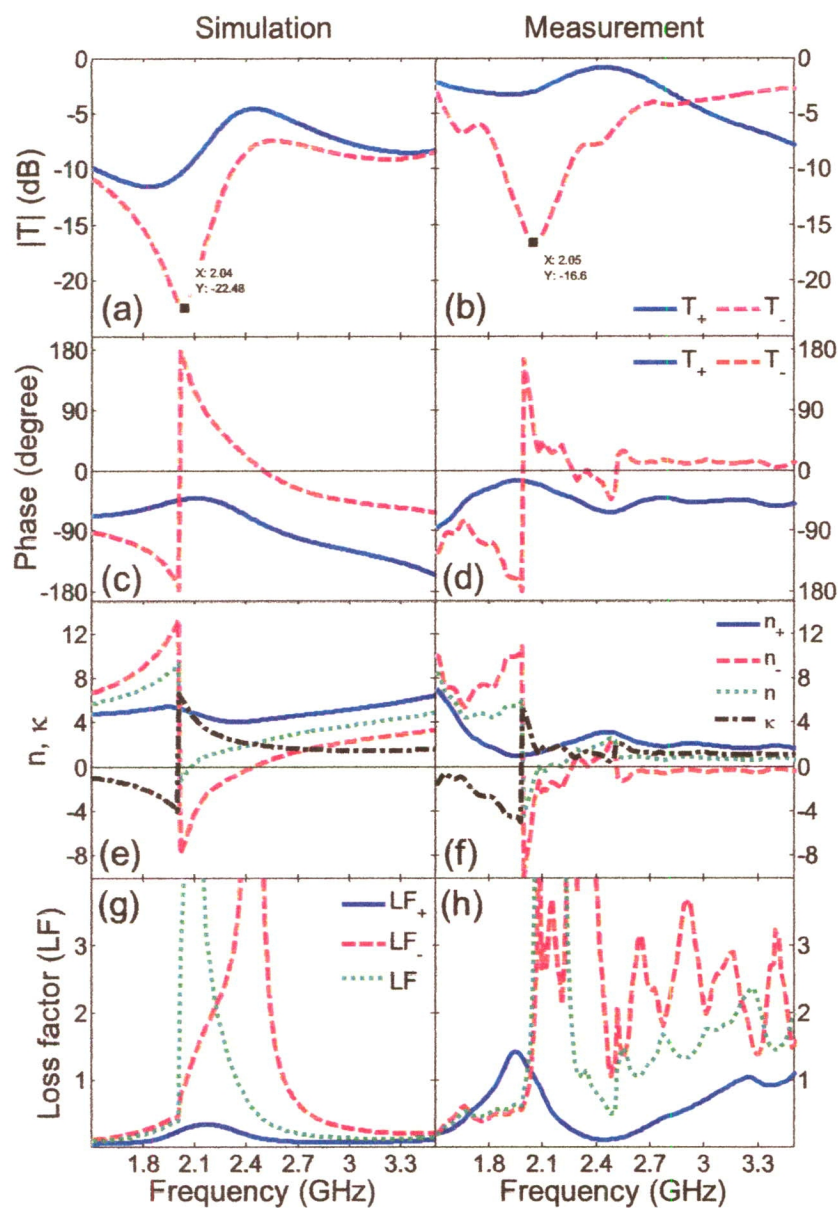
Acknowledgments

Figure 6. Simulation and experimental results of 3D planar double helices: (a) and (b) transmission amplitude, (c) and (d) transmission phase of the RCP and LCP wave. (e) and (f) refractive and chirality index, and (g) and (h) loss factor of the RCP, LCP wave and of the average value.

References

[1] Pendry J B 2004 A chiral route to negative refraction *Science* **306** 1353–5

[2] Wongkasem N and Akyurtlu A 2010 Light splitting effects in chiral metamaterials *J. Opt.* **12** 035101

[3] Jin Y and He S 2005 Focusing by a slab of chiral medium *Opt. Express* **13** 4974–9

[4] Zhao R, Koschny Th, Economou E N and Soukoulos C M 2010 Comparison of chiral metamaterial designs for repulsive Casimir force *Phys. Rev.* B **81** 235126

[5] McCauley A P, Zhao R, Homer Reid M T, Rodriguez A W, Zhou J, Rosa F S S, Joannopoulos J D, Dalvit D A R, Soukoulis C M and Johnson S G 2010 Microstructure effects for Casimir forces in chiral metamaterials *Phys. Rev.* B **82** 165108

[6] Plum E, Zhou J, Dong J, Fedotov V A, Koschny Th, Soukoulis C M and Zheludev N I 2009 Metamaterial with negative index due to chirality *Phys. Rev.* B **79** 035407

[7] Zhou J, Dong J, Wang B, Koschny T, Kafesaki M and Soukoulis C M 2009 Negative refractive index due to chirality *Phys. Rev.* B **79** 121104(R)

[8] Li Z, Zhao R, Koschny Th, Kafesaki M, Alici K B, Colak E, Caglayan H, Ozbay E and Soukoulis C M 2010 Chiral metamaterials with negative refractive index based on four 'U' split ring resonators *Appl. Phys. Lett.* **97** 081901

[9] Zhao R, Zhang L, Zhou J, Koschny Th and Soukoulis C M 2011 Conjugated gammadion chiral metamaterial with

uniaxial optical activity and negative refractive index *Phys. Rev.* B **83** 035105

[10] Wiltshire M C K, Pendry J B and Hajnal J V 2009 Chiral Swiss rolls show a negative refractive index *J. Phys.: Condens. Matter* **21** 292201

[11] Demetriadou A and Pendry J B 2009 Extreme chirality in Swiss roll metamaterials *J. Phys.: Condens. Matter* **21** 376003

[12] Wang B, Zhou J, Koschny T and Soukoulis C M 2009 Nonplanar chiral metamaterials with negative index *Appl. Phys. Lett.* **94** 151112

[13] Zhang S, Park Y S, Li J, Lu X, Zhang W and Zhang X 2009 Negative refractive index in chiral metamaterials *Phys. Rev. Lett.* **102** 023901

[14] Gansel J K, Thiel M, Rill M S, Decker M, Bade K, Saile V, Freymann G V, Linden S and Wegener M 2009 Gold helix photonic metamaterial as broadband circular polarizer *Science* **325** 1513

[15] Gansel J K, Wegener M, Burger S and Linden S 2010 Gold helix photonic metamaterials: a numerical parameter study *Opt. Express* **18** 1059

[16] Yang Z Y, Zhao M, Lu P X and Lu Y F 2010 Ultrabroadband optical circular polarizers consisting of double-helical nanowire structures *Opt. Lett.* **35** 2588–90

[17] Yang Z Y, Zhao M and Lu P X 2011 How to improve the signal-to-noise ratio for circular polarizers consisting of helical metamaterials? *Opt. Express* **19** 4255–60

[18] Wongkasem N, Kamtongdee C, Akyurtlu A and Marx K 2010 Artificial multiple helices: EM and polarization properties *J. Opt.* **12** 075102

[19] Green M M, Peterson N C, Sato T, Teramoto A, Cook R and Lifson S 1995 A helical polymer with a cooperative response to chiral information *Science* **268** 1860–6

[20] CST Microwave Studio: http://www.cst.com/

[21] Wang B, Zhou J, Koschny T, Kafesaki M and Soukoulis C M 2009 Chiral metamaterials: simulations and experiments *J. Opt. A: Pure Appl. Opt.* **11** 114003

[22] Sonsilphong A and Wongkasem N 2012 Transmission properties in chiral metamaterials *Int. J. Phys. Sci.* **7** 2829–37

[23] Panpradit W, Sonsilphong A, Soemphol C and Wongkasem N 2012 High negative refractive index in chiral metamaterials *J. Opt.* **14** 075101

บทความตีพิมพ์ในวารสารวิชาการระดับนานาชาติ

ก4.   W. Panpradit, A. Sonsilphong, C. Soemphol and **N. Wongkasem**, "High Negative Refractive Index Chiral Metamaterials," *Journal of Optics* **14** 075101, July 2012. **(IF 1.990)**

High negative refractive index in chiral metamaterials

W Panpradit, A Sonsilphong, C Soemphol and N Wongkasem

Metasolver Laboratory, Department of Electrical Engineering, Faculty of Engineering,
Khon Kaen University, Khon Kaen, 40002, Thailand

E-mail: nantakan@kku.ac.th

Abstract

Conjugated bi-layer C_8 metamaterials are proposed. Chirality and refractive index can be
controlled effectively by the structure geometry. Extreme chirality results in a high negative
refractive index for both right- and left-circular polarized excitations. The conjugated bi-layer
C_8 structures are fabricated and tested in microwave regimes. The measurement results are in
good agreement with the simulation results. These proposed structures are additional
promising candidates for high negative refractive index metamaterials which will facilitate
different applications.

Keywords: chiral, negative refractive index, metamaterials

(Some figures may appear in colour only in the online journal)

1. Introduction

Due to optical rotary dispersion (ORD) or optical activity,
as an electromagnetic (EM) wave propagates through lossy
chiral materials, the wave splits into two waves with different
phase velocities, refractive indices and different direction of
rotation, defined as left- and right-circular polarization (LCP
and RCP). The two circularly polarized waves then combine
at the chiral-end and propagate out from the chiral media
as an elliptically polarized wave based on circular dichroism
(CD). These two important features in chiral materials
are advantageous in optoelectronic devices, specifically for
polarization control and spitting light applications [1].

Chirality (κ) found in bi-isotropic and bi-anisotropic
materials in the magnetoelectric coupling term [2–4] is
typically weak for natural chiral materials, e.g., for quartz,
$\kappa = 5 \times 10^{-5}$ at $\lambda = 400$ nm [5]. There have been efforts
to design chiral metamaterials in three-dimensional (3D) and
planar orientations [6–23] in order to control the chirality
index and obtain special EM properties, for instance, negative
refractive index [5, 9–11, 14–18] and broadband polarizers [7,
24]. Chirality is connected to the refractive index as follows:
$n_\pm = \sqrt{\varepsilon\mu} \pm \kappa$ and $\kappa = (n_+ + n_-)/2$ [18], where ()$_+$ and
()$_-$ signify parameters of RCP and LCP waves respectively.
High chirality leads to negative refractive index [25], as

well as high refractive index, both of which are essential in
several photonics applications, e.g. LEDs [26], lenses [27],
multiplexing or demultiplexing devices [28] and fast-neutron
spectrometry and imaging [29], to name but a few.

This paper discusses how to geometrically manipulate the
chirality and refractive index in chiral metamaterial structures,
by focusing on the conjugated bi-layer C_8 structures [14,
21], based on their well-defined chiral properties [22], as
well as their easily adjustable orientations. The orientation
parameters consist of two main parts, being the direction of
the arms and the twist angle, to establish two study cases,
A and *B*. Three geometric parameters, i.e. the twist angle
between the structures on each layer, the ratio between the
main axis and the arm, and the angle between the main axis
and the connected arm are studied. These parameters are
observed to investigate the transmission coefficients, as well
as the chirality and refractive indices. High negative refractive
index conjugated bi-layer C_8 structures with low loss are
fabricated and measured to confirm the design concept.

2. Chirality control in C_n metamaterials

The C_8 structure, shown in figure 1, is selected to investigate
the EM parameters. The transmission properties are first
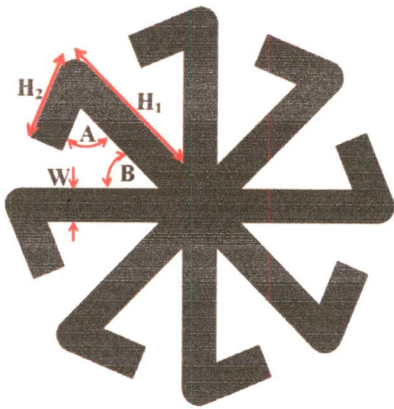obtained by CST Microwave Studio® and then used to

Figure 1. C_8 structure.

Figure 3. Case *A* of the conjugated bi-layer C_8 structures where the angle φ between the two structures is twisted.

extract the chirality and refractive index [15, 18, 19, 22]. The geometrical parameters are also illustrated, where H_1 and H_2, respectively, are the main axis and the arm of the structure. w is the linewidth, $A°$ is the angle between the main axis and the connected arms, and $B°$ is the angle between the adjacent main axis.

Two conjugated bi-layer formats of C_8 structures, shown in figure 2, are selected to investigate the electromagnetic properties, with regard to their well-defined chiral orientation. It is important to stress that the retrieval procedures [15, 18, 19, 22] can only apply in purely chiral structures, where the cross transmission coefficients (T_{+-} and T_{-+}), as well as the reflection coefficients (R_{--} and R_{++}), must be identical [22]. Case *A*, shown in figure 2(a), presents twisted structures with an angle φ, where the arms of each structure lie in opposite direction as 'the mirror' twisted layout. The two structures are located on top of each other, with a substrate inserted in between. In case *B*, illustrated in figure 2(b), the two structures with opposite arms are placed on top of each other; therefore, there is no twist angle. The bi-layer structures in both cases are set using a periodic boundary. The Propagation direction, $\vec{k}$, electric field, $\vec{E}$, and magnetic field, $\vec{H}$, are
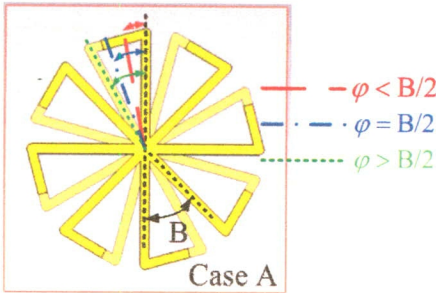
referenced in both cases. A double copper-clad Arlon Di 880 board is used as a substrate in all simulations. The dielectric constant of the substrate board, ε_r, is 2.2, with a dielectric loss tangent of 0.0001. The dimension parameters are given as follows: $a_x = a_y = 37$ mm, $w = 2.8$ mm, $H_1 = 15.7$ mm, $s = 0.254$ mm and $B = 360°/n$. The copper thickness, t_m, is 0.03 mm. These parameters are used in all studies. Based on the broken symmetry and therefore electromagnetic coupling, both conjugated bi-layer C_8 structures can generate chirality [21]. These formats are further investigated with respect to the twist angle (φ), the ratio between the main axis and the connected arm (H_1/H_2) and the angle between the main axis and arm (A). Chirality and refractive indices are both connected to the geometrical orientation of these C_8 structures.

2.1. The angle between two structures (twist angle: φ)

The transmission and reflection coefficients, refractive (n) and chirality (κ) indices of the conjugated bi-layer C_8 structures, where the angle φ between the two bi-layer structures is varied, are observed. The angle φ is adjusted by rotating the C_8 structure on the back side, as presented in figure 3. The three different twist angles are: $\varphi < B/2$, $\varphi = B/2$ and $\varphi > B/2$, where $B = 45°$. The dimension parameters are set
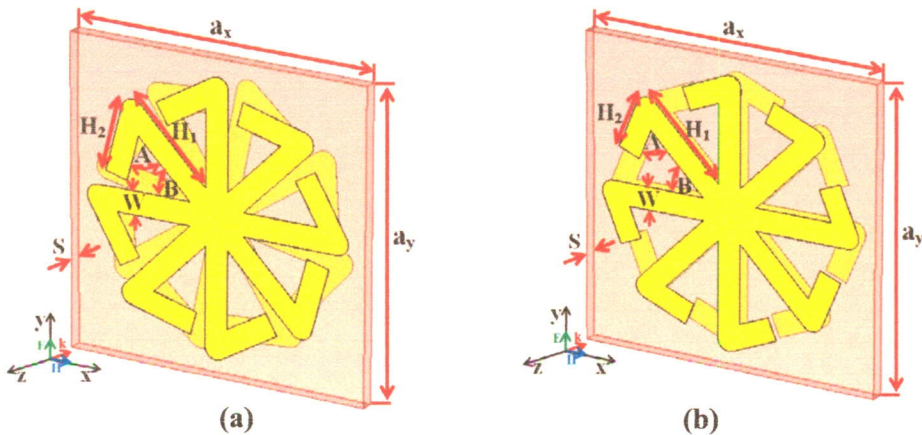

Figure 2. Two conjugated bi-layer formats of C_8 structures: (a) case *A*: twisted C_8 structures with opposite arm orientation and (b) case *B*: non-twisted C_8 structures with opposite arm orientation.
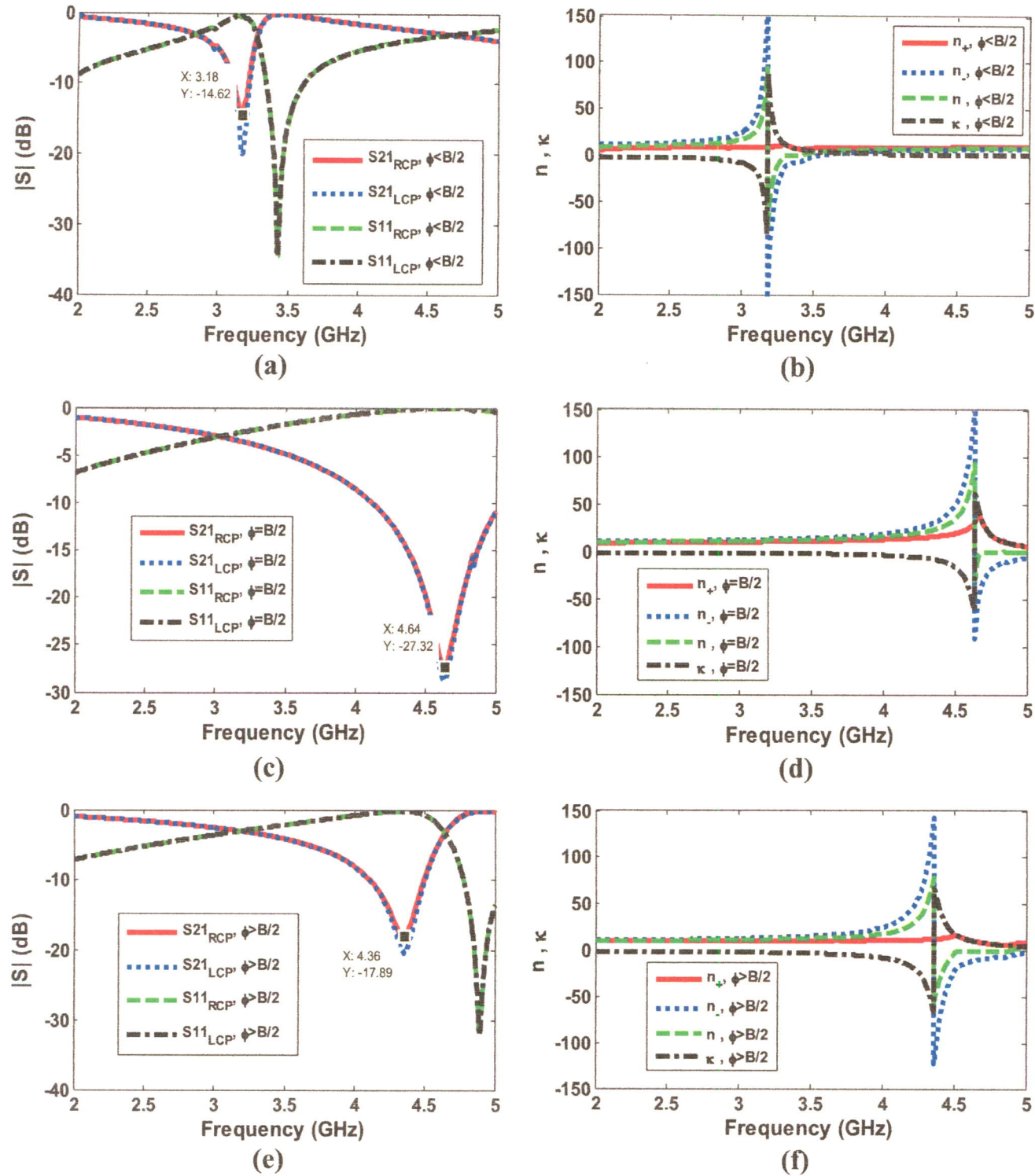
Figure 4. *S* parameters, refractive and chirality index of the conjugated bi-layer C$_8$ case *A*: (a), (b) $\varphi < B/2$, (c), (d) $\varphi = B/2$ and (e), (f) $\varphi > B/2$.

as $(H_1/H_2) = 2$ and $A = 60°$. Note that φ is always zero for case *B*. Therefore, in this study, the focus is only on case *A*.

Figure 4 illustrates *S* parameters, refractive and chirality index of the conjugated bi-layer C$_8$ structures case *A*. The transmission coefficients (S_{21}) of the RCP wave and LCP wave are different at the first or the dominant resonance at 3.18 GHz for $\varphi < B/2$, 4.64 GHz for $\varphi = B/2$, and 4.36 GHz for $\varphi > B/2$, as marked in figures 4(a), (c) and (e). These stress the occurrence of chirality presenting at the

same frequency. The refractive and chirality index are shown in figures 4(b), (d) and (f). The reflection coefficients of the RCP and LCP wave of each case of angle φ are alike. The small values of cross transmission coefficients (T_{+-} and T_{-+}) of each case are also identical (not shown in this paper). This proves that these conjugated bi-layer C$_8$ cases *A* have well-defined chirality. Based on the high chirality (-100 to $+100$), negative refractive indices are generated. The refractive index of the LCP wave (n_-) from all φ is
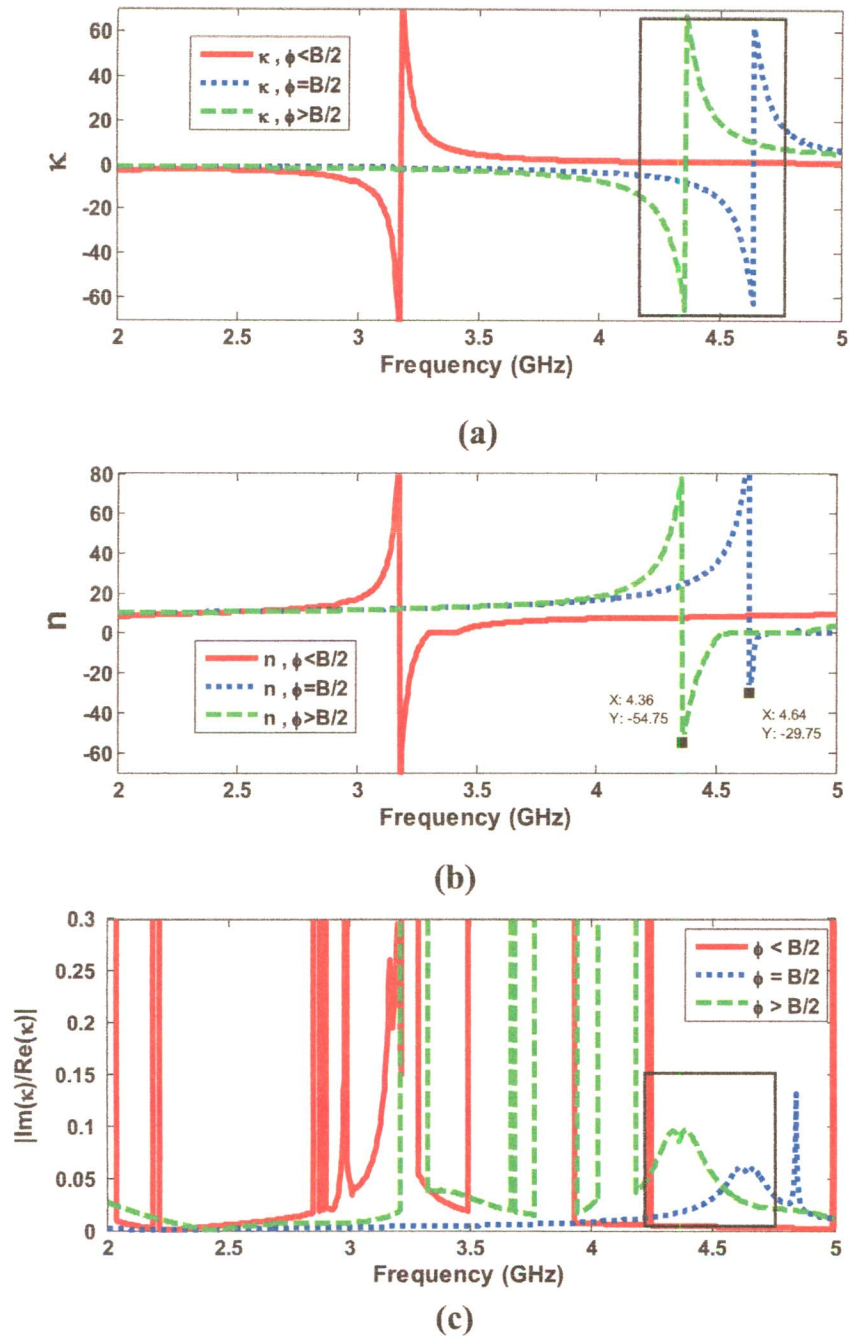
(a)

(b)

(c)

Figure 5. (a) Chirality index, (b) refractive index and (c) figure of merit of the conjugated bi-layer C_8 case A.

significantly high, resulting in a negative value of the effective or average refractive index (n).

The chirality and effective refractive indices, as well as their figure of merit ($\mathrm{Im}(\kappa)/\mathrm{Re}(\kappa)$) focusing on the negative refractive index, are shown in figure 5. A high negative index is generated at the chirality peak of the structure, which is $\varphi < B/2$ ($n = -70$ at 3.18 GHz), $\varphi = B/2$ ($n = -29.75$ at 4.64 GHz) and $\varphi > B/2$ ($n = -54.75$ at 4.36 GHz). It should be stated that the figure of merit of the structure, illustrated in figure 5(c), where $\varphi = B/2$ and $\varphi > B/2$, is significant low, less than 0.1, implying good transmission. These areas are surrounded by a square.
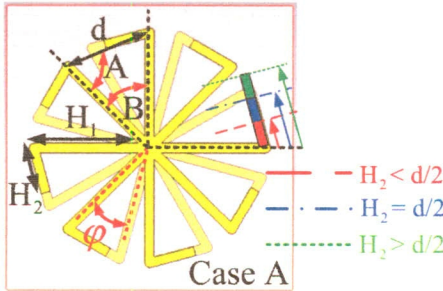

Figure 6. Case A of the conjugated bi-layer C_8 structures where the ratio of the main axis and the connected arm is varied.

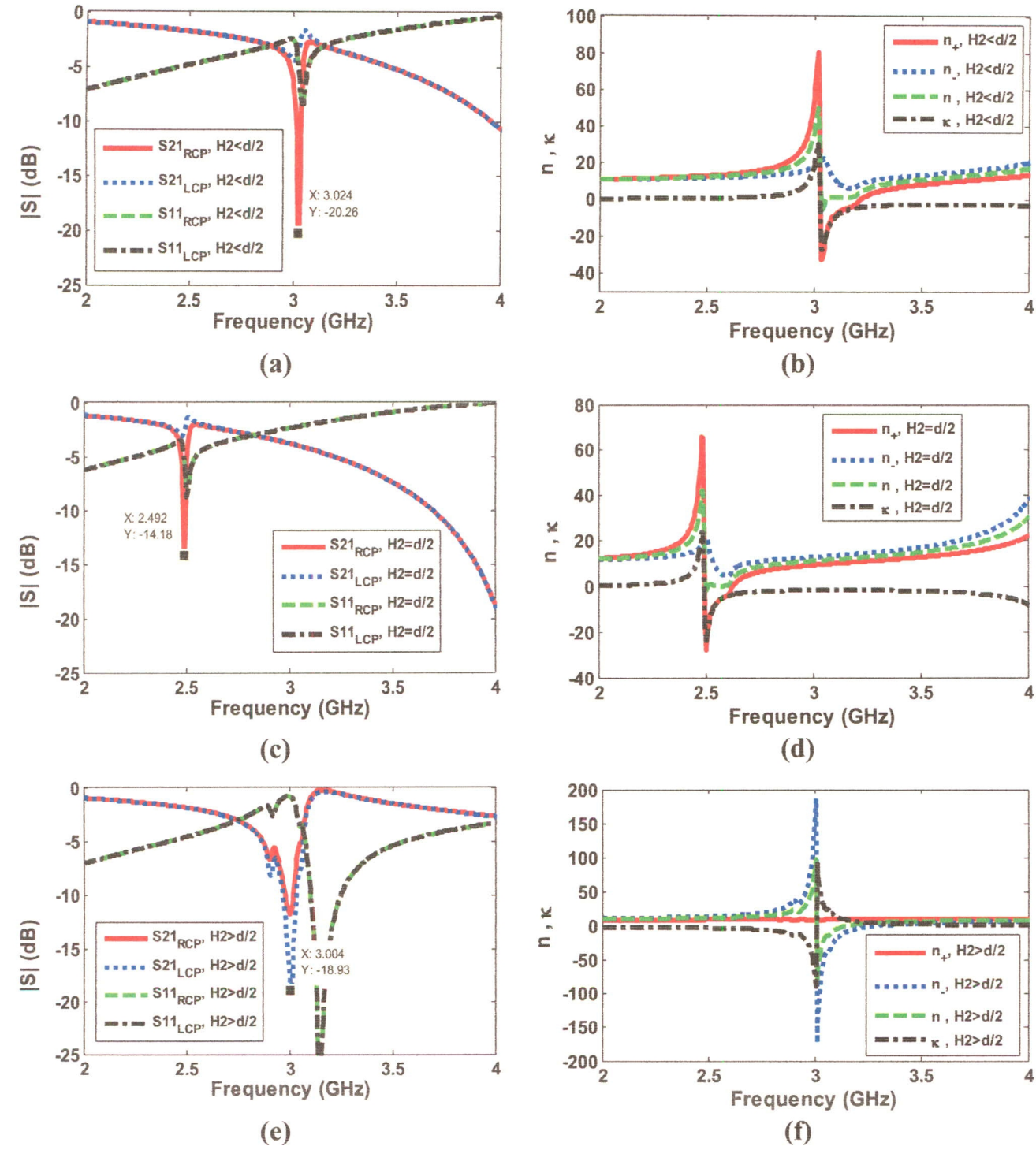**Figure 7.** S parameters, refractive and chirality index of the conjugated bi-layer C_8 case A: (a), (b) $H_2 < d/2$, (c), (d) $H_2 = d/2$ and (e), (f) $H_2 > d/2$.

2.2. Ratio of the main axis and the connected arm (H_1/H_2)

In this study, the main axis is fixed at 15.7 mm. The connected arm, H_2, is set with respect to the distance between the ends of the two adjacent main axes, d, where $H_2 < d/2$, $H_2 = d/2$ and $H_2 > d/2$, as shown in figure 6. The isosceles triangle theory is obtained to determine the angle between the main axis, A, and H_2, as follows: $A = (180 - B)/2$,

$d = 2\sqrt{H_1^2 - (H_1 \cos(B/2)^2)}$. S parameters, and the refractive and chirality index of case A and B are illustrated in figures 7 and 9, respectively.

The chirality peak of the conjugated bi-layer case A with $H_2 < d/2$ and $H_2 > d/2$ is located at a similar frequency, around 3.0 GHz, as shown in figures 7(b) and (f). The effective refractive index is negative due to the large negative value of n_+ and n_-, respectively. However, since
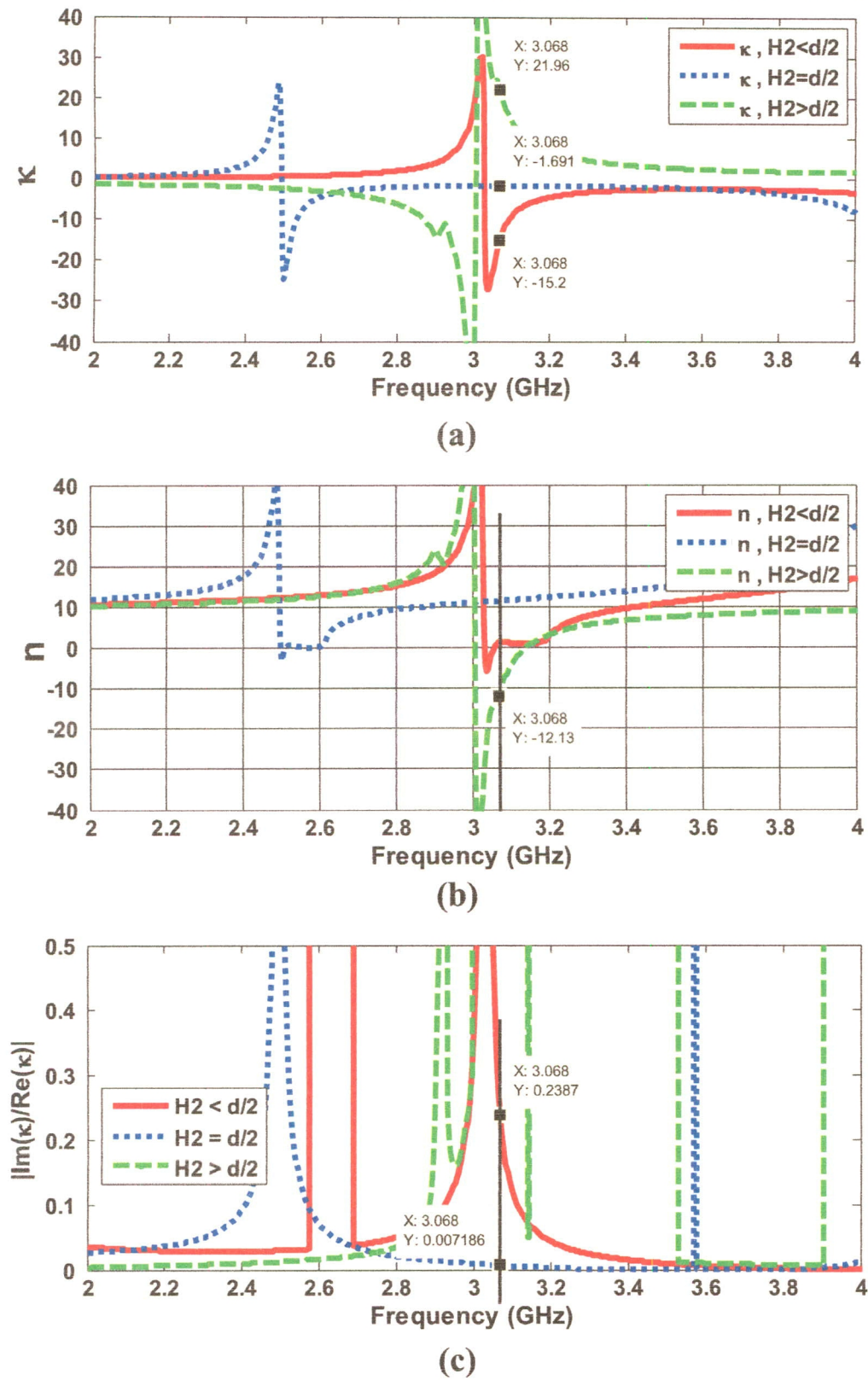
Figure 8. (a) Chirality index, (b) refractive index and (c) figure of merit of the conjugated bi-layer C_8 case A.

the transmission coefficient of the RCP and LCP wave of the bi-layer with $H_2 < d/2$ and $H_2 > d/2$ (figures 7(a) and (e)) is poor, respectively at -20.25 dB and -18.93 dB, these two structures are highly lossy. The figure of merit, shown in figure 8(c), supports the above-mentioned data.

The difference between the transmission coefficients of the RCP and LCP waves is found in all orientations of the bi-layer in case B, as shown in figures 9(a), (c) and (e), at 4.15 GHz, 3.28 GHz and 3.23 GHz, respectively. The chirality peak (figures 9(b), (d) and (f)) is found at the above-mentioned

Figure 9. *S* parameters, refractive and chirality index of the conjugated bi-layer C_8 case *B*: (a), (b) $H_2 < d/2$, (c), (d) $H_2 = d/2$ and (e), (f) $H_2 > d/2$.

frequency. In this case, the extended length of the connected arm raises the broken symmetry, so that the chirality is larger if H_2 is longer. There is a negative refractive index for $H_2 = d/2$ and $H_2 > d/2$, while for $H_2 < d/2$ the chirality is small and there is no occurrence of the negative index. The effective refractive index is negative due to the large negative value of n_-. The negative refractive indices are large, down to -80. The figure of merit of both cases presented in figure 10(c) is below 0.2 and 0.3, respectively, which is highly acceptable.

2.3. Angle between the main axis and the connected arms, $A°$

Figure 11 shows the bi-layer C_8 case *A*, where the angle between the main axis and the connected arms is varied at 15°, 45° and 75°. Other parameters are set as follows: $\varphi < B/2$, $H_1 = 15.7$ mm and $H_2 = d/2$ mm. The *S* parameters and indices of the bi-layer C_8 case *A* and *B* based on the angle $A°$ are illustrated in figures 12 and 14, respectively.
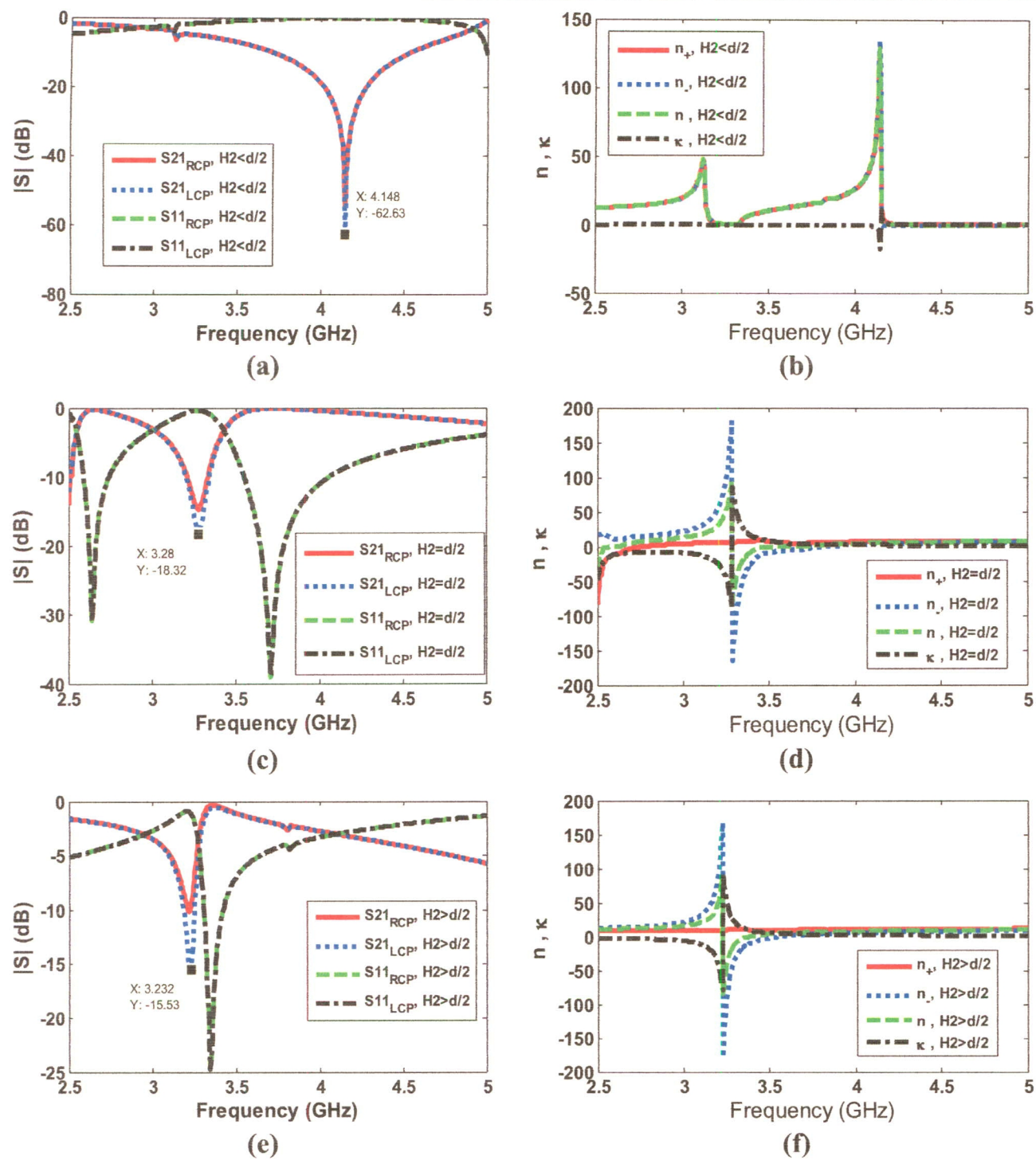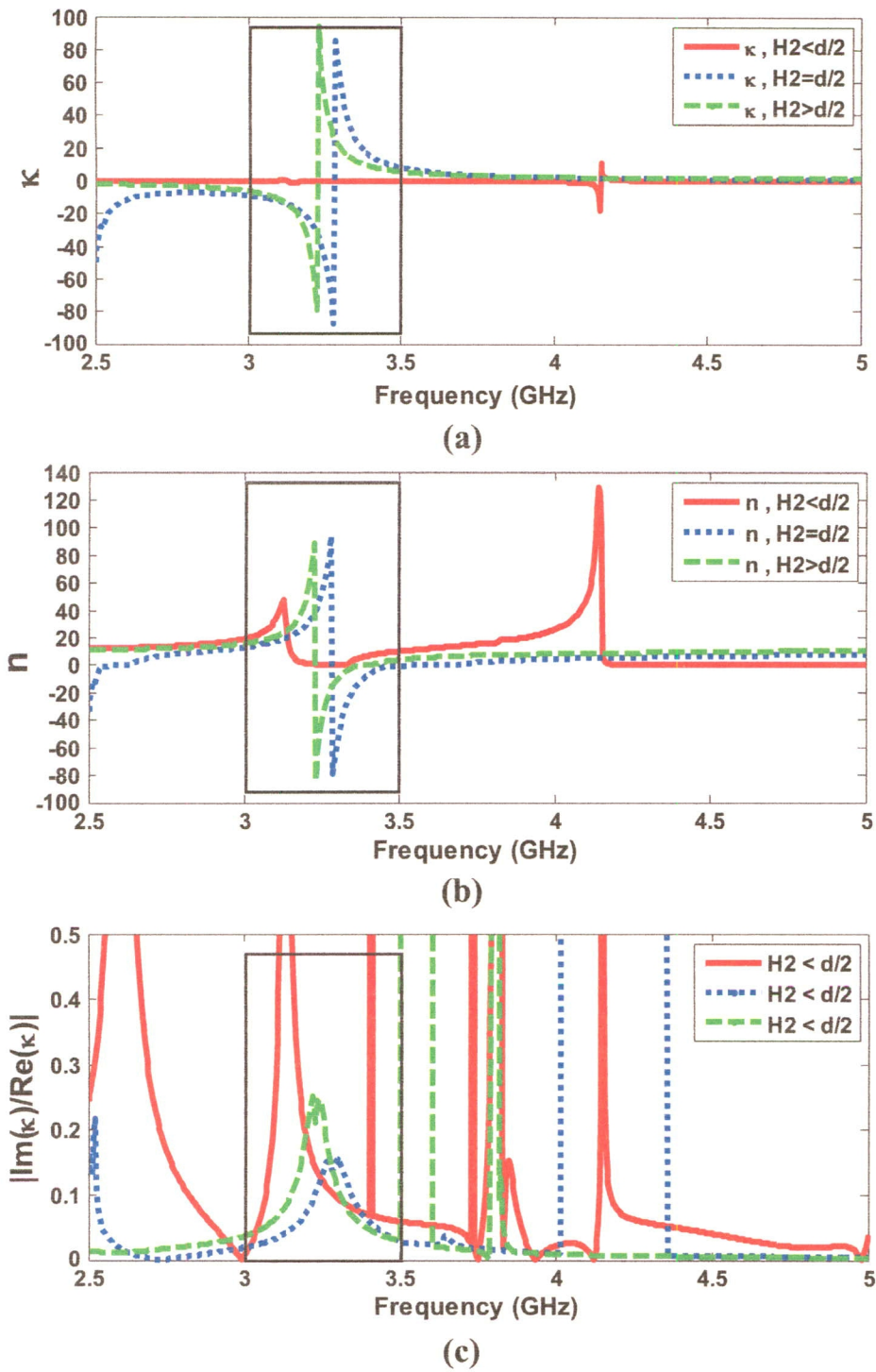
Figure 10. (a) Chirality index, (b) refractive index and (c) figure of merit of the conjugated bi-layer C_8 case *B*.

In case *A*, the angle $A°$ controls the resonance location due to the structure capacitance generated from the two arms or the mutual pair from the front and back board. As the angle $A°$ gets wider, the capacitance is larger; therefore, the resonance is found at a lower frequency, which is valid for both RCP and LCP excitations illustrated in figures 12(a), (c) and (e). The effective refractive index is negative at the resonance for all angles; however, the value is low, $n = -14.21$, $n = -3.46$, and $n = -4.54$ for $A = 15°$, $A = 45°$ and $A = 75°$, respectively, as shown in figure 13(b). Moreover,

these conjugated cases are highly lossy in the negative index band, as indicated (circled) in figure 13(c).

In case *B*, the angle is directly proportional to the broken symmetry and, therefore, the chirality. The chirality is very small when $A = 15°$, and there is no incidence of the negative refractive index, shown in figures 14(b), (d) and (f). There are three chirality peaks located within the operating frequency of the conjugated structures with $A = 45°$ and $75°$. The effective refractive index is found to be negative at those six chirality peaks, as illustrated in figures 15(a) and (b). The third negative
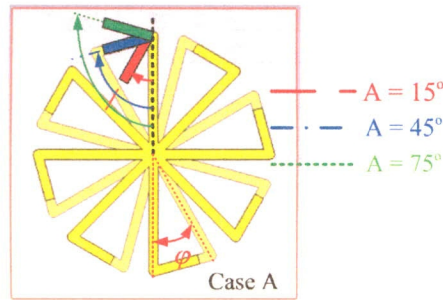
Figure 11. Case *A* of the conjugated bi-layer C_8 structures where the angle $A°$ between the main axis and the connected arms is varied.

refractive peak of the conjugated C_8, $n = -55.86$ at 3.7 GHz and $n = -79.68$ at 3.30 GHz, with $A = 45°$ and $A = 75°$, stress the good transmission regarding the low figure of merit at 0.12 and 0.2, respectively, as illustrated in figure 15(c).

3. High refractive index C_8 chiral metamaterials

The conjugated bi-layer C_8 case *B* shown in figure 16 is selected to further investigate the high indices. The structures are fabricated on Arlon Di 880 boards. The dielectric constant of Arlon Di 880 board is 2.2+0.0009i. The thickness of copper is 0.03 mm. The dimension parameters of the bi-layer

Figure 12. *S* parameters, refractive and chirality index of the conjugated bi-layer C_8 case *A*: (a), (b) $A = 15°$, (c), (d) $A = 45°$ and (e), (f) $A = 75°$.
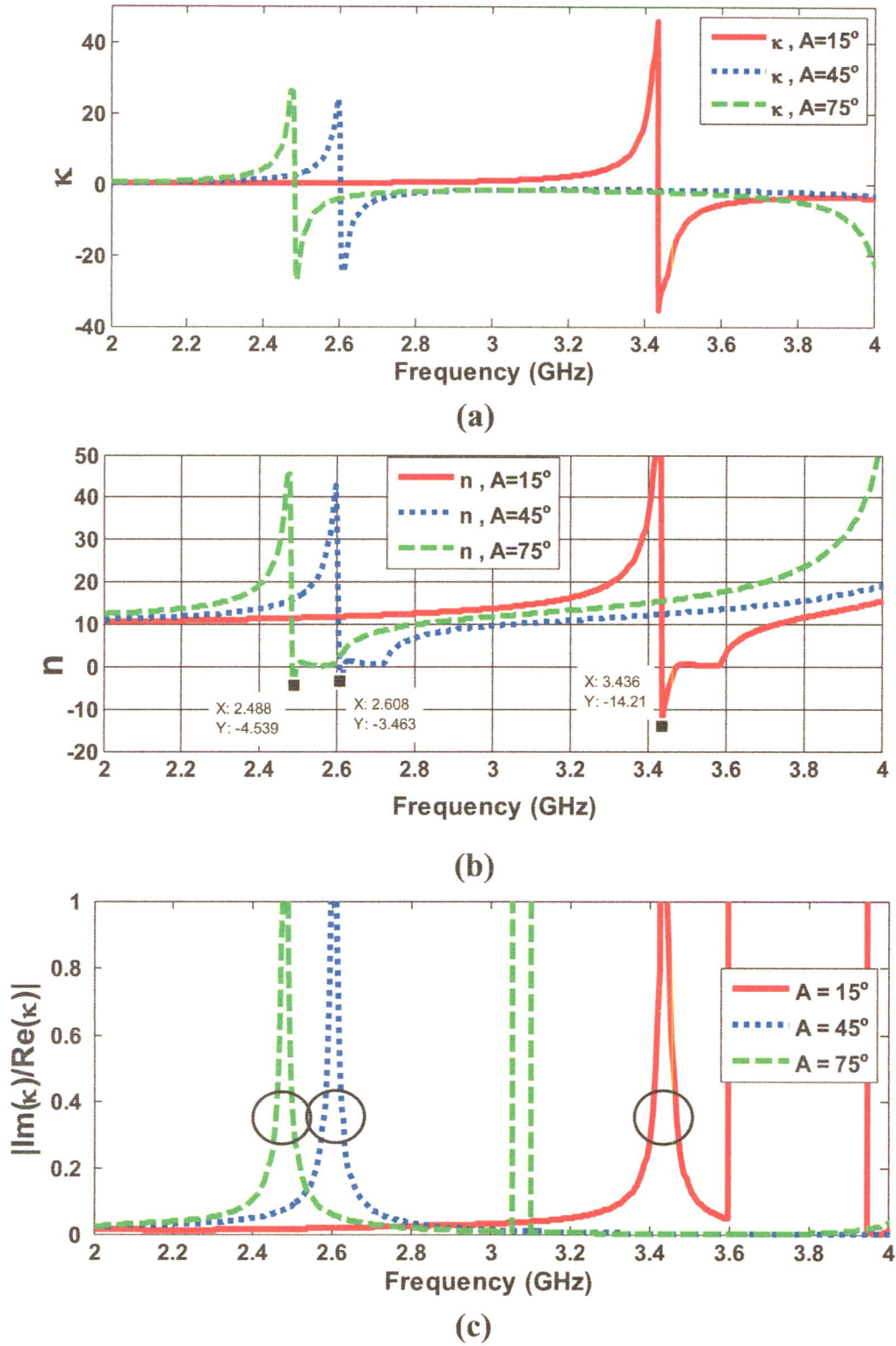
Figure 13. (a) Chirality index, (b) refractive index and (c) figure of merit of the conjugated bi-layer C_8 case *B*.
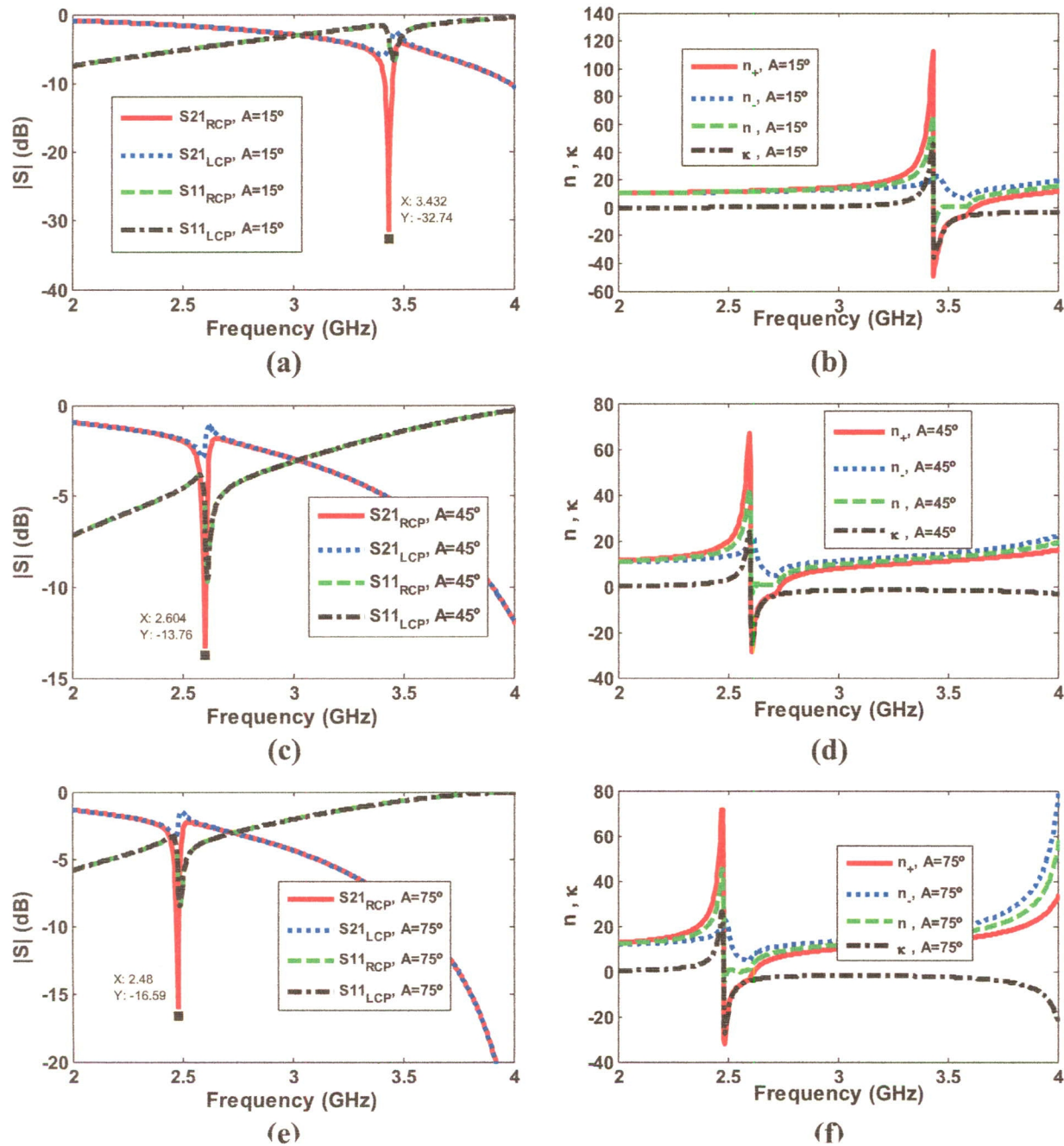
structures are set as: $x = y = 37$ mm, $w = 2.8$ mm, $H_1 = 15.7$ mm, $B = 360°/n$, $t = 0.03$ mm, $s = 0.254$ mm, $H_2 = d/2$ mm, $A = 50°$. The RCP and LCP excitations are set along the $-z$ direction. The transmission (S_{21}) and reflection (S_{11}) coefficients of the cross- and co-polarizations are measured by a vector network analyzer (HP8753D), using horn antennas as the excitation and receiving ports.

Figures 17(a) and (b) show the transmission coefficients of RCP and LCP waves, amplitude and phase, respectively, of the conjugated bi-layer C_8 structures, case *B*. There are two locations where the transmission coefficients (both amplitude and phase) of the RCP and LCP wave are different. The differences at the resonance locations confirm the chirality index. The chirality and refractive indices are illustrated in
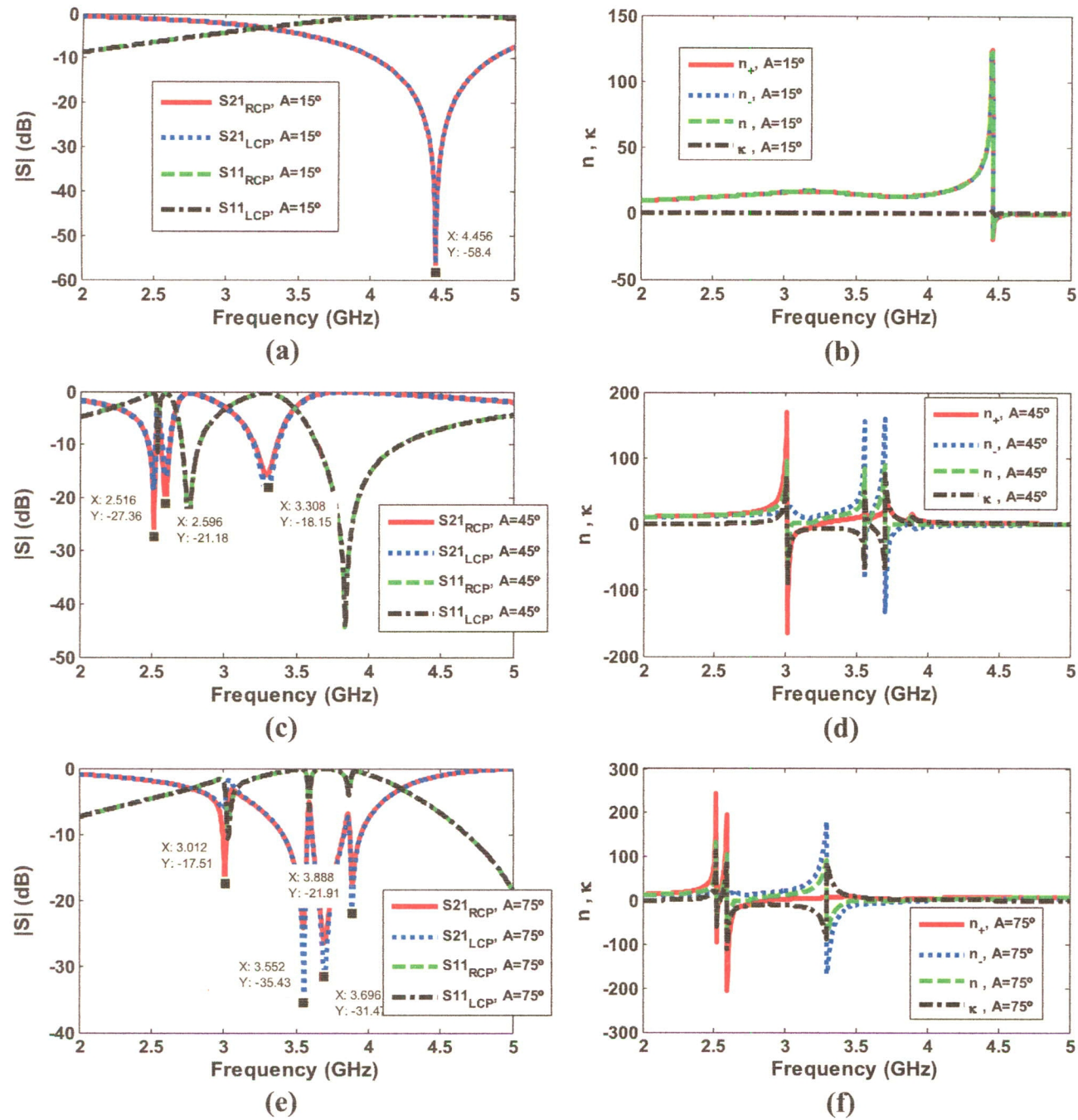
Figure 14. S parameters, refractive and chirality index of the conjugated bi-layer C$_8$ case *B*: (a), (b) $A = 15°$, (c), (d) $A = 45°$ and (e), (f) $A = 75°$.

figures 17(c) and (e). The first chirality peak ($f = 2.94$ GHz, simulation) changes sign from negative to positive, while for the second peak (3.11 GHz, simulation) the sign changes from positive to negative. The chirality is in the range of -60 to 80 (for both simulation and measurement). The negative refractive index values from both excitations are correspondingly extreme. Considering the RCP excitation, the negative refractive index, $n_{RCP} = -130$, is found at the second chirality peak. On the other hand, for the LCP wave, the negative refractive index, $n_{LCP} = -170$, is generated at the first chirality peak. The figure of merit value at the two

negative index peaks, shown in figure 17(d), is low, less than 0.3, resulting in good transmission.

4. Conclusions

Two orientation cases of the conjugated bi-layer C$_8$ metamaterials based on the arm direction and the twist angle are investigated. Three geometric parameters, i.e. the twist angle between the structures on each layer, the ratio between the main axis and the arm, and the angle between the main axis and the connected arm, can be designed to control
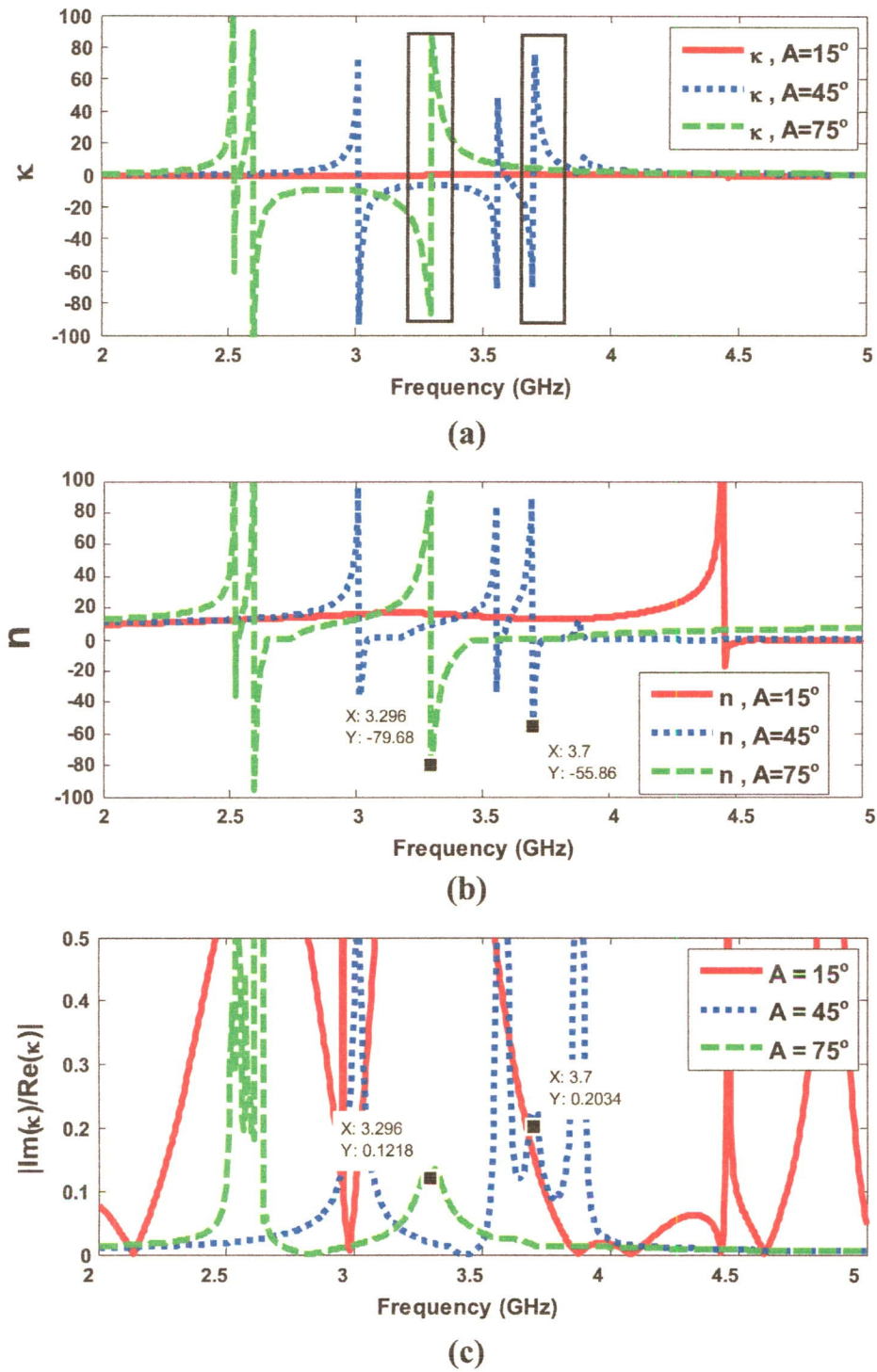
Figure 15. (a) Chirality index, (b) refractive index and (c) figure of merit of the conjugated bi-layer C_8 case *B*.

the structures' chirality. Structure modification based on the inductances, capacitances, self- and mutual couplings, and broken symmetry, extensively influences the locations and value of the chirality and therefore has a strong impact on negative refractive index properties. Conjugated bi-layer C_8 structures are fabricated and tested in the microwave regime. The measurement results show extreme chirality, as well as high negative refractive index, confirming the expectations.

Acknowledgments
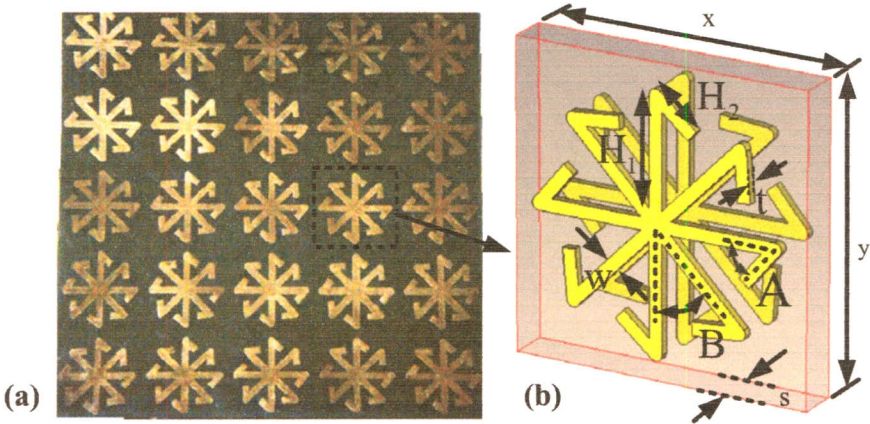
Figure 16. (a) A photograph (top view) and (b) a unit cell of the conjugated bi-layer C_8 structures. The geometric parameters of both structures are given as follows: $x = y = 37$ mm, $w = 2.8$ mm, $H_1 = 15.7$ mm, $B = 360°/n$, $t = 0.03$ mm, $s = 0.254$ mm, $H_2 = d/2$ mm.
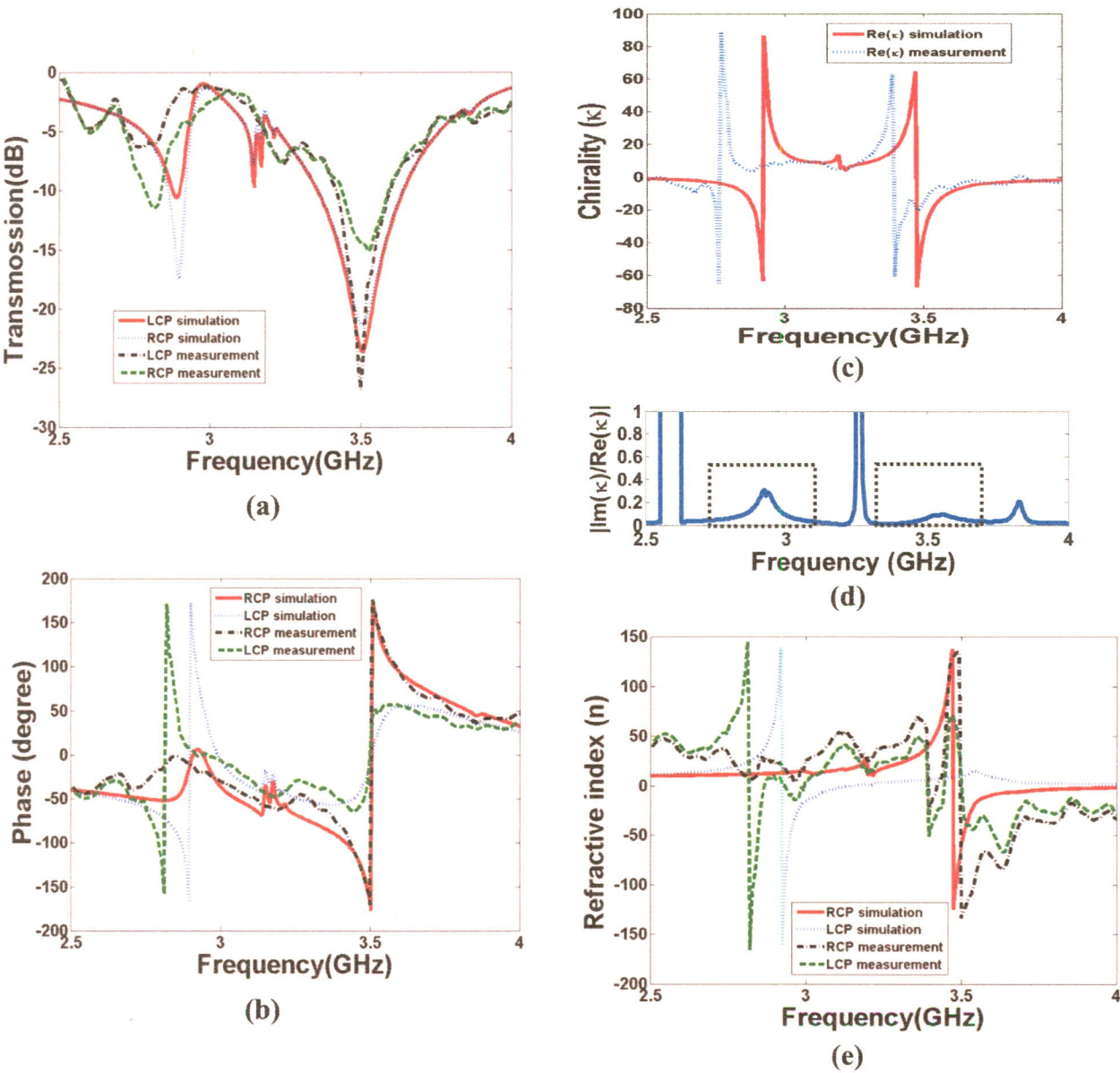
Figure 17. Simulation and experimental results of the conjugated bi-layer C_8 structures. Transmission coefficients of RCP and LCP wave: (a) amplitude and (b) phase. (c) Chirality, (d) figure of merit and (e) refractive index.

References

[1] Wongkasem N and Akyurtlu A 2011 Light splitting effects in chiral metamaterials *J. Opt.* **12** 035101

[2] Lindell I V, Sihvola A, Tretyakov S A and Viitanen A J 1994 *Electromagnetic Waves in Chiral and Bi-isotropic Media* (Boston: Artech House, Norwood)

[3] Sihvola A, Tretyakov S A and Baas de A 2007 Metamaterials with extreme material parameters *J. Commun. Electron.* **52** 986–90

[4] Sihvola A 2007 Metamaterials in electromagnetic *Metamaterials* **1** 2–11

[5] Zhao R, Zhang L, Zhou J, Koschny Th and Soukoulis C M 2011 Conjugated gammadion chiral metamaterial with uniaxial optical activity and negative refraction index *Phys. Rev.* B **83** 035105

[6] Gansel J K, Wegener M, Burger S and Linden S 2010 Gold helix photonic metamaterials: a numerical parameter study *Opt. Express* **18** 1059–69

[7] Gansel J K, Thiel M, Rill M S, Decker M, Bade K, Saile V, Freymann G V, Linden S and Wegener M 2009 Gold helix photonic metamaterial as broadband circular polarizer *Science* **325** 1513–5

[8] Wongkasem N, Kamtongdee C, Akyurtlu A and Marx K A 2010 Artificial multiple helices: polarization and EM properties *J. Opt.* **12** 075102

[9] Koschny T and Soukoulis C M 2009 Nonplanar chiral metamaterials with negative index *Appl. Phys. Lett.* **94** 151112

[10] Wongkasem N, Akyurtlu A, Marx K A, Goodhue W D, Li J, Dong Q and Ada E T 2007 Fabrication of a novel micron scale Y-structure-based chiral metamaterial: simulation and experimental analysis of its chiral and negative index properties in the terahertz and microwave regime *Microsc. Res. Technique* **70** 497–505

[11] Li Z, Zhao R, Koschy T, Kafesaki M, Alici K B, Colak E, Caglayan H, Ozbay E and Soukoulis C M 2011 Chiral metamaterials with negative refractive index based on four 'U' split ring resonators *Appl. Phys. Lett.* **97** 081901

[12] Xiong X, Sun W H, Beo Y J, Peng R W, Sun C, Lu X, Shao J, Li Z F and Ming N B 2010 Construction of a chiral metamaterial with a U-shaped resonator assembly *Phys. Rev.* B **81** 075119

[13] Xiong X, Sun W H, Beo Y J, Peng R W, Sun C, Lu X, Shao J, Li Z F and Ming N B 2009 Switching the electric and magnetic responses in a metamaterial *Phys. Rev.* B **80** 201105(R)

[14] Matra K and Wongkasem N 2009 Left-handed chiral isotropic metamaterials: analysis and detailed numerical study *J. Opt. A: Pure Appl. Opt.* **14** 074011

[15] Zhou J, Dong J, Wang B, Koschny T, Kafesaki M and Soukoulis C M 2009 Negative refractive index due to chirality *Phys. Rev.* B **79** 121104(R)

[16] Dong J, Zhou J, Koschny T and Soukoulis C M 2009 Bi-layer cross chiral structure with strong optical activity and negative refractive index *Opt. Express* **17** 14172–9

[17] Rogacheva A V, Fedotov V A, Schwanecke S A and Zheludev N I 2006 Giant gyrotropy due to electromagnetic-field coupling in a bi layered chiral stucture *Phys. Rev. Lett.* **97** 177401

[18] Plum E, Zhou J, Dong J, Fedotov V A, Koschny T, Soukoulis C M and Zheludev N I 2009 Metamaterials with negative index due to chirality *Phys. Rev.* B **79** 035407

[19] Wang B, Zhou J, Koschny T, Kafesaki M and Soukoulis C M 2009 Chiral metamaterials: simulations and experiments *J. Opt. A: Pure Appl. Opt.* **11** 114003

[20] Svirko Y, Zheludev N and Osipov M 2001 Layered chiral metallic microstructure with inductive coupling *Appl. Phys. Lett.* **78** 498

[21] Panpradit W, Sonsilphong A and Wongkasem N 2011 Chirality control in metamaterial by geometrical manipulation *ICEAA: 2011 Int. Conf. on Electromagnetics in Advanced Applications* pp 540–3

[22] Zhao R, Koschny T and Soukoulis C M 2010 Chiral metamaterials: retrieval of the effective parameters with and without substrate *Opt. Express* **18** 14553–67

[23] Zhao R, Koschny T, Economou E N and Soukoulis C M 2010 Comparison of chiral metamaterial designs for repulsive Casmir force *Phys. Rev.* B **81** 235126

[24] Yu Y, Yang Z Y, Zhao M and Lu P 2011 Broadband optical circularpolarizers in the terahertz region using helical metamaterials *J. Opt.* **13** 055104

[25] Zhang S, Park Y, Li J, Lu X, Zhang W and Zhan X 2009 Negative refractive index in chiral metamaterials *Phys. Rev. Lett.* **102** 023901

[26] Zhou Y, Tran N, Lin Y, He Y and Shi F G 2008 One-component, low-temperature, and fast cure epoxy encapsulant with high refractive index for LED applications *IEEE Trans. Adv. Packag.* **31** 484–9

[27] Zwiller V and Bjork G 2002 Improved light extraction from emitters in high refractive index materials using solid immersion lenses *J. Appl. Phys.* **92** 660

[28] Mayeh M and Farahi F 2008 Geometrically modified multimode interference waveguides using high refractive index SiON material, for application in wavelength multiplexing/demultiplexing *High Capacity Optical Networks and Enabling Technologies, HONET. International Symposium* pp 121–5

[29] Lauck R, Brandis M, Bromberger B, Dangendorf V, Goldberg M B, Mor I, Tittelmeier K and Vartsky D 2009 Low-afterglow, high-refractive-index liquid scintillators for fast-neutron spectrometry and imaging applications *IEEE Trans. Nucl. Sci.* **56** 989–93

สิทธิบัตรประเทศไทย

ข1. **นันทกานต์ วงศ์เกษม** และ อมรเทพ สอนศิลพงศ์, "วัสดุป้องกันคลื่นสัญญาณแม่เหล็กไฟฟ้า
ในย่านรังสีเอกซ์" ยื่นจดสิทธิบัตรประเทศไทย เมื่อวันที่ 2 เมษายน 2557
เลขที่คำขอ 1401001981

คำขอรับสิทธิบัตร/อนุสิทธิบัตร

☒ การประดิษฐ์
☐ การออกแบบผลิตภัณฑ์
☐ อนุสิทธิบัตร

ข้าพเจ้าผู้ลงลายมือชื่อในคำขอรับสิทธิบัตร/อนุสิทธิบัตรนี้
ขอรับสิทธิบัตร/อนุสิทธิบัตร ตามพระราชบัญญัติสิทธิบัตร พ.ศ 2522
แก้ไขเพิ่มเติมโดยพระราชบัญญัติสิทธิบัตร (ฉบับที่ 2) พ.ศ 2535
และ พระราชบัญญัติสิทธิบัตร (ฉบับที่ 3) พ.ศ 2542

สำหรับเจ้าหน้าที่	
วันรับคำขอ 1 0 เม.ย. 2557	เลขที่คำขอ
วันยื่นคำขอ - 2 เม.ย. 2557	140100 1981 (นางสาวจีรนันท์ ภูดงดาร) นักวิชาการพาณิชย์
สัญลักษณ์จำแนกการประดิษฐ์ระหว่างประเทศ	
ใช้กับแบบผลิตภัณฑ์ ประเภทผลิตภัณฑ์	
วันประกาศโฆษณา	เลขที่ประกาศโฆษณา
วันออกสิทธิบัตร/อนุสิทธิบัตร	เลขที่สิทธิบัตร/อนุสิทธิบัตร
ลายมือชื่อเจ้าหน้าที่	

1.ชื่อที่แสดงถึงการประดิษฐ์/การออกแบบผลิตภัณฑ์
    วัสดุป้องกันคลื่นสัญญาณแม่เหล็กไฟฟ้าในย่านรังสีเอ็กซ์

2.คำขอรับสิทธิบัตรการออกแบบผลิตภัณฑ์นี้เป็นคำขอสำหรับแบบผลิตภัณฑ์อย่างเดียวกันและเป็นคำขอลำดับที่
    ในจำนวน   คำขอ ที่ยื่นในคราวเดียวกัน

3.ผู้ขอรับสิทธิบัตร/อนุสิทธิบัตร และที่อยู่ (เลขที่ ถนน ประเทศ)
    มหาวิทยาลัยขอนแก่น

    123 ถนนมิตรภาพ ต.ในเมือง อ. เมือง จ. ขอนแก่น 40002

3.1 สัญชาติ ไทย	
3.2 โทรศัพท์ 0-4320-2222-41	
3.3 โทรสาร	
3.4 อีเมล์ -	

4.สิทธิในการขอรับสิทธิบัตร/อนุสิทธิบัตร

    ☐ ผู้ประดิษฐ์/ผู้ออกแบบ   ☒ ผู้รับโอน   ☐ ผู้ขอรับสิทธิโดยเหตุอื่น

5.ตัวแทน(ถ้ามี)/ที่อยู่ (เลขที่ ถนน จังหวัด รหัสไปรษณีย์)
    นางจิราภรณ์ เหลืองไพรินทร์
    สำนักงานบริหารจัดการทรัพย์สินทางปัญญา
    123 มหาวิทยาลัยขอนแก่น ต.ในเมือง อ.เมือง จ.ขอนแก่น ประเทศไทย 40002

5.1 ตัวแทนเลขที่ 2217	
5.2 โทรศัพท์ 0-4320-2733	
5.3 โทรสาร 0-4320-2733	
5.4 อีเมล์ ip@kku.ac.th	

6.ผู้ประดิษฐ์/ผู้ออกแบบผลิตภัณฑ์ และที่อยู่ (เลขที่ ถนน ประเทศ)

    6.1 ผู้ช่วยศาสตราจารย์นันทกานต์ วงศ์เกษม

    6.2 นายอมรเทพ สอนศิลพงศ์

        ที่อยู่ คณะวิศวกรรมศาสตร์ มหาวิทยาลัยขอนแก่น ต.ในเมือง อ.เมือง จ. ขอนแก่น 40002

7. คำขอรับสิทธิบัตร/อนุสิทธิบัตรนี้แยกจากหรือเกี่ยวข้องกับคำขอเดิม

    ผู้ขอรับสิทธิบัตร/อนุสิทธิบัตร ขอให้ถือว่าได้ยื่นคำขอรับสิทธิบัตร/อนุสิทธิบัตรนี้ ในวันเดียวกับคำขอรับสิทธิบัตร

    เลขที่   วันยื่น   เพราะคำขอรับสิทธิบัตร/อนุสิทธิบัตรนี้แยกจากหรือเกี่ยวข้องกับคำขอเดิมเพราะ

    ☐ คำขอเดิมมีการประดิษฐ์หลายอย่าง   ☐ ถูกคัดค้านเนื่องจากผู้ขอไม่มีสิทธิ   ☐ ขอเปลี่ยนแปลงประเภทของสิทธิ

หมายเหตุ ในกรณีที่ไม่อาจระบุรายละเอียดได้ครบถ้วน ให้จัดทำเป็นเอกสารแนบท้ายแบบพิมพ์นี้โดยระบุหมายเลขกำกับข้อและหัวข้อที่แสดงรายละเอียด
    เพิ่มเติมดังกล่าวด้วย

การยื่นคำขอนอกราชอาณาจักร

วันยื่นคำขอ	เลขที่คำขอ	ประเทศ	สัญลักษณ์จำแนกการประดิษฐ์ระหว่างประเทศ	สถานะคำขอ
1				
2				
3				

4 ☐ ผู้ขอรับสิทธิบัตร/อนุสิทธิบัตรขอสิทธิให้ถือว่าได้ยื่นคำขอนี้ในวันที่ได้ยื่นคำขอรับสิทธิบัตร/อนุสิทธิบัตรในต่างประเทศเป็นครั้งแรกโดย

☐ ได้ยื่นเอกสารหลักฐานพร้อมคำขอนี้   ☐ ขอยื่นเอกสารหลักฐานหลังจากวันยื่นคำขอนี้

การแสดงการประดิษฐ์ หรือการออกแบบผลิตภัณฑ์ ผู้ขอรับสิทธิบัตร/อนุสิทธิบัตรได้แสดงการประดิษฐ์ที่หน่วยงานของรัฐเป็นผู้จัด

วันแสดง   วันเปิดงานแสดง   ผู้จัด

10.การประดิษฐ์เกี่ยวกับจุลชีพ

10.1 เลขทะเบียนฝากเก็บ	10.2 วันที่ฝากเก็บ	10.3 สถาบันฝากเก็บ/ประเทศ

11 ผู้ขอรับสิทธิบัตร/อนุสิทธิบัตร ขอยื่นเอกสารภาษาต่างประเทศก่อนในวันยื่นคำขอนี้ และจะจัดยื่นคำขอรับสิทธิบัตร/อนุสิทธิบัตรนี้ที่จัดทำในภาษาไทยภายใน 90 วัน นับจากวันยื่นคำขอนี้ โดยขอยื่นเป็นภาษา

☐ อังกฤษ   ☐ ฝรั่งเศส   ☐ เยอรมัน   ☐ ญี่ปุ่น   ☐ อื่นๆ

12 ผู้ขอรับสิทธิบัตร/อนุสิทธิบัตร ขอให้อธิบดีประกาศโฆษณาคำขอรับสิทธิบัตร หรือรับจดทะเบียน และประกาศโฆษณาอนุสิทธิบัตรนี้หลังจากวันที่   เดือน   พ.ศ

ผู้ขอรับสิทธิบัตร/อนุสิทธิบัตรขอให้ใช้รูปเขียนหมายเลข   ในการประกาศโฆษณา

13.คำขอรับสิทธิบัตร/อนุสิทธิบัตรนี้ประกอบด้วย

ก. แบบพิมพ์คำขอ   2 หน้า

ข. รายละเอียดการประดิษฐ์
   หรือคำพรรณนาแบบผลิตภัณฑ์   3 หน้า

ค. ข้อถือสิทธิ   1 หน้า

ง. รูปเขียน   4 รูป   2 หน้า

จ. ภาพแสดงแบบผลิตภัณฑ์

   ☐ รูปเขียน   รูป   หน้า

   ☐ ภาพถ่าย   รูป   หน้า

ฉ. บทสรุปการประดิษฐ์   1 หน้า

14.เอกสารประกอบคำขอ

☐ เอกสารแสดงสิทธิในการขอรับสิทธิบัตร/อนุสิทธิบัตร

☐ หนังสือรับรองการแสดงการประดิษฐ์/การออกแบบผลิตภัณฑ์

☒ หนังสือมอบอำนาจ

☐ เอกสารรายละเอียดเกี่ยวกับจุลชีพ

☐ เอกสารการขอนับวันยื่นคำขอในต่างประเทศเป็นวันยื่นคำขอในประเทศไทย

☐ เอกสารขอเปลี่ยนแปลงประเภทของสิทธิ

☐ เอกสารอื่น ๆ

15. ข้าพเจ้าขอรับรองว่า

☒ การประดิษฐ์นี้ไม่เคยยื่นขอรับสิทธิบัตร/ อนุสิทธิบัตรมาก่อน

☐ การประดิษฐ์นี้ได้พัฒนาปรับปรุงมาจาก..

16.ลายมือชื่อ (☐ ผู้ขอรับสิทธิบัตร / อนุสิทธิบัตร; ☒ ตัวแทน)

(นางจิราภรณ์ เหลืองไพรินทร์)

<u>หมายเหตุ</u> บุคคลใดยื่นขอรับสิทธิบัตรการประดิษฐ์หรือการออกแบบผลิตภัณฑ์ หรืออนุสิทธิบัตร โดยการแสดงข้อความอันเป็นเท็จแก่พนักงานเจ้าหน้าที่ เพื่อให้ได้ไปซึ่งสิทธิบัตรหรืออนุสิทธิบัตร ต้องระวางโทษจำคุกไม่เกินหกเดือน หรือปรับไม่เกินห้าพันบาท หรือทั้งจำทั้งปรับ

หนังสือสัญญาโอนสิทธิขอรับสิทธิบัตร/อนุสิทธิบัตร

เขียนที่ มหาวิทยาลัยขอนแก่น

123 ถ. มิตรภาพ ต.ในเมือง อ. เมือง

จ. ขอนแก่น 40002

วันที่

          สัญญาระหว่างผู้โอน คือ 1.ผู้ช่วยศาสตราจารย์นันทกานต์ วงศ์เกษม และ 2.นายอมรเทพ สอนศิลพงศ์ ที่อยู่ 123 คณะวิศวกรรมศาสตร์ มหาวิทยาลัยขอนแก่น ถ.มิตรภาพ อ.เมือง จ.ขอนแก่น 40002 และผู้รับโอน คือ 1.**มหาวิทยาลัยขอนแก่น** โดย ศาสตราจารย์วีระชัย โควสุวรรณ รองอธิการบดีฝ่ายวิจัยและการถ่ายทอดเทคโนโลยี มหาวิทยาลัยขอนแก่น ที่อยู่บ้านเลขที่ 123 ถ.มิตรภาพ ต.ในเมือง อ. เมือง จ.ขอนแก่น 40002 2. **สำนักงานกองทุนสนับสนุนการวิจัย** โดย ศาสตราจารย์สุทธิพันธ์ จิตพิมลมาศ ผู้อำนวยการสำนักงานกองทุนสนับสนุนการวิจัย ที่อยู่ 979/17-21 อาคารเอส เอ็ม ทาวเวอร์ ชั้น 14 ถ.พหลโยธิน แขวงสามเสนใจ เขตพญาไท กรุงเทพฯ 10400 โดยสัญญานี้ ผู้โอนซึ่งเป็นผู้ประดิษฐ์ **"วัสดุป้องกันคลื่นสัญญาณแม่เหล็กไฟฟ้าในย่านรังสีเอ็กซ์"** ขอโอนสิทธิในการประดิษฐ์ดังกล่าว ซึ่งรวมถึงสิทธิขอรับสิทธิบัตร/อนุสิทธิบัตร และสิทธิอื่นๆ ที่เกี่ยวข้องให้แก่ผู้รับโอน เพื่อเป็นพยานหลักฐานแห่งการนี้ ผู้โอนและผู้รับโอนได้ลงลายมือชื่อไว้ข้างล่างนี้

(ลงชื่อ) .... ผู้โอน   (ลงชื่อ) .... ผู้โอน

(ผู้ช่วยศาสตราจารย์นันทกานต์ วงศ์เกษม)   (นายอมรเทพ สอนศิลพงศ์)

(ลงชื่อ) .... ผู้รับโอน   (ลงชื่อ) .... ผู้รับโอน

(ศาสตราจารย์วีระชัย โควสุวรรณ)   (ศาสตราจารย์สุทธิพันธ์ จิตพิมลมาศ)

(ลงชื่อ)......................................พยาน   (ลงชื่อ)......................................พยาน

(นายเศกสิทธิ์ พรหมพฤฒา)   (นางสาวนฤมล เบญจปัก)

สิทธิบัตรประเทศไทย

ข2. **นันทกานต์ วงศ์เกษม** และ มนตรี มาลาทอง, "วัสดุปิดกั้นคลื่นสัญญาณแม่เหล็กไฟฟ้า"
ยื่นจดสิทธิบัตรประเทศไทย เมื่อวันที่ 31 มกราคม 2556 เลขที่คำขอ 1301000619

คำขอรับสิทธิบัตร/อนุสิทธิบัตร

☒ การประดิษฐ์
☐ การออกแบบผลิตภัณฑ์
☐ อนุสิทธิบัตร

ข้าพเจ้าผู้ลงลายมือชื่อในคำขอรับสิทธิบัตร/อนุสิทธิบัตรนี้
รับสิทธิบัตร/อนุสิทธิบัตร ตามพระราชบัญญัติสิทธิบัตร พ.ศ 2522
ไขเพิ่มเติมโดยพระราชบัญญัติสิทธิบัตร (ฉบับที่ 2) พ.ศ 2535
ะ พระราชบัญญัติสิทธิบัตร (ฉบับที่ 3) พ.ศ 2542

เอที่แสดงถึงการประดิษฐ์/การออกแบบผลิตภัณฑ์
ัสดุปิดกั้นคลื่นสัญญาณแม่เหล็กไฟฟ้า

่ำขอรับสิทธิบัตรการออกแบบผลิตภัณฑ์นี้เป็นคำขอสำหรับแบบผลิตภัณฑ์อย่างเดียวกันและเป็นคำขอลำดับที่
นจำนวน   คำขอ ที่ยื่นในคราวเดียวกัน

สำหรับเจ้าหน้าที่		
วันรับคำขอ − 6 ก.พ. 2556		เลขที่คำขอ
วันยื่นคำขอ 3 1 ม.ค. 2556		1301000619
สัญลักษณ์จำแนกการประดิษฐ์ระหว่างประเทศ		
ใช้กับแบบผลิตภัณฑ์		
ประเภทผลิตภัณฑ์		
วันประกาศโฆษณา		เลขที่ประกาศโฆษณา
วันออกสิทธิบัตร/อนุสิทธิบัตร		เลขที่สิทธิบัตร/อนุสิทธิบัตร
ลายมือชื่อเจ้าหน้าท		

ุ่ขอรับสิทธิบัตร/อนุสิทธิบัตร และที่อยู่ (เลขที่ ถนน ประเทศ)
มหาวิทยาลัยขอนแก่น
123 ถนนมิตรภาพ ต.ในเมือง อ. เมือง จ.ขอนแก่น 40002

3.1 สัญชาติ	ไทย
3.2 โทรศัพท์	0-4320-2222-41
3.3 โทรสาร	-
3.4 อีเมล์	-

ิทธิในการขอรับสิทธิบัตร/อนุสิทธิบัตร

☐ ผู้ประดิษฐ์/ผู้ออกแบบ   ☒ ผู้รับโอน   ☐ ผู้ขอรับสิทธิโดยเหตุอื่น

ัวแทน(ถ้าม)/ที่อยู่ (เลขที่ ถนน จังหวัด รหัสไปรษณีย์)
นางจิราภรณ์ เหลืองไพรินทร์
สำนักงานบริหารจัดการทรัพย์สินทางปัญญา
123 มหาวิทยาลัยขอนแก่น ต.ในเมือง อ. เมือง จ.ขอนแก่น ประเทศไทย 40002

5.1 ตัวแทนเลขที่ 2217	
5.2 โทรศัพท์ 0-4336-4409	
5.3 โทรสาร 0-4336-4409	
5.4 อีเมล์ ip@kku.ac.th	

ู้ประดิษฐ์/ผู้ออกแบบผลิตภัณฑ์ และที่อยู่ (เลขที่ ถนน ประเทศ)

6.1 ผู้ช่วยศาสตราจารย์นันทกานต์ วงศ์เกษม

6.2 นายมนตรี มาลาทอง

    ที่อยู่ คณะวิศวกรรมศาสตร์ มหาวิทยาลัยขอนแก่น ต.ในเมือง อ. เมือง จ. ขอนแก่น 40002

คำขอรับสิทธิบัตร/อนุสิทธิบัตรนี้แยกจากหรือเกี่ยวข้องกับคำขอเดิม

    ผู้ขอรับสิทธิบัตร/อนุสิทธิบัตร ขอให้ถือว่าได้ยื่นคำขอรับสิทธิบัตร/อนุสิทธิบัตรนี้ ในวันเดียวกับคำขอรับสิทธิบัตร

เขที่   วันยื่น   เพราะคำขอรับสิทธิบัตร/อนุสิทธิบัตรนี้แยกจากหรือเกี่ยวข้องกับคำขอเดิมเพราะ

☐ คำขอเดิมมีการประดิษฐ์หลายอย่าง ☐ ถูกคัดค้านเนื่องจากผู้ขอไม่มีสิทธิ ☐ ขอเปลี่ยนแปลงประเภทของสิทธิ

หมายเหตุ ในกรณีที่ไม่อาจระบุรายละเอียดได้ครบถ้วน ให้จัดทำเป็นเอกสารแนบท้ายแบบพิมพ์นี้โดยระบุหมายเลขกำกับข้อและหัวข้อที่แสดงรายละเอียด
เพิ่มเติมดังกล่าวด้วย

9.การยื่นคำขอนอกราชอาณาจักร

วันยื่นคำขอ	เลขที่คำขอ	ประเทศ	สัญลักษณ์จำแนกการประดิษฐ์ระหว่างประเทศ	สถานะคำขอ
9.1				
9.2				
9.3				

9.4 ☐ ผู้ขอรับสิทธิบัตร/อนุสิทธิบัตรขอสิทธิให้ถือว่าได้ยื่นคำขอนี้ในวันที่ได้ยื่นคำขอรับสิทธิบัตร/อนุสิทธิบัตรในต่างประเทศเป็นครั้งแรกโดย

☐ ได้ยื่นเอกสารหลักฐานพร้อมคำขอนี้   ☐ ขอยื่นเอกสารหลักฐานหลังจากวันยื่นคำขอนี้

9.การแสดงการประดิษฐ์ หรือการออกแบบผลิตภัณฑ์ ผู้ขอรับสิทธิบัตร/อนุสิทธิบัตรได้แสดงการประดิษฐ์ที่หน่วยงานของรัฐเป็นผู้จัด

วันแสดง   วันเปิดงานแสดง   ผู้จัด

10.การประดิษฐ์เกี่ยวกับจุลชีพ

10.1 เลขทะเบียนฝากเก็บ	10.2 วันที่ฝากเก็บ	10.3 สถาบันฝากเก็บ/ประเทศ

11.ผู้ขอรับสิทธิบัตร/อนุสิทธิบัตร ขอยื่นเอกสารภาษาต่างประเทศก่อนในวันยื่นคำขอนี้ และจะจัดยื่นคำขอรับสิทธิบัตร/อนุสิทธิบัตรนี้ที่จัดทำในภาษาไทยภายใน 90 วัน นับจากวันยื่นคำขอนี้ โดยขอยื่นเป็นภาษา

☐ อังกฤษ   ☐ ฝรั่งเศส   ☐ เยอรมัน   ☐ ญี่ปุ่น   ☐ อื่นๆ

12.ผู้ขอรับสิทธิบัตร/อนุสิทธิบัตร ขอให้อธิบดีประกาศโฆษณาคำขอรับสิทธิบัตร หรือรับจดทะเบียน และประกาศโฆษณาอนุสิทธิบัตรนี้
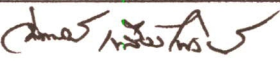
ตั้งแต่วันที่   เดือน   พ.ศ

☐ ผู้ขอรับสิทธิบัตร/อนุสิทธิบัตรขอให้ใช้รูปเขียนหมายเลข   ในการประกาศโฆษณา

13.คำขอรับสิทธิบัตร/อนุสิทธิบัตรนี้ประกอบด้วย

ก. แบบพิมพ์คำขอ   2 หน้า

ข. รายละเอียดการประดิษฐ์
หรือคำพรรณนาแบบผลิตภัณฑ์   5 หน้า

ค. ข้อถือสิทธิ   2 หน้า

ง. รูปเขียน   4   รูป   2 หน้า

จ. ภาพแสดงแบบผลิตภัณฑ์
  ☐ รูปเขียน   รูป   หน้า
  ☐ ภาพถ่าย   รูป   หน้า

ฉ. บทสรุปการประดิษฐ์   1 หน้า

14.เอกสารประกอบคำขอ

☐ เอกสารแสดงสิทธิในการขอรับสิทธิบัตร/อนุสิทธิบัตร

☐ หนังสือรับรองการแสดงการประดิษฐ์/การออกแบบผลิตภัณฑ์

☒ หนังสือมอบอำนาจ

☐ เอกสารรายละเอียดเกี่ยวกับจุลชีพ

☐ เอกสารการขอนับวันยื่นคำขอในต่างประเทศเป็นวันยื่นคำขอในประเทศไทย

☐ เอกสารขอเปลี่ยนแปลงประเภทของสิทธิ

☐ เอกสารอื่น ๆ

15. ข้าพเจ้าขอรับรองว่า

☒ การประดิษฐ์นี้ไม่เคยยื่นขอรับสิทธิบัตร/ อนุสิทธิบัตรมาก่อน

☐ การประดิษฐ์นี้ได้พัฒนาปรับปรุงมาจาก...

16.ลายมือชื่อ (☐ ผู้ขอรับสิทธิบัตร / อนุสิทธิบัตร; ☒ ตัวแทน)

(นางจิราภรณ์ เหลืองไพรินทร์)

หมายเหตุ บุคคลใดยื่นขอรับสิทธิบัตรการประดิษฐ์หรือการออกแบบผลิตภัณฑ์ หรืออนุสิทธิบัตร โดยการแสดงข้อความอันเป็นเท็จแก่พนักงานเจ้าหน้าที่ เพื่อให้ได้ไปซึ่งสิทธิบัตรหรืออนุสิทธิบัตร ต้องระวางโทษจำคุกไม่เกินหกเดือน หรือปรับไม่เกินห้าพันบาท หรือทั้งจำทั้งปรับ

หนังสือสัญญาโอนสิทธิขอรับสิทธิบัตร/อนุสิทธิบัตร

เขียนที่ มหาวิทยาลัยขอนแก่น

123 ถ. มิตรภาพ ต.ในเมือง อ. เมือง

จ. ขอนแก่น 40002

วันที่ 31 กรกฎาคม 2556

    สัญญาระหว่างผู้โอน คือ   1.ผู้ช่วยศาสตราจารย์นันทกานต์ วงศ์เกษม   และ 2.นายมนตรี มาลาทอง ที่อยู่ 123 คณะวิศวกรรมศาสตร์ มหาวิทยาลัยขอนแก่น ถ.มิตรภาพ อ.เมือง จ.ขอนแก่น 40002 และผู้รับโอน คือ 1.**มหาวิทยาลัยขอนแก่น** โดย ศาสตราจารย์วีระชัย โควสุวรรณ รองอธิการบดีฝ่ายวิจัยและการถ่ายทอดเทคโนโลยี มหาวิทยาลัยขอนแก่น ที่อยู่บ้านเลขที่ 123 ถ.มิตรภาพ ต.ในเมือง อ. เมือง จ.ขอนแก่น 40002 2. **สำนักงานกองทุนสนับสนุนการวิจัย** โดย ศาสตราจารย์สุทธิพันธ์ จิตพิมลมาศ ผู้อำนวยการสำนักงานกองทุนสนับสนุนการวิจัย ที่อยู่ 979/17-21 อาคารเอส เอ็ม ทาวเวอร์ ชั้น 14 ถ.พหลโยธิน แขวงสามเสนใน เขตพญาไท กรุงเทพฯ 10400 โดยสัญญานี้ ผู้โอนซึ่งเป็นผู้ประดิษฐ์   **"วัสดุปิดกั้นคลื่นสัญญาณแม่เหล็กไฟฟ้า"** ขอโอนสิทธิในการประดิษฐ์ดังกล่าว ซึ่งรวมถึงสิทธิขอรับสิทธิบัตร/อนุสิทธิบัตร และสิทธิอื่นๆ ที่เกี่ยวข้องให้แก่ผู้รับโอน เพื่อเป็นพยานหลักฐานแห่งการนี้ ผู้โอนและผู้รับโอนได้ลงลายมือชื่อไว้ข้างล่างนี้

(ลงชื่อ) .... ผู้โอน

(ผู้ช่วยศาสตราจารย์นันทกานต์ วงศ์เกษม)

(ลงชื่อ) .... ผู้โอน

(นายมนตรี มาลาทอง)

(ลงชื่อ) .... ผู้รับโอน

(ศาสตราจารย์วีระชัย โควสุวรรณ)

(ลงชื่อ) .... ผู้รับโอน

(ศาสตราจารย์สุทธิพันธ์ จิตพิมลมาศ)

(ลงชื่อ) ....พยาน

(นายเศกสิทธิ์ พรหมพฤฒา)

(ลงชื่อ) ....พยาน

(นางสาวนฤมล เบญจปัก)

หนังสือมอบอำนาจ

มหาวิทยาลัยขอนแก่น

อ.เมือง จ. ขอนแก่น 40002

วันที่ 31 กรกฎาคม 2556

โดยหนังสือฉบับนี้ ข้าพเจ้า 1.มหาวิทยาลัยขอนแก่น โดย ศาสตราจารย์วีระชัย โควสุวรรณ รองอธิการบดีฝ่ายวิจัยและการถ่ายทอดเทคโนโลยี มหาวิทยาลัยขอนแก่น ที่อยู่บ้านเลขที่ 123 ถ.มิตรภาพ ต.ในเมือง อ. เมือง จ.ขอนแก่น 40002 2. สำนักงานกองทุนสนับสนุนการวิจัย โดย ศาสตราจารย์สุทธิ พันธ์ จิตพิมลมาศ ผู้อำนวยการสำนักงานกองทุนสนับสนุนการวิจัย ที่อยู่ 979/17-21 อาคารเอส เอ็ม ทาวเวอร์ ชั้น 14 ถ.พหลโยธิน แขวงสามเสนใจ เขตพญาไท กรุงเทพฯ 10400 ขอมอบอำนาจและแต่งตั้งให้ นางจิรา ภรณ์ เหลืองไพรินทร์ อยู่บ้านเลขที่ 123 สำนักงานบริหารจัดการทรัพย์สินทางปัญญา มหาวิทยาลัยขอนแก่น ต.ในเมือง อ.เมือง จ.ขอนแก่น 40002 เป็นตัวแทนและผู้รับมอบอำนาจของข้าพเจ้ามีอำนาจในการยื่นขอรับ สิทธิบัตร/อนุสิทธิบัตรและดำเนินการจดทะเบียนสำหรับสิทธิบัตร/อนุสิทธิบัตรสำหรับการประดิษฐ์ "วัสดุปิดกั้น คลื่นสัญญาณแม่เหล็กไฟฟ้า โดยให้ตัวแทนดังกล่าวมีสิทธิลงชื่อในเอกสารทั้งมวลในนามของข้าพเจ้าแทน ข้าพเจ้า แก้ไขเปลี่ยนแปลงเอกสารและเอกสารอื่นๆ ที่เกี่ยวข้อง รวมทั้งการอุทธรณ์ต่างๆ ด้วย

ข้าพเจ้าขอรับผิดชอบในการที่ผู้รับมอบอำนาจได้กระทำไปตามหนังสือมอบอำนาจ ที่เสมือนว่า ข้าพเจ้าได้กระทำด้วยตนเองทั้งสิ้น

เพื่อเป็นหลักฐาน ข้าพเจ้าได้ลงลายมือชื่อไว้เป็นสำคัญต่อหน้าพยาน

(ลงชื่อ)..........................ผู้มอบอำนาจ   (ลงชื่อ)..........................ผู้มอบอำนาจ

(ศาสตราจารย์วีระชัย โควสุวรรณ)   (ศาสตราจารย์สุทธิพันธ์ จิตพิมลมาศ)

(ลงชื่อ)..........................ผู้รับมอบอำนาจ

(นางจิราภรณ์ เหลืองไพรินทร์)

(ลงชื่อ)..........................พยาน   (ลงชื่อ)..........................พยาน

(นายเศกสิทธิ์ พรหมพฤฒา)   (นางสาวนฤมล เบญจปัก)

บทความตีพิมพ์ใน **Proceedings** การประชุมวิชาการระดับนานาชาติ

ค1.   **N. Wongkasem** and A. Sonsilphong, "Narrow-Band Wave Block by Chiral Metamaterials," PIER 2013, Stockholm, Sweden, August 2013.

Narrow-band Wave Block by Chiral Metamaterials

Nantakan Wongkasem and Amornthep Sonsilphong

Metasolver Laboratory, Department of Electrical Engineering
Faculty of Engineering, Khon Kaen University, Khon Kaen 40002, Thailand

Abstract— EM wave block design using double-layer chiral metamaterials in microwave regimes is proposed. One of the well-known chiral structures, C_8, proven to have low loss narrow bandwidth, is employed in this design. The first layer is used to block one of the CP waves, while the other CP wave is filtered out by the same chiral structure with opposite handedness. Different distances between the two chiral layers are observed for the stopband location. These proposed designs are additional promising candidates in EM wave block applications.

1. INTRODUCTION

Based on optical activity or optical rotary dispersion (ORD), as an arbitrary polarized electromagnetic (EM) wave propagates through lossy chiral media, the wave splits into two waves with different phase velocities. These two eigenmodes, left and right circularly polarized waves (LCP and RCP wave), with different refractive indices, cause the rotation of the polarization plane. At the chiral-end, the two CP waves are then coupled and exit the media in one polarization configuration, typically as an elliptically polarized wave due to the circular dichroism (CD) or absorption loss.

Chiral metamaterials have been proposed for broadband [1–3] and multi-band circular polarizers [4,5], where different transformation responses for the LCP and RCP waves have been investigated. A designated CP wave of the two CP waves is blocked or filtered out depending on the handedness or enantiomer orientation of the chiral structures [6]. However, when high values of chirality index are generated, low loss circular birefringence is found [7,8]. In this study, we propose an EM wave block design using double-layer chiral metamaterials in microwave regimes One of the well-known chiral structures, C_8 [8,9], proven to have low loss narrow bandwidth, is employed in this design. The first layer is used to block one of the CP waves while the other CP wave is filtered out by the same chiral structure with opposite handedness. Different distances between the two chiral layers are observed for the resonance location of the composite. These proposed designs are additional promising candidates in EM wave block applications.

2. WAVE BLOCK BY C_8 STRUCTURE

A low loss isotropic chiral structure, C_8 [9], shown in Figure 1(a), is used in this study. An earlier report has shown that chirality and refractive index can be controlled effectively by the structure geometry [7]. H_1 and H_2, respectively, are the main axis and the arm of the structure; w is the linewidth, $A°$ is the angle between the main axis and the connected arms, and $B°$ is the angle between the adjacent main axis. With regard to its well-defined chiral orientation, a non-twisted C_8 structure with opposite arm illustrated in Figure 1(b) is employed to generate handedness properties. The two structures with opposite arms are placed on top of each other; hence, there is no twisted angle. The bi-layer structures are set using a periodic boundary. A double copper-clad Arlon Di 880 board is used as a substrate. The dielectric constant of the substrate board, ε_r, is 2.2, with a dielectric loss tangent of 0.0001. The dimension parameters are given as follows:
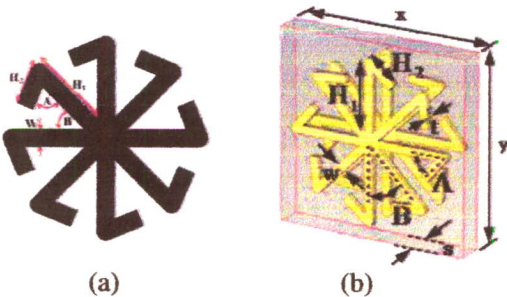

Figure 1: (a) C_8 structure and (b) a unit cell of the conjugated bi-layer C_8 structures [7].

$a_x = a_y = 37 \, \text{mm}$, $w = 2.8 \, \text{mm}$, $H_1 = 15.7 \, \text{mm}$, $s = 0.254 \, \text{mm}$ and $B = 360°/n$. The copper thickness, t_m, is $0.03 \, \text{mm}$.

A unit cell of left-handed (LH) and right-handed (RH) conjugated bi-layer C_8 structures are presented in Figure 2. The excitation is launched along $-z$ axis. Electric field, $\vec{E}$, and magnetic field, $\vec{H}$, are set along $+y$ and $+x$ axis, respectively. Figure 3 shows scattering (S) parameters of the LH and the RH conjugated bi-layer C_8 structures. The LCP wave can propagate through the RH structures at the operating frequency $f = 3.43 \, \text{GHz}$; while the RCP wave is truncated. Opposite results are found from the LH structures.
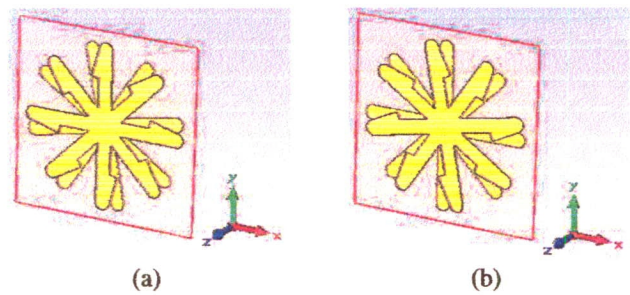
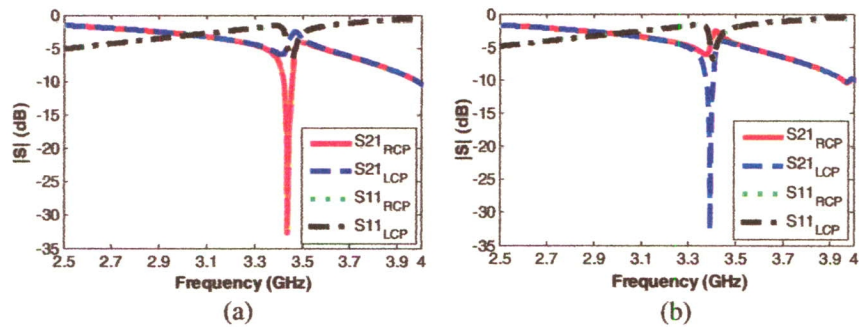Figure 2: A unit cell of (a) LH and (b) RH conjugated bi-layer C_8 structures.

Figure 3: S parameters of (a) left-handed and (b) right-handed conjugated bi-layer C_8 structures.
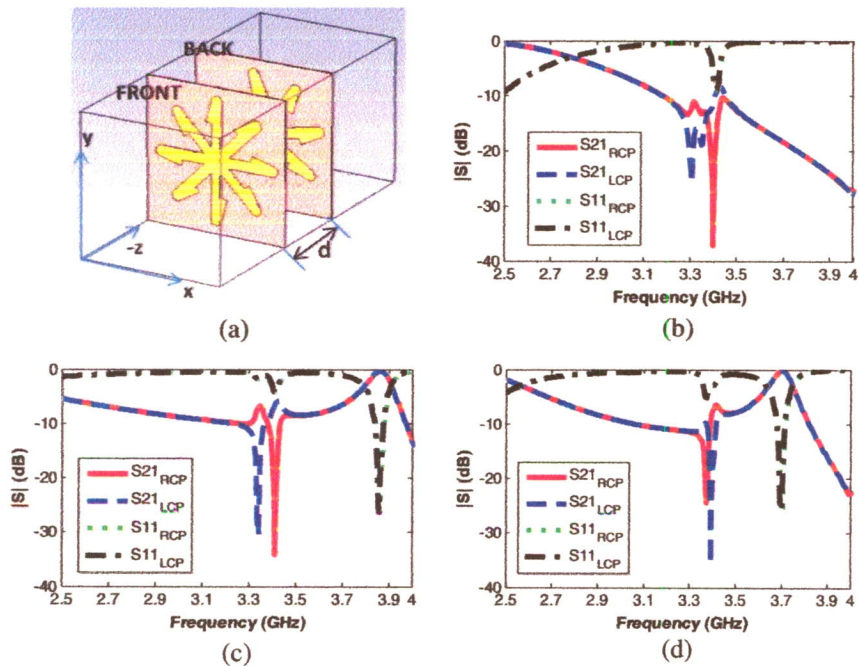

Figure 4: (a) CMM wave block and S parameters of the CMM wave block where (b) $d = \lambda/4$, (c) $d = \lambda/2$ and (d) $d = \lambda$.

The LH and the RH conjugated bi-layer C_8 structures are combined to perform as a CMM wave block. The two bi-layers are separated by a distance, d, as shown in Figure 4(a). S parameters of the CMM wave block are investigated when $d = \lambda/4$, $d = \lambda/2$ and $d = \lambda$. The resonances (S_{21}) of the LCP and RCP wave are almost overlapped when $d = \lambda$, confirming the complete CP wave block at the composite resonance frequency $f = 3.40\,\text{GHz}$.

3. CONCLUSIONS

Double-layer LH/RH chiral metamaterials are designed as EM wave block. The conjugated bi-layer C_8 structures are selected as low loss chiral metamaterials. The composite structure is composed of an array of LH and an array of RH chiral metamaterials. RCP wave is blocked by the LH set while LCP wave is filtered out by the RH set. The complete CP block is found when the distance between the two layers equals a wavelength at the operating frequency.

ACKNOWLEDGMENT

REFERENCES

1. Gansel, J. K., M. Thiel, M. S. Rill, M. Decker, K. Bade, V. Saile, G. V. Freymann, S. Linden, and M. Wegener, "Gold helix photonic metamaterial as broadband circular polarizer," *Science*, Vol. 325, 1513, 2009.
2. Gansel, J. K., M. Wegener, S. Burger, and S. Linden, "Gold helix photonic metamaterials: A numerical parameter study," *Optics Express*, Vol. 18, 1059, 2010.
3. Yang, Z. Y., M. Zhao, P. X. Lu, and Y. F. Lu, "Ultrabroadband optical circular polarizers consisting of double-helical nanowire structures," *Optics Letters*, Vol. 35, 2588–2590, 2010.
4. Ma, X., C. Huang, M. Pu, Y. Wang, Z. Zhao, C. Wang, and X. Luo, "Dual-band asymmetry chiral metamaterial based on planar spiral structure," *Appl. Phys. Lett.*, Vol. 101, 161901, 2012.
5. Wang, B., T. Koschny, and C. M. Soukoulis, "Wide-angle and polarization independent chiral metamaterials absorbers," *Phys. Rev. B*, Vol. 80, 033108, 2009.
6. Wongkasem, N., C. Kamtongdee, A. Akyurtlu, and K. Marx, "Artificial multiple helices: EM and polarization properties," *J. Opt.*, Vol. 12, 075102, 2010.
7. Panpradit, W., A. Sonsilphong, C. Soemphol, and N. Wongkasem, "High negative refractive index chiral metamaterials," *J. Opt.*, Vol. 14, 075101, 2012.
8. Sonsilphong, A. and N. Wongkasem, "Three-dimensional artificial double helices with high negative refractive index," *J. Opt.*, Vol. 14, 105103, 2012.
9. Matra, K. and N. Wongkasem, "Left-handed chiral isotropic metamaterials: Analysis and detailed numerical study," *J. Opt. A: Pure and Applied Optics*, Vol. 11, 074011, 2009.

บทความตีพิมพ์ใน **Proceedings** การประชุมวิชาการระดับนานาชาติ

ค2.   A. Sonsilphong and **N. Wongkasem**, "Light-weight radiation protection by non-lead materials in x-ray regimes," ICEAA – IEEE APWC 2014, Aruba, August 2014.

Light-weight radiation protection by non-lead materials in X-ray regimes

A. Sonsilphong[1]   and   N. Wongkasem[2]

Abstract – **A double-layer W/Bi sheet is proposed for a X-ray radiation protection at the energy range of 70 keV to 90 keV. Comparison of X-ray transmission intensity between simulation and measurement results is presented. Transmission intensity of X-rays with various incident angles is observed. This designed W/Bi sheet, only 0.14 mm thick, provides the same X-ray protection properties as the standard 0.50 mm Pb, and is 47% lighter.**

1   INTRODUCTION

X-ray is an electromagnetic wave widely used in many applications such as medical radiography, X-ray crystallography, and security systems etc. Lead (Pb) is a standard material used to shield X-ray propagation in an X-ray imaging system. Because lead is a heavy metal, the weight of Pb protective garments is high, which can lead to back pain when lengthily used [1]. Moreover, lead becomes toxic when it is out of date, approximately after 10 years [2]. Therefore, most recent research focuses on reducing the weight of protective garments by using composite materials with different K-edge absorption, for example, bi-layer of tungsten (W) and bismuth (Bi), and nano-metal with polymer metric, etc.

The powdered compounds such as bismuth oxide (Bi_2O_3), and gadolinium oxide (Gd_2O_3), and bi-layer of tungsten (W) and bismuth (Bi) were studied to reduce the transmission spectra and the weight of garments [2,3]. Nano-metal with polymer metric or rubber was presented as well [4-7]. The standard lead thicknesses are 0.50 mm, 0.35 mm, and 0.25 mm. The thickness depends on the transmission intensity which is directly related to the applied voltage at an X-ray tube. The energy range of 40 keV to 120 keV is normally used in the diagonal X-ray.

This paper discusses the protective non-lead materials for diagnostic imaging within the X-ray energy range of 70 keV to 90 keV. The transmission, reflection, and absorption spectra will be observed and compared with the standard 0.50 mm Pb sheet. The electromagnetic (EM) properties are obtained by Fresnel's equations. The EM properties from various incident angles of X-rays will be also investigated.

2   THEORIES AND METHODS

The transmission, reflection, and absorption spectra are calculated from Fresnel's equations [8-10]. The multi-layer stack used in this design is shown in fig. 1.

The incident wave propagates from left to right with the angle, θ_i. n and d are the refractive index and the thickness of each layer, respectively, where the subscription N, is the number of the layers. n_a and n_N are the refractive indices of the free space. The transmitted angle of each layer can be obtained from Snell's law. If the excited wave propagates perpendicularly to the multilayer stack, θ_i is equal to zero. i is the integer number, 1, 2, 3,..., i, $i+1$,..., N, indicating the number of layers.
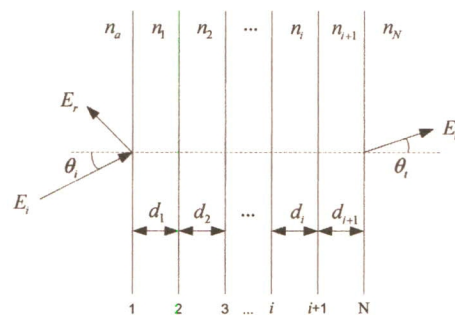

Figure 1: Multi-layer stack.

The refractive index at X-ray regimes used in this calculation is obtained from the NIST Physical Measurement Laboratory [11,12]. The weight ratio can be obtained from:

$$\%W_{ratio} = \frac{W_m}{W_{Pb}} = \frac{\sum_1^N \rho_m (xyz)_m}{\rho_{Pb}(xyz)_{Pb}} \qquad (1)$$

When the materials have the same dimensions but different thickness, the weight ratio can be obtained by:

$$\%W_{ratio} = \frac{\sum_1^N \rho_m z_m}{\rho_{Pb} z_{Pb}} \qquad (2)$$

where ρ and z are the density (g/cm^3) and the thickness (cm) of materials, respectively. From equation 2, we can calculate the weight ratio. If the weight ratio is less than 1, it means that the weight of the designed materials is lighter than the standard 0.50 mm Pb.

Metasolver Laboratory, Department of Electrical Engineering,
Faculty of Engineering, KhonKaen University, KhonKaen, 40002, Thailand
[1]e-mail: a.sonsilphong@gmail.com
[2]e-mail: nantakan@gmail.com

3 SIMULATION RESULTS

To validate a multi-layer method, the simulation results are compared with the measurement results [13], as illustrated in fig. 2. Three thicknesses, 0.5 mm, 1.0 mm, and 2.0 mm, of a Pb sheet are studied. The X-ray intensity decreases when the Pb thickness increases. The simulation results are in good agreement with the measurement results.
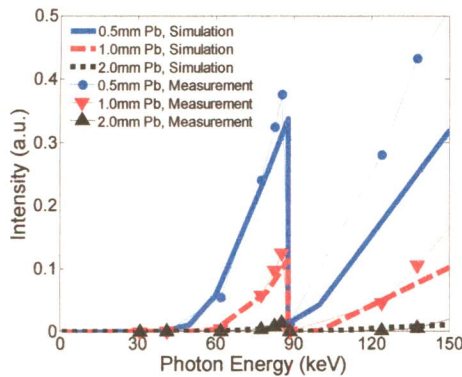

Figure 2: Comparison of X-ray transmission intensity between simulation and measurement results.
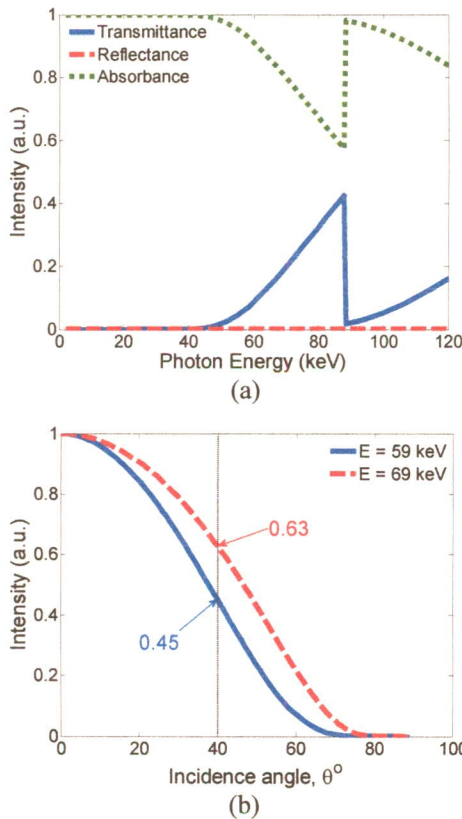

(a)

(b)

Figure 3: (a) Transmission, reflection and absorption spectra versus energy and (b) normalized transmission intensity of a 0.50 mm Pb sheet with different incident angles.

Figure 3 shows the EM properties of the standard 0.50 mm Pb sheet. Within the energy range of 70 keV to 90 keV, the 0.50 mm Pb sheet can absorb more than 60% of X-rays, as shown in figure 3(a). The reflectance of the 0.50 mm Pb sheet is significantly small, close to zero. Figure 3(b) shows the transmittance of the X-rays with various incident angles at 59 keV and 69 keV. It can be seen that at 59 keV the 0.5 mm Pb sheet can absorb the X-ray better than at 69 keV (less transmission intensity); for instance at 40 degrees, the transmission intensity at 59 keV is 45%, while it is 63% at 69 keV. Note that this is because of the higher value of the imaginary part of the refractive index term.
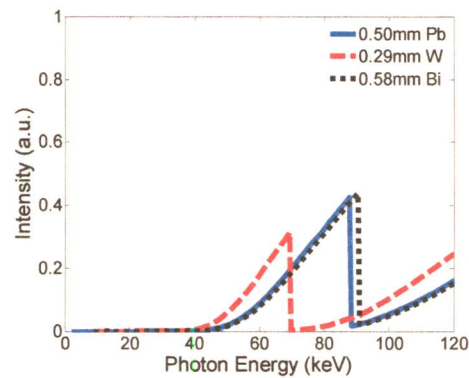

Figure 4: Transmission spectra of W and Bi and 0.50 mm PB at the same weight.
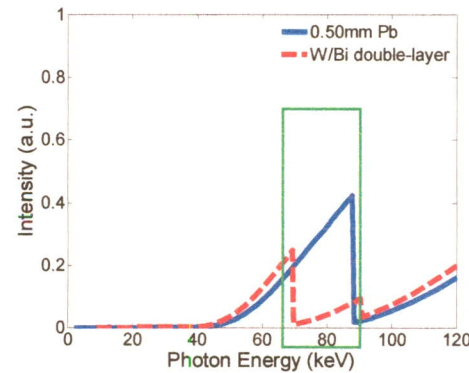

Figure 5: Transmission spectra of double-layer W/Bi sheet and 0.50 mm PB at same weight.

The transmission properties of tungsten (W) and bismuth (Bi) are investigated in X-ray regimes. It is important to stress that both W and Bi are relatively inexpensive and also easy to find in nature. Figure 4 illustrates the simulation results of the transmission spectra of a single-layer W and a single-layer Bi sheet. The W sheet and Bi sheet both have the same weight as the 0.50 mm Pb sheet. The thicknesses of W and Bi are 0.29 mm and 0.58 mm, respectively. The transmission intensity of the W sheet is lower than that

of the 0.50 mm Pb in the energy range of 70 keV to 90 keV, while the transmission intensity of the Bi sheet is similar to that of the 0.50 mm Pb sheet.

The double-layer W/Bi sheet is investigated. This W/Bi sheet is set to have the same weight as the standard 0.5 mm Pb sheet. The thickness ratio between W and Bi, γ, is equal to 0.5. Therefore, the thicknesses of W and Bi are 0.20 mm. The transmission spectra of the W/Bi sheet is lower than that of the 0.50 mm Pb sheet in the energy range of 70 keV to 90 keV, which is illustrated in figure 5.
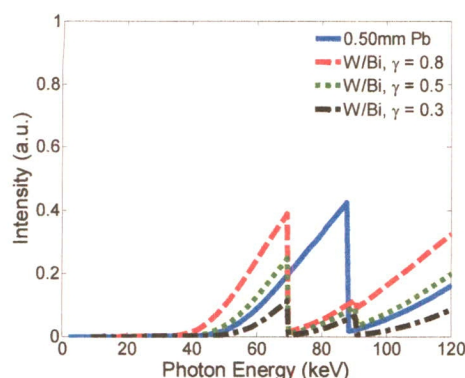

Figure 6: Transmission spectra of double-layer W/Bi and 0.50 mm Pb, where γ is varied.

The double-layer W/Bi sheet is then observed in different thickness ratios at γ = 0.8, 0.5, and 0.3. The thickness of W is fixed at 0.20 mm. The thicknesses of Bi are 0.05 mm, 0.20 mm, and 0.47 mm for the thickness ratio of 0.8, 0.5, and 0.3, respectively. At γ = 0.8, the 0.25 mm double-layer W/Bi sheet is 24% lighter than that of the standard 0.5 mm Pb sheet. Furthermore, to obtain the same transmission intensity, the double-layer W/Bi sheet is 47% lighter than that of the standard 0.50 mm Pb in the energy range of 70 keV to 90 keV. Here, γ = 0.5, where W and Bi have the thickness of 0.07 mm.

4   CONCLUSIONS

A double-layer W/Bi sheet is designed and proposed to shield X-ray radiation in the energy range of 70 keV to 90 keV. This 0.17 mm W/Bi sheet is proved to provide the same protection properties as the standard 0.50 mm Pb and is 47% lighter.

References

[1]   B. Moore, E. VanSonnenberg, G. Casola, and R. A. Novelline, "The relationship between back pain and lead apron use in radiologists.," *Ajr Am. J. Roentgenol.*, vol. 158, no. 1, pp. 191–193, 1992.

[2]   J. P. McCaffrey, H. Shen, B. Downton, and E. Mainegra-Hing, "Radiation attenuation by lead and nonlead materials used in radiation shielding garments," *Med. Phys.*, vol. 34, no. 2, p. 530, 2007.

[3]   J. P. McCaffrey, F. Tessier, and H. Shen, "Radiation shielding materials and radiation scatter effects for interventional radiology (IR) physicians," *Med. Phys.*, vol. 39, no. 7, pp. 4537–4546, Jul. 2012.

[4]   M. H. Al-Maamori, O. H. Al–Bodairy, and N. A. Saleh, "Effect if PbO with rubber composite on transmission of (x-ray)," *Nat. Appl. Sci.*, vol. 3, no. 3, pp. 113–119, 2012.

[5]   S. Nambiar and J. T. W. Yeow, "Polymer-Composite Materials for Radiation Protection," *Acs Appl. Mater. Interfaces*, vol. 4, no. 11, pp. 5717–5726, Nov. 2012.

[6]   S. Nambiar, E. K. Osei, and J. T. W. Yeow, "Polymer nanocomposite-based shielding against diagnostic X-rays," *J. Appl. Polym. Sci.*, vol. 127, no. 6, pp. 4939–4946, Mar. 2013.

[7]   H. Uthoff, C. Peña, J. West, F. Contreras, J. F. Benenati, and B. T. Katzen, "Evaluation of Novel Disposable, Light-Weight Radiation Protection Devices in an Interventional Radiology Setting: A Randomized Controlled Trial," *Am. J. Roentgenol.*, vol. 200, no. 4, pp. 915–920, Apr. 2013.

[8]   C. A. Balanis, *Advanced Engineering Electromagnetics*, Solution Manual edition. New York: Wiley, 1989.

[9]   V. G. Kohn, "On the Theory of Reflectivity by an X-Ray Multilayer Mirror," *Phys. Status Solidi B*, vol. 187, no. 1, pp. 61–70, Jan. 1995.

[10] M. Born, E. Wolf, A. B. Bhatia, P. C. Clemmow, D. Gabor, A. R. Stokes, A. M. Taylor, P. A. Wayman, W. L. Wilcock, and & 3 more, *Principles of Optics: Electromagnetic Theory of Propagation, Interference and Diffraction of Light*, 7th edition. Cambridge ; New York: Cambridge University Press, 1999.

[11] C. T. Chantler, "Theoretical Form Factor, Attenuation, and Scattering Tabulation for Z=1–92 from E=1–10 eV to E=0.4–1.0 MeV," *J. Phys. Chem. Ref. Data*, vol. 24, no. 1, pp. 71–643, 1995.

[12] N. US Department of Commerce, "NIST Physical Measurement Laboratory Homepage." [Online]. Available: http://www.nist.gov/pml/index.cfm.

[13] G. W. C. Kaye and W. Binks, "The emission and transmission of x and gamma radiation," *Br. J. Radiol.*, vol. 13, no. 150, pp. 193–212, 1940.